MULTISPECIES BACTERIAL ATTACHMENT TO A106 GB INDUSTRY-FINISHED STEEL USED IN HEAT EXCHANGERS

Submitted By

ALICIA PRITHIRAJ

A dissertation submitted in partial fulfilment of the requirements for the degree

of

DOCTOR OF PHILOSOPHY

(CHEMICAL ENGINEERING)

In the

FACULTY OF ENGINEERING, BUILT ENVIRONMENT AND INFORMATION TECHNOLOGY

DEPARTMENT OF CHEMICAL ENGINEERING

UNIVERSITY OF PRETORIA

2024

ABSTRACT

Title: **Multispecies bacterial attachment to A106 GB industry-finished steel used in heat exchangers**

Author: Alicia Prithiraj

Supervisor: Professor Evans Martin Nkhalambayausi Chirwa

Co-supervisor: Professor Shepherd Masimba Tichapondwa

Department: Chemical Engineering

University: University of Pretoria

Degree: Doctor of Philosophy (Chemical Engineering)

Multispecies bacterial attachment to industrial-finished alloys is not understood. It is not well understood as to why certain bacterial species selectively attach to differently finished steel surfaces. It is also a matter of curiosity as to why the attachment of certain bacteria influences corrosion. Bacterial attachment in heat exchangers leads to biofouling, corrosion, and downtime costs. This study evaluated the synergistic effect of bacterial attachment to smooth and rough (industrial standard) surfaces unique to the petrochemical industry. From the results there were no significant time-related differences in colonisation ($p(perm)>0.05$), and bacterial levels on the surfaces ($p>0.05$). However, quantification of surfaces using Atomic Force Microscopy (AFM) showed significant differences ($p<0.05$) in the root mean square surface roughness (RMS) of the differently finished surfaces, elucidating that bacterial colonisation was not proportional to surface roughness. It was observed that *Clostridium sp.* colonised the rough surfaces abundantly, and *Pseudomonas sp.* favoured the rough surface during early colonisation which influenced the corrosion rate. In bacterial presence, the corrosion rate on the rough alloy surface on day 3, exhibited corrosion resistance. This was owing to the synergistic behaviour of the bacteria which selectively attached to the rough surface and formed biofilm. Increased corrosion rates were then observed when compared to the smooth alloy. On the rough surface on day 6, the corrosion rate was observed to be the highest with 38.72 ± 0.15 mm/y. Smooth surfaces exhibited unusual corrosion rates on this day. On day 13 both surfaces exhibited a corrosion protection phenomenon. In light of the findings, it was

observed that there were significant differences observed on day 6, in the corrosion rate value between the rough and smooth surfaces ($p<0.05$). The growth model confirmed that exponential growth phase took place from day 6. Total Organic Carbon (TOC) results revealed that during bacterial growth, the bacteria utilised the carbon sources and produced acetic acid and lactic acid which played an important role in the corrosion process.

Unlike sulfate-reducing bacteria (SRB), *Clostridium sp.* and *Pseudomonas sp.* described in this study are rarely reported in the petrochemical environment. These microorganisms are ubiquitous; however, their dominance in these systems showed that they play a significant role in steel corrosion. This study used next-generation sequencing with qPCR into microbial species colonising steel with AFM, which are rarely reported jointly in the literature. These bacteria can survive nutrient-depleted conditions for extended periods. The results provided a basis to explicate metabolic pathways. Long-term steel exposure to the bacterial consortia indicated steel protection rather than corrosion. Innovative insights on carbon-metal bonding were also determined, which could be a basis for future work. The synergistic behaviour of the bacteria provided a new dimension of thinking regarding the corrosion of carbon steel. In this study, the smooth-finished alloy performed best in this process system based on the corrosion evaluation.

Keywords: multispecies biofilm, cooling tower water, corrosion remediation, heat exchanger, microbial attachment, atomic force microscopy

DECLARATION

I, the undersigned hereby declare that:

- I understand what plagiarism is and I am aware of the University's policy in this regard;
- The work contained in this thesis is my own original work;
- I did not refer to work of current or previous students, lecture notes, handbooks or any other study material without proper referencing;
- Where other people's work has been used this has been properly acknowledged and referenced;
- I have not allowed anyone to copy any part of my thesis;
- I have not previously in its entirety or in part submitted this thesis at any University for a degree.

DISCLAIMER:

The work presented in this report is that of the student alone. Students were encouraged to take ownership of their projects and to develop and execute their experiments with limited guidance and assistance. The content of the research does not necessarily represent the observations of the supervisor or any staff member of the University of Pretoria, Department of Chemical Engineering. The supervisor has read the final report to provide recommendations based on the institutional guidelines and is not responsible for any technical inaccuracies, statements or errors. The conclusions and recommendations provided in the report are also not necessarily that of the supervisor, sponsors or companies involved in the research.

_____ _____

Alicia Prithiraj Date

ACKNOWLEDGEMENTS

My sincere gratitude to the following persons and institutions:

- My study leaders, Prof. Chirwa and Prof. Shepherd, thank you for believing in me and for the opportunity to take on this project. The guidance and technical expertise I received from my study leaders ensured the success of this project.
- Prof. Brink from the Chemistry Department (UP) for sharing his knowledge on HPLC and TOC methods.
- Prof. Nel, for your support with AFM (UP); your kindness lifted me, and your interest in my topic motivated me.
- Vusani, from Physics Department (UP), for assisting with Raman spectroscopy analysis.
- Charity, from the Microscopy Lab (UP), for her time and support with SEM.
- Tiaan, from the industrial chemistry department, for his kindness and support with FTIR.
- Monoko—for all the assistance on HPLC (UP).
- Deon from the metallurgy department has been a great support from the petrochemical industry, and I am grateful to have met him on my journey.
- Austin and James from the industry for their kindness and interest in my work and their specialist advice.
- Stephanus, Jean, and the Buckman team for always being willing to assist me with the cooling tower work.
- Due to my relocation to Cape Town, I could not finish SEM work for the corrosion tests; therefore, I humbly thank Prof. Robert and Miranda from the University of Cape Town for supporting me with SEM imaging.
- Some of my challenges from this project included time management (work and family), travelling to use various equipment in various locations and expert resource availability to operate the equipment. I am grateful to everyone who provided their time to support me.
- I thank Amith for proofreading this document.
- My appreciation to my language editor, Elizabeth Marx, from Academic and Professional Editing Services (APES).
- I acknowledge my spouse Ashish and daughter Aditi, my only support structure. I would like to dedicate this thesis to both of you.

Funding:

- National Research Fund (NRF) of South Africa for funding the project through the Grant No's SRUG2204072544 and EQP180503325881 awarded to Prof Evans M. N. Chirwa and the Rand Water Chair in Water Utilisation Project No. RW01413/18 also awarded to Prof Evans Chirwa.
- Additional NRF funding provided via the Thuthuka Grant No. TTK18024324064 awarded to Prof Shepherd M. Tichapondwa of the Department of Chemical Engineering at the University of Pretoria.
- MINTEK South Africa for funding support on next-generation sequencing.

TABLE OF CONTENTS

LIST OF FIGURES

LIST OF TABLES

LIST OF EQUATIONS AND REACTIONS

$$Cr = \frac{(W_1 - W_4)\times 365\times 100}{\rho_c . A . t} \quad \text{(Equation 1)}$$

$$\mu = \frac{\mu_{max} S}{K_s + S} \quad \text{(Equation 2)}$$

$$CH_3COO^- + 8Fe(OH)_3 \rightarrow 8Fe^{2+} + 15OH^- + 2HCO_3^- + 5H_2O \quad \text{(Equation 3)}$$

$$4Fe + SO_4^{2-} + 8H^+ \rightarrow 4FeS + 4H_2O \quad \text{(Equation 4)}$$

$$2C_3CHOHCOO^- + SO_4^{2-} + H^+ \rightarrow 2CH_3COO^- + 2CO_2 + HS^- + 2H_2O \quad \text{(Equation 5)}$$

$$Fe^{2+} + S^{2-} \rightarrow FeS \quad \text{(Equation 6)}$$

$$Fe^{2+} + CO_2 + OH^- \rightarrow FeCO_3 + H^+ \quad \text{(Equation 7)}$$

LIST OF ABBREVIATIONS/DEFINITIONS/ACRONYMS

ASTM:	American Society for Testing and Materials
Amorphous:	Irregular or curved surfaces
EDX:	Energy Dispersive X-Ray Analysis
SEM:	Scanning Electron Microscopy
AFM:	Atomic Force Microscopy
TOC:	Total Organic Carbon
VOA:	Volatile Organic Analysis
NDIR:	Non-Dispersive Infrared
HPLC:	High-Performance liquid chromatography
Ni-P-rGO:	Ni–P–graphene oxide
PTFE:	Polytetrafluoroethylene
Ni-P:	Nickel-phosphorus
DLVO/ XDLVO:	Derjaguin-Landau-Verwey-Overbeek and the extended theorem
Biofilm:	A consortia of bacteria within a polymer matrix attached to a surface
SRB:	Sulfate-reducing bacteria
TSA:	Tryptic Soy Agar
MTT:	3-(4,5- dimethylthiazol-2-yl)-2,5-diphenyl tetrazolium bromide
XRD:	X-Ray Diffraction analysis
Ecology:	relationships among living organisms
Homogenous:	comprising the same parts or elements

Planktonic:	free-living bacteria
Topography:	the arrangement of features on the surface
PMMA:	polymethyl methacrylate
PDMS:	polydi-Methylsiloxane
BSA:	bovine serum albumin
FTIR:	Fourier Transform Infrared Spectroscopy
PERMANOVA:	Permutational analysis of variance
Acetogens:	organisms that generate acetate (and water) as the main by-product. All acetogens characterised since 2019 belong to bacteria.
Metagenomics:	the study of genetic material recovered directly from environmental samples.
qPCR:	quantitative polymerase chain reaction

Absolute copy number: Bacterial levels

LIST OF SYMBOLS

S	simulated concentration of the nutrient in the media at time t (g/L)
S_{meas}	measured concentration of the nutrient in the media at time t (g/L)
μ	specific growth rate
μ_{max}	maximum specific growth rate
K_s	half-life saturation constant
k	concentration constant
C	simulated concentration (g/L)
C_{meas}	measured concentration (g/L)
Cr	corrosion rate (mm/y)
W_1	weight 1 initial weight of coupon taken before exposure (g)
W_4	weight 4 final weight taken after cleaning biofilm/corrosion product (g)
$\boldsymbol{\rho_c}$	density of the coupon (g/dm^3)
A	surface area of the coupon (dm^2)
Cq	quantification cycle
g to bp	constant (1.096 x 10^{-21}g)

PEER-REVIEWED JOURNAL ARTICLES

Prithiraj, A., Tichapondwa, S., & Chirwa, E.M.N. 2023. Kinetic growth model and metabolic effect of a bacterial consortia from a petrochemical processing plant. **Status:** Accepted. Wiley: *Canadian Journal of Chemical Engineering*.

Prithiraj, A., Tichapondwa, S., Nel., J.M., & Chirwa, E.M.N. 2023. Influence of surface finish on colonisation and surface erosion by a mixed bacterial culture. **Status:** Accepted. *Taylor and Francis: Biotechnology and Biotechnological Equipment*.

PEER-REVIEWED CONFERENCE PROCEEDINGS AND CONFERENCES

Conference abstract submission: 9th International Conference on Industry Biotechnology 2024: Biofilms in industry and medicine. **Topic:** Morphological evaluation of a multispecies biofilm on A106 GB industry-finished steel used from heat exchangers. **Status:** Accepted.

Conference abstract submission: Global Congress of Chemical Engineering 2024. **Topic:** Characterization of corrosion products formed on carbon steel after exposure to a bacterial consortium from a cooling tower. **Status:** Abstract accepted, reviews submitted.

Conferences: Presented at Materials global summit 2020.

Conferences: Presented at SEM symposium 2021.

CHAPTER 1 INTRODUCTION

1.1 BACKGROUND

Microbial communities in complex environments typically co-exist in syntropic synergy to optimise resource utilisation. Microbial cultures growing on surfaces, such as bacteria facilitating surface corrosion of metallic surfaces, are not an exemption from the above behaviours (Xi *et al.,* 2020). Despite decades of work conducted on bacterial attachment, it is still a challenge in bioengineering applications attributable to complex initial dynamics in cells, formation of exopolysaccharides (EPS), and complex initial interaction between the cell/biofilm matrix and surface conditioning (Achinas *et al*., 2019, Tuck *et al.,* 2021, Yuan *et al.,* 2019).

Biofilm formation is a process step involved with bacterial attachment to the substrate. The biofilm formation process includes four steps: initial attachment, microcolony formation, maturation, and dispersion. Extracellular polymeric substance (EPS) formation in heat exchangers causes biofouling—which can also be termed biofilm (Yang *et al*., 2004)—leading to a loss in heat transfer efficiency and tube failures (Mathew *et al.,* 2021). Most heat exchanger devices are made of carbon steel that is susceptible to biofouling.

Surface modifications to reduce initial attachment and biofilm formation range across various fields of study. In the petrochemical industry, carbon steel tubes were coated with nickel-phosphorus graphene oxide (Ni-P-rGO) (Xu *et al.,* 2020) to investigate the properties of iron bacteria biofouling. Food industries used stainless steel 304 plates modified by electroless plating nickel-phosphorus (Ni-P) and limited amounts of Polytetrafluoroethylene (PTFE) on *Escherichia coli* (*E.coli)* adhesion (Zhao *et al.,* 2007). In industrial cooling water systems various polymeric surfaces and stainless steel were studied during the biofouling process of *E.coli* (Pohl *et al.,* 2017).

In biological sciences, the effect of substratum roughness on the attachment of *Pseudomonas aeruginosa* and *Staphylococcus epidermidis* was investigated using polymethyl methacrylate (Taylor *et al.,* 1998). In dentistry, an invitro study was conducted to assess the roughness and attachment of *Streptococcus sanguinis* after treatment of smooth and rough titanium surfaces with an erbium-doped: yttrium, aluminium, and garnet (Er: YAG) laser, metal, and plastic curettes, and an air-power abrasive system (Duarte *et al.,* 2009). For the marine environment, the non-fouling properties of hyaluronic acid and chondroitin sulphate against marine fouling

organisms (marine bacterium *Cobetia marina*, zoospores of seaweed *Ulva linza* and cells of a diatom *Navicula incerta*) were investigated (Bauer *et al.,* 2013).

There is limited research into attaching a mixed bacterial culture to steel used in the petrochemical industry. A few authors studied multispecies attachment in dentistry; however, the conclusions are contrasting (Park *et al.,* 2019; Dezelic & Schmidlin, 2009). Multispecies attachment differs from single-species studies by ecology and the surface finish of materials used in a specific environment/field of study and bacterial appendages (Fimbriae, Pili, and flagella), which strengthen the attachment among the bacterial cell on the surface once the bacteria encounter the material surface (Jamal *et al.,* 2018). From the existing reports, there is an apparent need for research involving multispecies attachment from the petrochemical industry, owing to the conflicting reports and downtime of equipment and maintenance, distinctly associated with a mixed bacterial culture.

Two theorems explain cell-surface interactions, the DLVO/XDLVO (Derjaguin-Landau-Verwey-Overbeek and the extended theorem), used to describe the net interaction between a cell and a surface as a balance between two interactions: Van der Waals (generally attractive) and Coulomb (repulsive owing to the negative charge of cells and substratum), the other being the thermodynamic theorem—the second physiochemical approach used to describe bacterial attachment to surfaces. It considers the attractive and repulsive interactions and expresses them collectively concerning free energy, a thermodynamic term (Katsikogianni & Missirlis, 2004). Both theorems, often used in microbial systems, might not apply to all microorganisms, experimental conditions, and surfaces. The theorems have not identified various attachment behaviours in bacterial systems (Ninham *et al*., 2017); therefore, these theorems were not evaluated extensively in this study.

Traditional methods of evaluating the attachment of bacteria were by counting bacterial cells attached to the surface through microscopic image analysis (Dezelic & Schmidlin, 2009 and An & Friedman, 1997). Electron microscopy (Knutton, 1995) and confocal laser scanning microscopy (Park *et al.,* 2019) were used for this purpose; however, all these methods are imprecise, indirect, and tedious (Yuan *et al.,* 2019). The latest development in atomic force microscopy (AFM) offers new opportunities in characterising the bacterial surface (Yuan *et al.,* 2019). AFM analysis is the most applicable data collection method providing an avenue to examine colloid and bacterial attachment at atomic, nanoscale, and microscale levels.

1.2 PROBLEM STATEMENT

Petrochemical processing plants experience production and efficiency losses owing to severely corroded tubes on heat exchangers using cooling water as a cooling medium (Prithiraj *et al*., 2019). At 3.4% of the global gross domestic product (GDP) in 2013, estimated the global cost of corrosion to be US$ 2.5 trillion. The heat exchangers are being replaced in-kind three times a year with no detailed projects to guide the tube failures prevalent within the first year of replacement. During operation root cause analysis conducted by the plant supervisor in which sludge samples were taken directly from the heat exchanger tube, cooling water quality and microbial corrosion were identified as the drivers for accelerated corrosion. This is a broad understanding of the mechanism of corrosion.

Biofilm and localised corrosion were observed by the industry engineers during the on-site inspection of the heat exchanger tubes. During the replacement of the heat exchanger, it was observed that there was no material finish specification for steel delivered to site. Literature reports that surface finish influences the attachment of bacterial cells (Nouri *et al*., 2023), however, there are inconsistent conclusions on this subject. It is imperative to understand how multiple bacterial species interact and attach to the steel specifications and determine their corrosion mechanisms to recommend an optimum surface finish and cut costs. This study uses third-generation sequencing together with qPCR and AFM to provide new insights into bacterial colonisation of industry carbon steel tube material, A106 GB, finished to rough (400 grit) and smooth (3 µm polished). This study establishes formative standards when designing heat exchangers for cooling water service to broaden the comparison to literature while presenting a better understanding of multispecies attachment to surfaces. Moreover, the study highlights key role players responsible for corrosion in the petrochemical industry.

1.3 RESEARCH AIM AND OBJECTIVES

The main aim of this study was to identify a surface finish specification for future use in heat exchanger cooling systems to reduce multispecies biofilm facilitated corrosion.

Specific objectives:

- To determine bacterial growth for 15 days
- To evaluate bacterial metabolites produced and consumed with their functions
- To characterise bacterial species on colony plates

- To evaluate the roughness parameters
- To determine differences in bacterial colonisation on rough and smooth surfaces
- To determine differences in bacterial levels on rough and smooth surfaces
- To characterise bacterial species attached to the alloy surfaces
- To determine the corrosion rate and characterise the corrosion products

1.4 OUTLINE OF THE RESEARCH PROBLEM

Figure 1.1 presents an outline of the research problem. The outline highlights the early commonly asked questions on multispecies attachment to surfaces, the problem statement is summarised with a basic proposition on how to go forward in answering the questions. The Integration Definition for Process Modelling (IDEF0) in Figures (1.2-1.4), gives a visual representation of the overall project together with the order in which each experiment will be conducted. Included in the figures are the outputs indicating how the hypothesis should be structured. The controls represent the main constant parameter during the experiment, and the inputs includes what will be needed in order to start the experimental process. The mechanisms represent the various analysis that will be conducted. Lastly an output hypothesis is generated. In the chapters that follow, a table of hypothesises is presented in more detail.

1.5 EXPERIMENTAL ANALYSIS

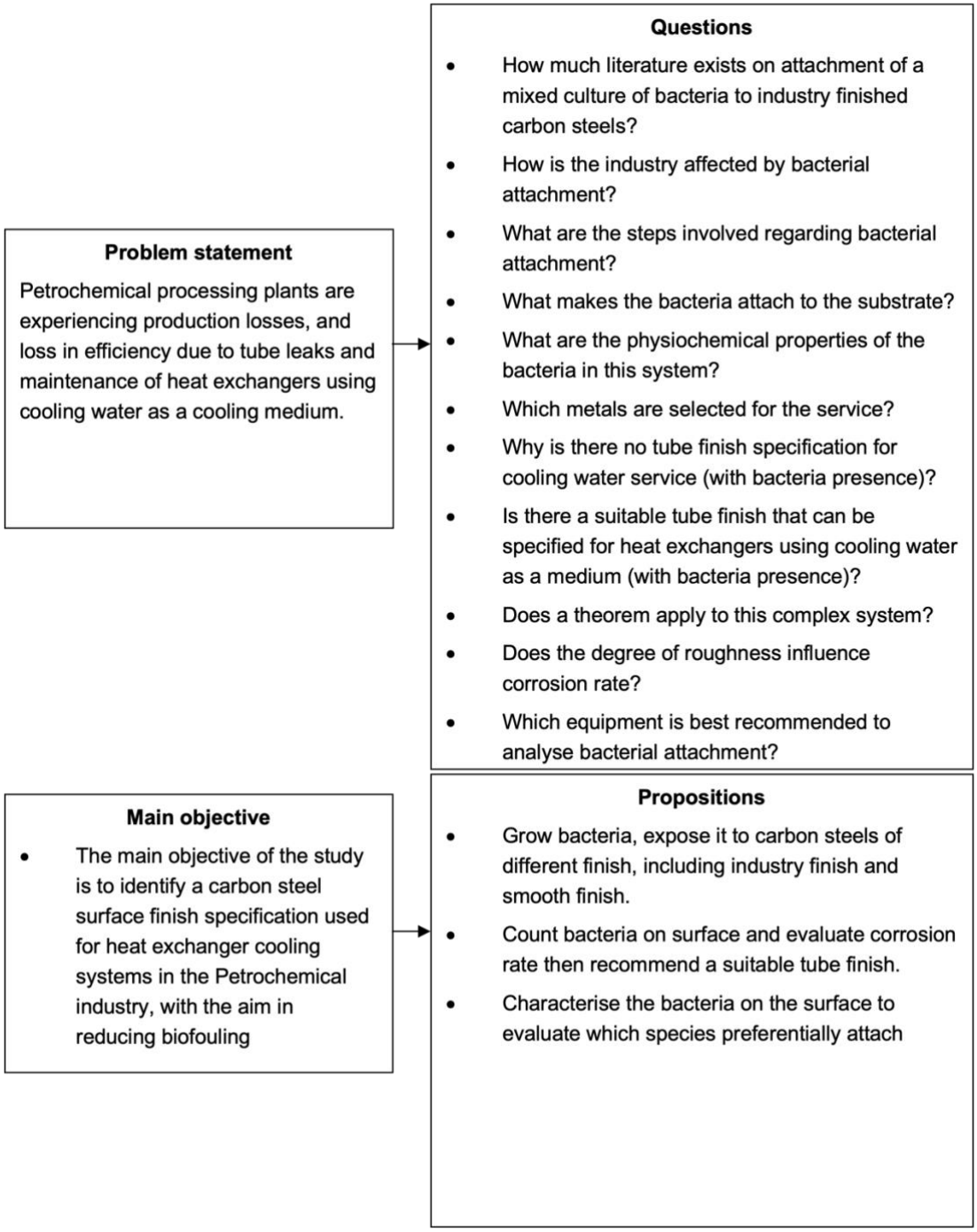

Figure 1.1: Outline of the research problem

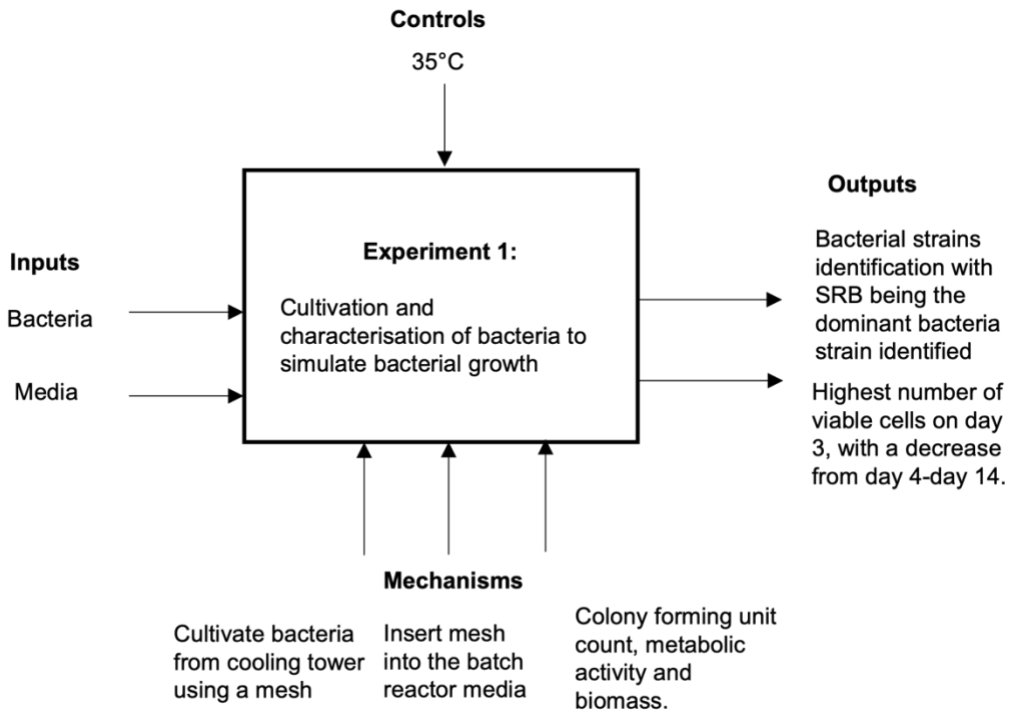

Figure 1.2: IDEF0 diagram of Experiment 1

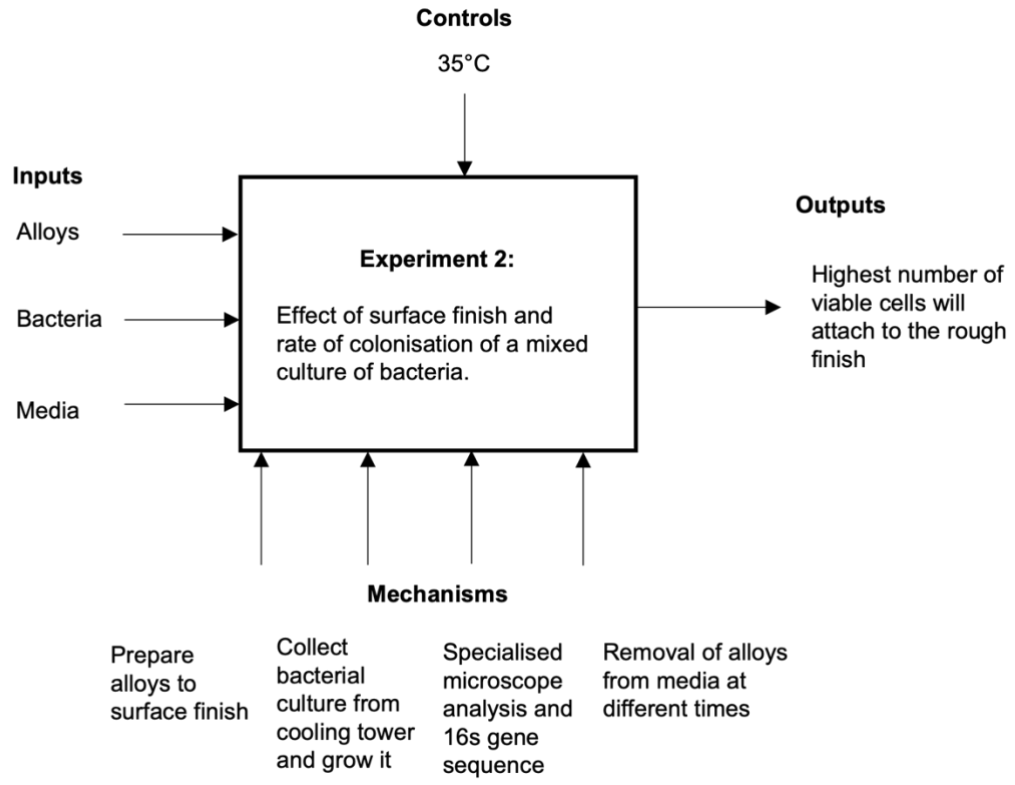

Figure 1.3: IDEF0 diagram of Experiment 2

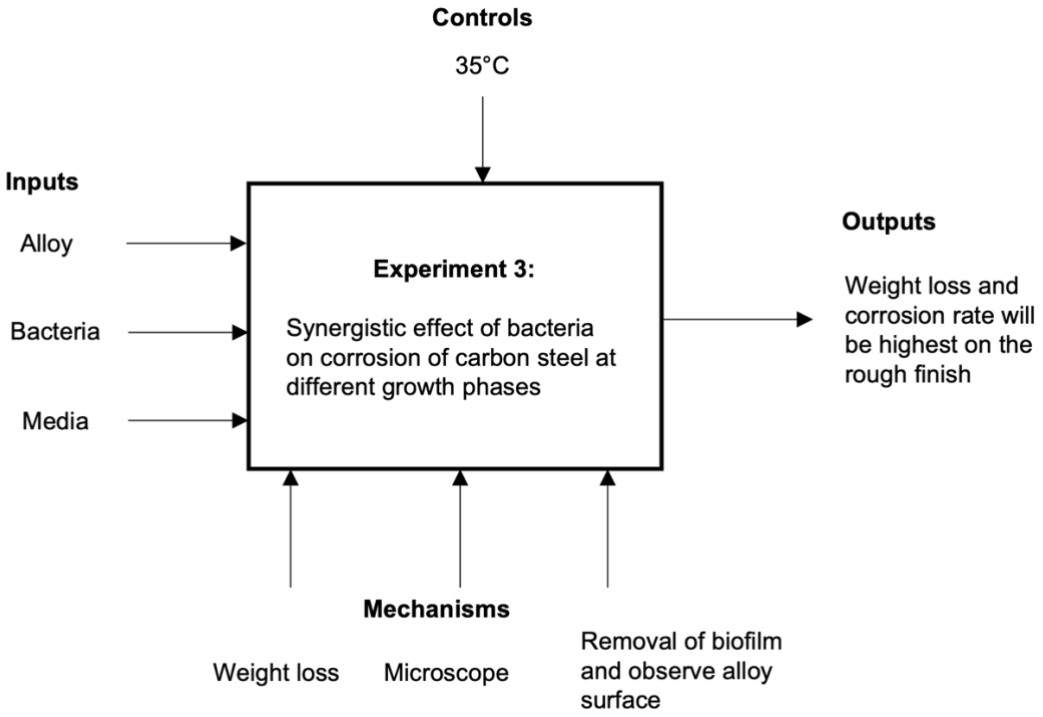

Figure 1.4: IDEF0 diagram of Experiment 3

1.6 ASSUMPTIONS

The study assumed that:

- Microorganisms identified on colony plates would differ from that of the bacteria in the prepared nutrient media.
- The training received on colony plating and conducting MTT assays was sufficient.
- The laminar flow hood used to conduct colony plating and MTT assays were in working. condition, and quality checks were conducted to certify the lab.

1.7 LIMITATIONS

The limitations were:

- Carbon sources were used in the batch media as the cooling water also contains carbon sources.
- Aerobic conditions were established in this study.
- Batch reactor set-ups inoculated with bacteria were prepared twice in this study. The first batch set-up evaluated the growth of bacteria without alloy exposure. The second batch reactor set-up with alloys evaluated TOC, HPLC, surface roughness, colonisation, and corrosion rate. The stainless-steel mesh designed to collect bacteria was left in the cooling tower coupon rack for 11 months, before being incubated in the nutrient batch reactor.
- The number of days was limited to 15 days, therefore, long-term stationary phase was not investigated.
- A stainless-steel mesh coupon designed to collect bacteria was inserted on-site in the cooling tower coupon rack and could only house one mesh at a time.

1.8 RESEARCH SCOPE

CHAPTER 1 Introduces the background of the study with a problem statement. The research objectives are presented with the research outline and experimental analysis. The assumptions and limitations are then defined.

CHAPTER 2 The literature review focuses on a broad discussion of bacterial attachment to a surface, then narrows down to the influences of surface roughness on the colonisation of bacteria. Presented first are basic concepts introducing the typical arrangement of a cooling

tower network in a petrochemical industry. The fundamental understanding of biofilm formation is introduced and is the most important factors in this multispecies study. The sections then interlink into the life cycle of bacterial biofilm with a discussion on how complex structures are formed and their emergent properties. The properties of biofilm communities comprise novel structures, activities, patterns, and properties and self-organisation in complex systems. A fundamental understanding of the factors controlling cell attachment is further presented.

The literature provides insight into preventing biofilm formation and emphasises inconsistencies, including irregular and patterned surfaces. Two theories explain bacterial attachment to surfaces; however, these theories do not consider multispecies systems. Reports on attachment studies are discussed, showcasing the range of fields this topic transcends. Typical equipment used to analyse bacterial attachment is presented. Surface roughness characterisation is lastly discussed. This study aimed to broaden the understanding of multispecies bacterial attachment while providing an apparent relationship between cell attachment and substrate roughness.

CHAPTER 3 This chapter presents the methodology with the selected research designs and hypotheses. Section 3.1 presents the method to develop a multispecies kinetic growth model specifically for the petrochemical process environment. The instruments used throughout the study are presented with a detailed methodology. Section 3.3 discusses the method chosen to evaluate differences in bacterial colonisation on rough and smooth-finished surfaces. Section 3.5 provides the corrosion methodology selected for the cooling water system because of bacterial attachment and metabolic activity.

CHAPTER 4 This chapter presents a newly developed kinetic model and metabolic growth curve for multispecies bacteria. Section 4.2 introduces the growth curve. Section 4.3 presents the kinetic growth model. Section 4.4 presents the colony-forming units, indicating that bacterial growth is still observed beyond 13 days. Section 4.5 presents the TOC and HPLC results, which provide more information on bacterial growth. Section 4.6 provides the method for developing a kinetic growth model for a multispecies batch system using AQUASIM. The chapter then concludes all sections.

CHAPTER 5 This study evaluated differences in bacterial colonisation on rough and smooth-finished surfaces. The bacteria cultivated for attachment studies are from the same cooling water system mentioned in Chapter 4. Chapter 5 comprises three sections. The chapter

introduces the reactor set-up on day 1 and provides the microscopy results with a discussion on spatial patterns. Section 5.2 provides the statistical results of bacterial colonisation because of surface roughness. Section 5.3 presents the surface roughness parameters obtained before and after bacterial exposure. Section 5.4 presents the microscopy images using SEM and AFM. The chapter then concludes on surface roughness and colonisation.

CHAPTER 6 This study evaluated corrosion because of bacterial attachment and metabolic activity. Section 6.2 comprises elemental mapping and spectra of alloy A after bacterial exposure. Section 6.3 covers the corrosion rates obtained for alloys A rough and smooth-finished surfaces to recommend the best candidate steel finish. Section 6.4 presents the Raman spectroscopy results of alloy A, which could provide more insight into the corrosion rates obtained. Last, Section 6.5 includes a detailed discussion of the results obtained from Fourier Transform Infrared spectroscopy (FTIR) on alloy A to evaluate the functional groups involved in the corrosion process.

CHAPTER 7 This chapter reveals the recommendations and key findings from the study.

CHAPTER 8 In this chapter the future work to be conducted is presented.

CHAPTER 2 LITERATURE REVIEW

2.1 INTRODUCTION

The literature review focuses on a broad discussion of bacterial attachment to a surface, then narrows down to the influences of surface roughness on colonising bacteria (Figure 2.1). Presented first are basic concepts introducing the typical arrangement of a cooling tower network in a petrochemical industry. The fundamental understanding of biofilm formation is introduced and is the most important factor in this multispecies study. The sections then interlink into the life cycle of bacterial biofilm with a discussion on how complex structures are formed and their emergent properties.

The properties of biofilm communities comprise novel structures, activities, patterns, properties, and self-organisation in complex systems. A fundamental understanding of the factors controlling cell attachment is further presented. The literature provides insight into preventing biofilm formation and emphasises inconsistencies, including irregular and patterned surfaces. Two theories explain bacterial attachment to surfaces; however, these theories do not consider multispecies systems.

Reports on attachment studies are discussed, showcasing the range of fields this topic transcends. Equipment used to analyse bacterial attachment is presented. Surface roughness characterisation is lastly discussed. This study aimed to broaden the understanding of multispecies bacterial attachment while providing an apparent relationship between cell attachment and substrate roughness.

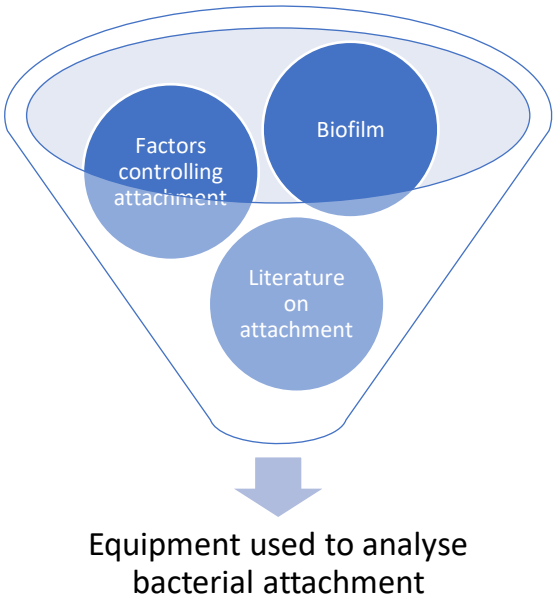

Figure 2.1: Summary of the literature review

2.2 TYPICAL COOLING WATER NETWORK INVOLVING HEAT EXCHANGERS

The cooling water network comprises a cooling tower where water is pumped from a Dam (Figure 2.2). The water is then transported to various sections of the plant that require process cooling, such as gases (polypropylene gas) or liquids (lube oil). The heat exchanger type used in these systems are shell and tube by design, and carbon steel tube materials are used (Prithiraj *et al.,* 2019). Cooling water flows on the tube side and processes fluid on the shell side. It was reported that biofilms forming on metallic surfaces owing to bacterial attachment and were also reported (Zhao *et al.,* 2007, Prithiraj *et al.,* 2019, Tran *et al*., 2021 and Queirroz *et al*., 2018), causing loss of efficiency and downtime. In the referenced studies it was observed that the steel experienced high corrosion and corrosion resistance at specific exposure times.

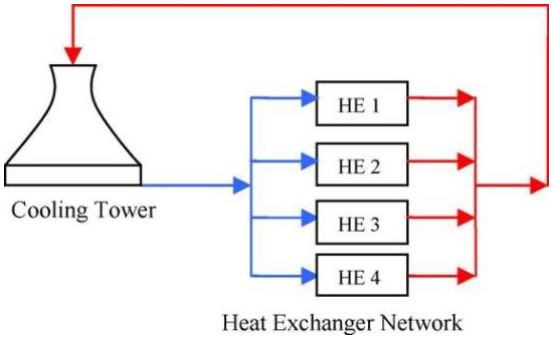

Figure 2.2: Typical cooling water network set-up with heat exchangers (Panjeshahi *et al.*, 2009)

2.3 WHAT IS BIOFILM, AND HOW DOES IT FORM?

Costerton *et al*. (1999) define a biofilm as "a structured community of bacterial cells enclosed in a self-produced polymeric matrix and adherent to an inert or living surface." Elder *et al.* (1995) described a biofilm as "a functional consortium of microorganisms organised within an extensive exopolymer matrix," whereas Carpentier and Cerf (1993) simplified the concept as "a community of microbes embedded in an organic polymer matrix, adhering to a surface." Considering these definitions, it is observed that a biofilm encompasses microbes, glycocalyx, and a surface. If one component is not included, a biofilm does not develop. The colonisation of bacteria would occur on any surface, including an animal, mineral, or vegetable. It is possible that biofilm forms on surfaces, such as contact lenses, ship hulls, dairy, and petroleum pipelines, rocks in streams, and all varieties of biomedical implants and transcutaneous devices (Carpentier & Cerf, 1993) (Costerton *et al.,* 1987), (Costerton *et al.,* 1995), (Costerton *et al*.,1999), and (Elder *et al.,* 1995).

The surface may also be a nutrient source, such as cellulose, in the paper industry (Costerton *et al.,* 1995). Some surface coatings resisting bacterial attachment are described (Sheng *et al.,* 2000). No bacterial species was observed in a planktonic state under all growth conditions (Carpentier & Cerf, 1993). Bacterial exopolysaccharides are the main component of the biofilm glycocalyx, and in earlier times was also identified as the slime layer (Costerton *et al*.,1985). The glycocalyx is primarily water when it is hydrated (Costerton *et al.,* 1985). In most species, the glycocalyx is used to trap minerals and nutrients from the environment while protecting the bacteria attached to the surface (Carpentier & Cerf, 1993, Costerton *et al.,* 1987, Carpentier & Cerf, 1993, Costerton *et al.,* 1987, Costerton *et al.,* 1995, Costerton & Lappin-Scott, 1995 and Flemming & Wingender, 2010).

When a biofilm comprises a diverse number of species (observed in nature and not by single species), the metabolic by-products of one organism may support the growth of another. In contrast, the attachment of one species might provide ligands allowing others' attachment (Costerton *et al.,* 1987, Leung *et al.,* 1998, Wimpenny, 2000). The competition for nutrients and accumulation of waste generated by initial colonisers could limit the species diversity within a biofilm (Wimpenny, 2000).

2.4 FORMATION STEPS OF BIOFILM

Initial attachment, microcolony formation, maturation, and dispersion form the biofilm process (Figure 2.3). The first step is the process where bacteria become close to the metal surface. This is caused by physical factors and chemical forces (Bispo *et al*., 2015). The bacterial cell appendages strengthen the attachment to the metal surface (Jamal *et al.,* 2018), pH and temperature can also influence bacterial attachment. The hydrophobicity of the material surface also reduces specific repulsion forces between the bacteria and the material (Bispo *et al.,* 2015). Di Ciccio *et al.* (2015) eluded that the bacteria are more inclined to attach to hydrophobic surfaces (polystyrene) than hydrophilic surfaces (stainless steel) (Di Ciccio *et al.,* 2015). Bacterial attachment is reversible, and biofilm growth could be prevented.

Bacteria multiplication and division follow the attachment stage. This leads to the EPS originating as a layer that protects the bacteria. This is also called irreversible attachment (Santos *et al.,* 2018, Hoffman *et al.,* 2015). The complex structure of various microcolonies that form on the surface is resistant to harsh environments. The interactions among microcolonies affect the metabolic products (Katsikogianni & Missirlis, 2004). In this stage, specific molecules, called autoinducers, are used as signalling molecules to communicate from cell-to-cell (Waters & Bassler, 2005). The autoinducers use a communication mechanism called quorum sensing, allowing adaptation of the EPS. Protecting the complex EPS architecture allows the bacteria to grow into a bulb-like structure (Kolter & Greenberg 2006).

The three-dimensional structures of EPS (formed among colonies) comprise channels providing nutrients which allow the bacteria to grow and survive (Persat *et al.,* 2015). In the last stage, an oversaturation of microbial cells is observed. Bacteria would disperse from the biofilm into the liquid phase once the EPS temporarily removes the protective layer at the top of the bulb-like structure. The sessile cells are then converted into motile forms, causing dispersion of the bacterial cells.

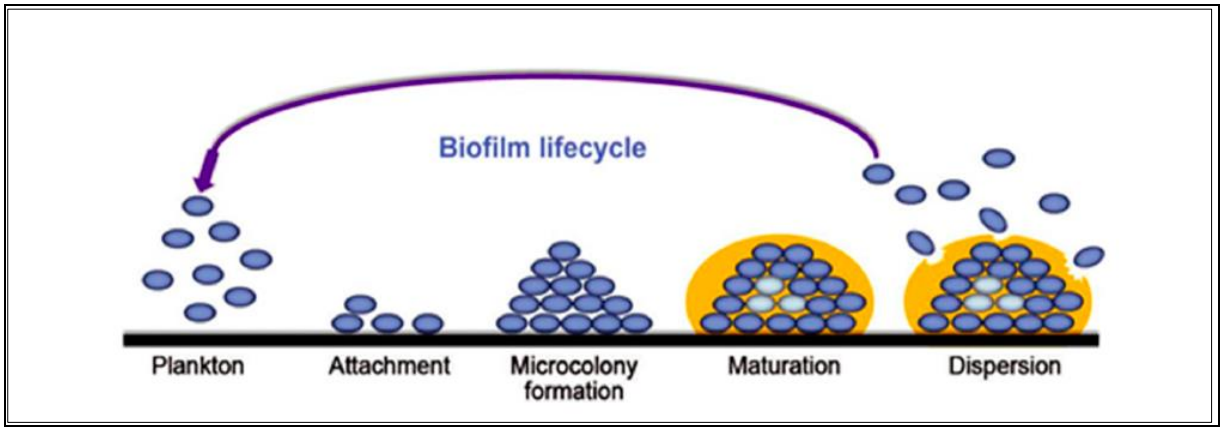

Figure 2.3: The formation steps of biofilm (Dos Santos *et al.,* 2018)

A complex biofilm structure is only formed when there is a consortium of bacteria present on a surface. This study evaluated the life cycle of the bacteria (Figure 2.3) and the new structures formed on the surface.

2.5 BIOFILM AS AN EMERGENT FORM OF BACTERIAL LIFE

Now that the fundamental understanding of biofilms has been discussed. The focus is drawn to bacterial communities and how the characteristic features of biofilms present the functional properties of the matrix, such as social cooperation, resource capture, and survival. Communities within an EPS matrix form bacterial biofilms. The bacteria in the biofilm have emergent properties, differing from free-living bacterial cells. Biofilms are groups of microorganisms where cells are frequently embedded in an EPS matrix attached and a surface (Vert *et al.,* 2012). The bacterial cells in layered biofilms experience cell-to-cell contact. This can be on biofilms attached to the surface, where one layer is in direct contact with the substratum, or mobile biofilms formed in the absence of any substratum. Through intercellular interactions—social and physical—with the properties of the matrix, the biofilm state is distinct from that of free-living bacterial cells.

Biofilm communities have new non-predictable properties from studying free-living bacterial cells (Konopka, 2009). Biofilms are complex systems with high cell densities, ranging from 10^8 to 10^{11} cells g^{-1} wet weight (Balzer *et al.,* 2010). The emergent properties of biofilm communities comprise novel structures, activities, patterns, and properties arising during the process which may lead to biogenic habitat formation (Corning, 2002). Physical and social

interactions (such as synergistic microconsortia) exist with emergent properties. Formation of the matrix is a dynamic process and depends on nutrient availability. The synthesis and secretion of extracellular material, shear stress, social competition, and nutrient in-take by other organisms generate an ecological perspective. This proves dissimilar when comparing single and multispecies biofilms; a need exists to study biofilms in diverse environments other than laboratories.

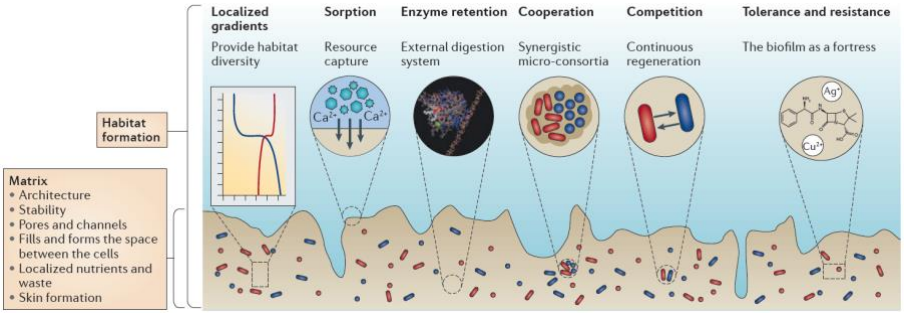

Figure 2.4: Bacterial cells in biofilms can be considered habitat formers, and the matrix forms the foundation of the biofilm (Flemming *et al.,* 2016)

Figure 2.4 depicts the biofilm, which comprises EPS providing stability to the biofilm. Nutrients and other molecules are trapped by sorption to EPS molecules though the channels. Skin formation by hydrophobic EPS molecules enhances the ability of the biofilm to survive drying. Biofilms derive several emergent properties, which include diversity, nutrient supply, enzyme control, social interactions, and the ability to resist harsh environmental conditions (Flemming *et al.,* 2016). The diverse organisms living in the matrix interact according to the organisation of the biofilms. This enables the exchange of metabolites, signalling molecules, genetic material, and defensive compounds, organising interactions among organisms. Heterogenous bacterial cells with diverse metabolic capacities or physiochemical gradients provide an opportunity for cooperation (Flemming *et al.,* 2016).

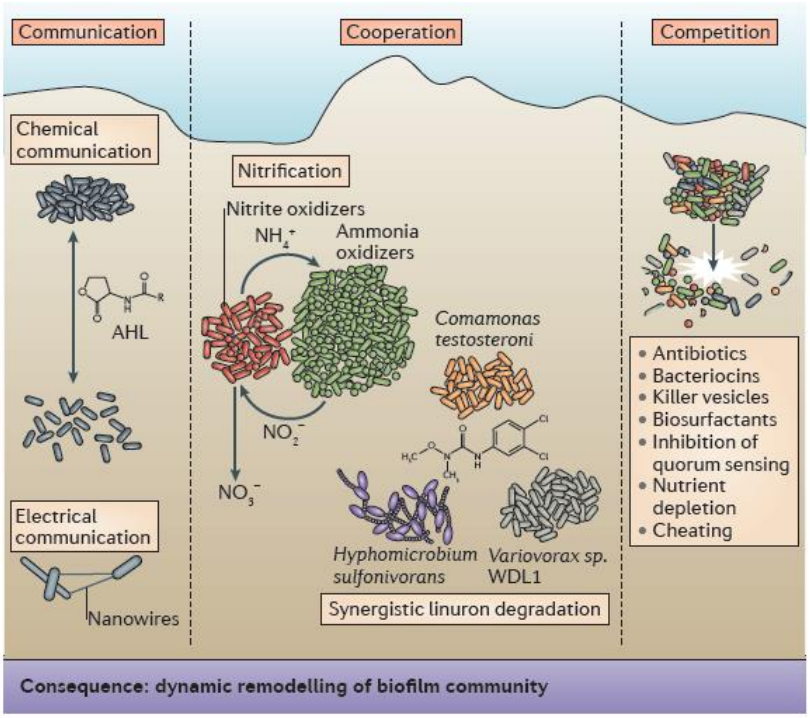

Figure 2.5: Social interactions in the matrix (Flemming *et al.,* 2016)

The interactions among the bacterial cells (Figure 2.5) within the biofilm can affect the entire biofilm community. Cooperation can be facilitated by chemical or electrical communication, and it can involve cooperative metabolism. With the nitrification process, ammonia-oxidising bacteria produce nitrite, further oxidised by nitrite-oxidising bacteria. These interactions rely on the proximity of cells that exchange metabolites to enable efficient exchange by diffusion. Negative interactions, such as competition or cheating, have also been observed in biofilms.

Competition or cheating among cells in biofilms can involve killing mechanisms or strategies that compromise growth, such as nutrient depletion or quorum sensing inhibition (Flemming *et al.,* 2016). It was discussed that a consortium of bacteria, other than the free-living bacteria, have emerging properties. From this understanding, biofilm structures and interactions of the bacterial species established in this petrochemical system are unknown. Competition and growth of bacteria in conditions with no carbon sources would prove interesting.

2.6 FACTORS THAT CONTROL CELL ATTACHMENT

There is significant socioeconomic interest globally in the attachment and colonisation of surfaces by bacteria (Costerton *et al*., 1987, Costerton *et al*., 1995, Davey & O'Toole, 2000, De Nys & Steinberg, 2000, Hall-Stoodley *et al*., 2004 and Costerton *et al*., 2007). Bacterial

contamination and biofilm growth influence several aspects of society, ranging from bio-induced corrosion of industrial piping and other materials to profound health implications in infected individuals (Costerton *et al.,* 1987, Scardino & de Nys 2011). Biofilms are persistent and may be prevented by inhibiting the initial colonisation step of the biofilm life cycle (Figure 2.6) (Costerton *et al.,* 1987, Costerton *et al.,* 1995, Davey, & Toole, 2000, Hall-Stoodley *et al.,* 2004 and Xavier, Picioreanu, & van Loosdrecht, 2005). The fundamental factors controlling cell attachment are presented below.

Several factors control the attachment of bacterial cells to a substratum surface. The physical chemistry properties of the surface and the environmental conditions under which the attachment occurs (An & Friedman, 1997). The interest was towards determining surface topography's role in the attachment process (Bazaka *et al*., 2012). Two samples with the same surface chemistry may present diverse attachment profiles owing to differences in surface architecture and roughness (Russell *et al.,* 2012).

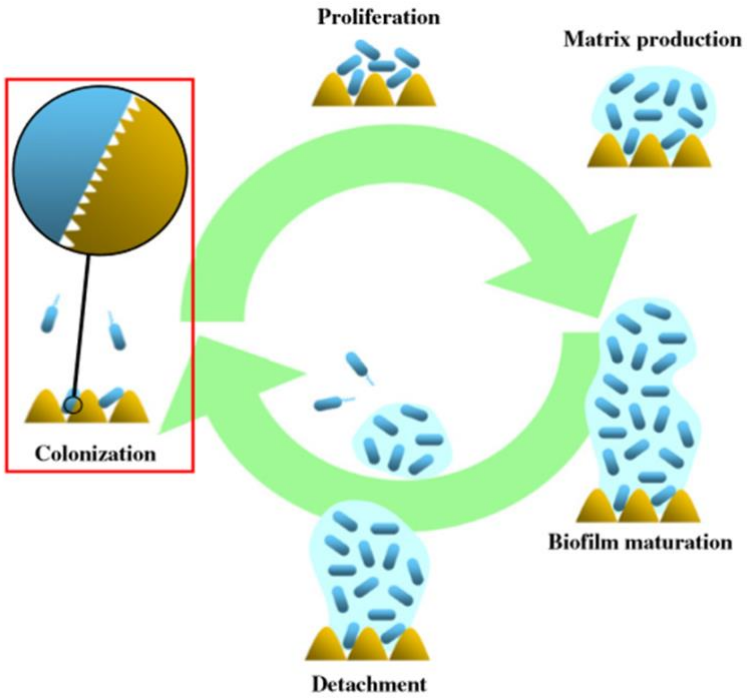

Figure 2.6: Biofilm formation and its life cycle on a hierarchically rough substrate (Russell *et al.*, 2012, Bazaka *et al.*, 2012)

The interactions between bacterial cells and various material surfaces, such as lass, silica, metals, and polymers, are reported (Chew & Lange, 2009, Salta *et al*., 2010, Callow & Callow,

2011, Lui, 2008, Russell *et al.,* 2012 and Shi *et al.,* 2009). Much of the research alluded to the elimination of the initial attachment of bacterial cells on the surfaces using several approaches, including chemical modification/functionalisation of surfaces, development of self-assembled monolayers and manipulating the surface topography (Lui, 2008, Ivanova *et al.,* 2011, Chua *et al.,* 2008 and Ivanova *et al.,* 2011).

Conflicting results are reported in describing the influence of surface roughness on the extent of bacterial attachment (Bazaka *et al.,* 2011, Anselme *et al.,* 2010, Truong *et al.,* 2010, Taylor *et al.,* 1998 and Bazaka *et al.*, 2011). It was postulated that the conflicts have arisen because distinct types of surface patterning often complicate the investigation of cell-substratum interactions. Surface topographies can be grouped into three general patterns:(i) irregular 'random' surface topographies, (ii) regularly patterned surfaces and (iii) hierarchical surface structures.

2.7 IRREGULAR/RANDOM SURFACE TOPOGRAPHIES

Table 2.1 presents the works conducted on irregular or random surface topographies, and there are no apparent conclusions to these studies.

Table 2.1: Irregular random surface topographies

Work conducted on irregular random surface topographies	**References**
In these investigations, there was no clarity on the influence of surface features on single-species bacterial attachment. In one study, there was no statistical significance on bacterial attachment to the surface. In the other study coating a titanium surface did not affect bacterial attachment.	Parham *et al.* (1989) and Harris & Richards (2004)
Single-species studies using mathematical evaluation of an irregular surface (R_a 1.25-0.43 µm) to understand how topographical dimensions exert and influence attachment were studied; however, no apparent relationship between roughness parameters and colonisation of bacterial cells was determined.	Bazaka *et al*. (2011), Medilanski *et al*. (2002), Mitik-Dineva *et al*. (2009), Whitehead *et al*. (2006), Boulangé-Petermann *et al*., (1997)

Work conducted on irregular random surface topographies	**References**
Four species were studied on topographies with sub-micron features and reported minimum bacterial attachment was observed on stainless steel surfaces with an average roughness of 0.16 µm measured over 50 × 50 µm scan areas. In contrast, smoother or rougher surfaces exhibited greater degrees of bacterial attachment. Only average roughness parameters were reported.	Medilanski *et al*. (2002)
Biofilm volume on a surface compared to roughness parameters was evaluated. The number of bacteria attached to the surface compared to roughness parameters was observed to have an inverse correlation. The two bacterial species studied (with various physiology rods and sphere-shaped) indicated preferential attachment to the differently modified surfaces.	Truong *et al*. (2009), Truong *et al*. (2010)
On surface nano topography studies. The attachment levels of the three bacterial strains in these studies appeared to be inversely correlated with surface roughness, and bacteria attached more to the nano-smooth surfaces (1.3 nm).	Mitik-Dineva *et al*. (2009) and Mitik-Dineva *et al*. (2009)
Studies using smooth nano topographies play in bacterial attachment. Cell attachment and EPS production for two strains was enhanced for thin titanium film substrata with lower average roughness, whereas on polished bulk titanium surfaces, decreasing roughness was established to enhance the adhesive behaviour of only *Pseudomonas aeruginosa,* whereas *S. aureus* exhibited a decreased propensity for adhesion. Conversely, smooth titanium films on silicone containing an average roughness below 0.5 nm enhanced the adhesive behaviour and EPS production of *S. aureus* but not for *P. aeruginosa* cells. Some suggested that the differences in the attachment profiles of these two bacteria in smooth films resulted from variations in cell deformability arising from their morphologies.	Ivanova *et al*. (2010), Truong *et al*. (2010) and Ivanova *et al*. (2011)

Most work involves studies on limited bacterial strains. A need exists to report on colonisation rates of multispecies bacterial cells. The inconsistent results arise not only from the surface finish/modifications but also considering the ecological perspective with the preferential attachment of the bacterial cells.

2.8 PATTERNED SURFACES

Bacterial attachment to irregular surface topographies was studied using a wide range of surfaces; however, the bacterial attachment behaviour on regularly patterned microscale and nanoscale topographies has not been a topic of interest. Several microscale patterns, including etched grooves, pits, squared-features, and shark-skin-inspired surfaces, were fabricated to develop anti-biofouling surfaces, and directing bacterial attachment (Chung *et al.,* 2007, Rozhok *et al.,* 2006). Rowan *et al*. (2002) fabricated flat surfaces with evenly distributed square corrals, 10 µm across, which trapped *E. coli* cells (Rowan *et al.,* 2002). Similarly, Rozhok *et al*. (2006) fabricated surfaces containing 3 µm holes with a depth of 0.5 µm, which also localised single cells of *E. coli* (Rozhok *et al.,* 2006)

Both studies did not contribute to the fundamental understanding of the topographical factors in controlling cell attachment, as they used surface chemistry to aid bacterial attachment (Rowan *et al*., 2002). More comprehensive testing of a single surface pattern was conducted, where regularly spaced arrays of square protrusions with controlled dimensions fabricated on polydimethylsiloxane (PDMS) surfaces were tested to control *E. coli* cell attachment and biofilm formation (Hou *et al.,* 2011). It was established that *E. coli* cells preferentially attached to and formed biofilms in the valleys among the square- shapes, indicating that surface patterns may promote bacterial attachment and biofilm formation (Hou *et al.,* 2011). The study did not include controlling cell attachment by surface topography.

There is insufficient information on roughness characterisation in most studies involving microscale-patterned surfaces; however, it was demonstrated that grooved, pitted surfaces and edged pits protect cells from external forces (Scheuerman *et al*., 1998, Whitehead *et al.,* 2005). An investigation of the attachment behaviour of *S. aureus* and *P. aeruginosa* on surfaces with 0.2-2 µm diameter pits indicated that larger diameter pits offered sheltered cells. On the nanoscale, several attempts were made to simplify the surface patterning and bacterial attachment responses on various surfaces (Bazaka *et al.,* 2011, Díaz *et al.,* 2010, Hochbaum & Aizenberg, 2010).

Periodic nanoscale arrays of high aspect ratio polymer pots were reported to direct the attachment behaviour of *P. aeruginosa*, *Bacillus subtilis,* and *E. coli* cells (Hochbaum & Aizenberg, 2010). The pots were produced with a diameter of 300 nm and height of 2 µm, where bacteria took on definite patterns. On quasi-random surface architectures, bacterial cells oriented themselves with the naturally existing patterns. For example, engineered and randomly nanostructured gold substrata established that *P. fluorescens* cells formed along the nanogrooves (Díaz *et al.,* 2007).

It is still observed that even on irregular and pattered surfaces, conflicting data arise. Mitik-Dineva *et al*. (2010) indicate that bacteria attached more to the nano smoother glass surface. Different diameters (20, 40, 60 and 80 µm) of titanium nanotubes created by anodising were revealed to affect the extent of attachment of *S. epidermidis* and *S. aureus* cells. The results indicated that the number of live cells was reduced in all nanotubular structures except 20 µm for *S. epidermidis* or at 60 nm and 80 nm for *S. aureus* (Ercan *et al.,* 2011).

2.9 HIERARCHICAL SURFACE STRUCTURES

Most hierarchical surface patterns studied were inspired by nature (Salta *et al*., 2010, Babu *et al*., 2010 and Bliznakov *et al*., 2009). There is insufficient data in the literature relating to bacterial attachment on these natural surfaces. Hierarchical surfaces are frequently superhydrophobic and include a self-cleaning ability. Investigations into cell attachment on superhydrophobic, hierarchical surfaces were studied to evaluate colonisation on the surfaces (Crick *et al.,* 2011, Ma *et al.,* 2011). The air trapped among the dual-scale surface features present on such surfaces limits the available contact area for the bacteria (Ma *et al.,* 2011).

Ma *et al*. (2011) studied bacteria attachment on the natural hierarchical surface of taro leaves, confirming that the structures on the surface are resistant to bacterial colonisation (Ma *et al.,* 2011). An investigation of the bacterial attachment on artificial superhydrophobic elastomeric silicone surfaces indicated a decrease in bacterial attachment (Crick *et al.,* 2011). Fadeeva *et al*. (2011) evaluated the bacterial attachment on titanium samples modified to mimic the dual-scale features of the lotus leaf (Nelumbo nucifera). The results indicated that *Staphylococcus sp.* cells dominated the attachment of the surface, whereas *Pseudomonas sp.* could not attach (Figure 2.7).

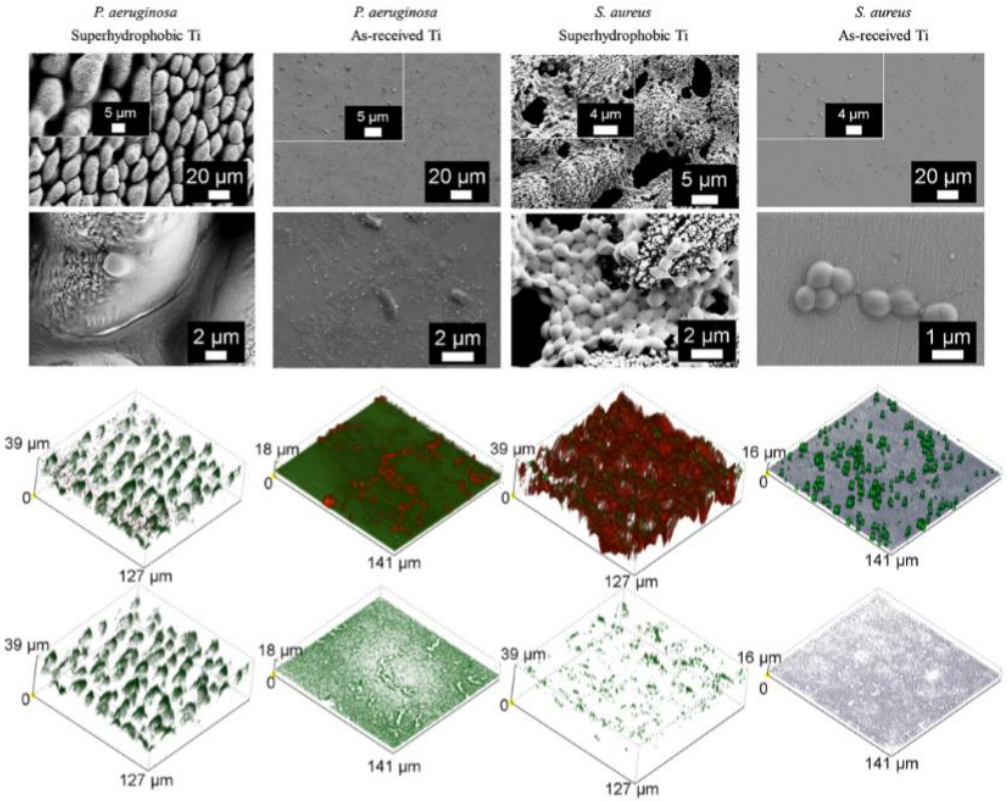

Figure 2.7: Cell attachment profiles of Pseudomonas sp. and Staphylococcus sp. aureus on lotus-like and polished titanium surfaces. Reprinted (adapted) with permission from {Fadeeva *et al.,* 2011}. Copyright {2011} American Society.

Despite studies conducted to reduce bacterial attachment on patterned and hierarchical surfaces, each environment selected a strain of bacteria or a few strains to be studied. Hierarchical patterns may reduce bacterial attachment when evaluating a single species; however, multispecies attachment could provide more insights. The preferential attachment of multispecies bacteria to nanopatterned smoother surfaces should be researched further.

2.10 SUMMARY OF STUDIES ON NANOSCALE SURFACE ROUGHNESS

The Table 2.2 presents the nanoscale surface properties of a material as a determinant in cell attachment.

Table 2.2: Surface properties of a material as a determinant in cell-surface interactions

Author	Study conducted
Scardino *et al.* (2009)	This study integrated hydrophobic materials with micro and nanoscale architectures to investigate fouling resistance. The results indicated that the nano roughness of the surfaces reduced the settlement of cells, whereas the surfaces possessing nano and micro scale architectures indicated selective attachment.
Fadeeva *et al*. (2011)	Created a lotus leaf-like morphology on a titanium surface. These superhydrophobic surfaces were reported to be highly effective in preventing *Pseudomonas aeruginosa* colonisation, although they could not prevent attachment and colonisation by the *Staphylococcus aureus* cells.

In the aforementioned studies, the rougher nano-modified surface would be suitable for preventing bacterial attachment, and studies are targeted in various areas of interest. These contrasts patterned surface studies as bacteria attached more to the smoother nano-modified surfaces.

2.11 THEORIES EXPLAINING HOW BACTERIA ATTACH TO A SURFACE

Two accepted theories on the attachment of bacteria to solid surfaces exist. The first of these theories includes two steps (Kumar & Anand, 1998). The first step involves the bacteria moving close to a surface where initial attachment occurs, with the forces involved with initial attachment are the van de Waals forces, electrostatic forces, and hydrophobic interactions (Carpentier & Cerf, 1993; Gilbert *et al.,* 1991). During this initial contact of bacteria to a surface, there is Brownian motion, and cells can be easily removed by fluid shear forces, such as through rinsing (Kumar & Anand, 1998).

In the attachment process, there is an irreversible attachment of cells to the surface, described by Dunne (2002) as bacteria locked onto the surfaces by producing exopolysaccharides and or specific ligands, such as pili or fimbriae. At the end of this stage, much stronger physical or chemical forces must remove the bacteria from the surface, such as scraping, scrubbing, or chemical cleaners. In the transition from reversible attachment to irreversible attachment,

various short-range forces are involved. This includes covalent hydrogen bonding and hydrophobic interactions (Kumar & Anand, 1998). Poortinga *et al*. (2002) expanded on covalent bonding in bacterial attachment and suggested that the bacteria either donated electrons to or accepted electrons from the substratum.

2.12 DERJAGUIN, LANDAU, VERWEY, AND OVERBEEK THEORY

The DLVO (Derjaguin, Landau, Verwey, & Overbeek) Theory of colloid stability was used by several groups to explain the attachment of microorganisms to surfaces (Hermansson, 1999, Rijnaarts *et al.,* 1995). According to the theory of cell attachment, there are repulsive or attractive forces with the charge of the two surfaces interacting. Rijnaarts *et al*. (1995) identified repulsive forces among positively charged inert surfaces. Negatively charged bacterial surfaces at neutral pH are owing to carboxyl, phosphate, and amino groups (Poortinga *et al.,* 2002) and ionic concentration (Van der Wal *et al.,* 1997) of the suspended medium. Rijnaarts *et al*. (1995:5, 1999) described as a low ionic strength of a solution dominates bacterial attachment, but at high ionic strength (>0.1 M), other factors, such as hydrophobicity, dominated. Many have now realised that the DLVO theory does not consider that the bacterial cell surface is a highly dynamic surface that responds to changes in ionic strength, pH, macromolecules, and other surfaces and is not merely a colloid particle (Poortinga *et al.,* 2002).

Environmental changes may influence changes to the surface structures, such as bacterial appendages, which may play a significant role in attachment. Work presented by Pembrey *et al*. (1999) and Castellanos *et al*., (1997) suggest that the bacterial cell surface is not just an inert, rigid structural component of the cell and is delicate; therefore, incorrect centrifuge speeds could damage the cells. Dan (2003) suggested that the DLVO approach to bacterial attachment treats bacterial cells as traditional colloidal particles. This was characterised by having an even surface and an evenly distributed surface charge; however, the bacterial cell appendages and complicated cell structures may exert their own localised cell charge (Tjalsma *et al.,* 2000).

This could mediate attachment through an attractive charge rather than repulsion. Various regions on the cell surface display various surface charges, even though the cell charge may be harmful (Jones *et al.,* 1996). Bacteria attach to the surface firmly and must rinse loosely attached bacterial cells on the surfaces before analysis. This provides information about

cleaning the surface well to obtain accurate corrosion rate results. The theory still lacks investigation into multispecies systems, as specified in the background section of this thesis.

2.13 SUMMARY OF BACTERIAL ATTACHMENT STUDIES ON ROUGH AND SMOOTH SURFACES

Tang *et al.* (2021) studied using biomaterials in implanted blood-contacting medical devices owing to microbial infection. He describes that the infection started from bacterial attachment and biofilm formation on the surface of biomaterials. In this research, new fluorinated alkoxyphosphazenes material was developed. Experiments were conducted using three bacterial strains, *Staphylococcal epidermidis*, *Staphylococcal aureus*, and *Pseudomonas aeruginosa,* and results indicated that bacterial attachment coefficients were significantly lower on poly [bis (octafluoropentoxy) phosphazene] (OFP) and cross-linkable OFP (X–OFP) smooth surfaces than on the polyurethane biomaterial. Surface texturing further reduced bacterial attachment owing to the reduced accessible surface contact area. In this study, single strains of bacteria were evaluated on surfaces.

Park *et al.* (2019) investigated the in vitro microbial changes in biofilms on composite resins of varying roughness (SR180 1.45 to 0.11 µm, SR400 0.62 to 0.05 µm and SR1500 0.35 to 0.02 µm grit and glass 0.15 to 0.1 µm) by using a multispecies biofilm model. Results display that increased roughness was not proportional to bacterial attachment. Gram-negative oral bacteria were used in this study. Decreased attachment of *S. mutans* and *S. sobrinus* and total bacteria was observed on glass.

Dezelic & Schmidlin (2009) studied the multispecies bacterial influence of surface roughness and contact time on forming a multispecies biofilm on dental materials. The statistical results present no difference in the biofilm formation rate among all the materials tested.

Medilanski *et al*. (2002) focused on four bacterial species comprising three phyla (*Desulfovibrio desulfuricans subsp. desulfuricans*, *Pseudomonas aeruginosa, and Pseudomonas putida*) in a batch set-up. The physiochemical characteristics of the cells were influenced by the surface topography of AISA 304 stainless steel. Stainless steel surface finishes used were P80 (0.89 µm), P500 (0.25 µm), P1000 (0.16 µm), diamond-polished (0.05 µm) and electropolished (0.3 µm). Results indicated that the attachment of all four bacteria was reduced at Ra = 0.16 µm (roughness), whereas smoother and rougher surfaces provided rise to more attachment.

Taylor *et al*. (1998) studied the effect of surface roughness on the attachment of *Pseudomonas aeruginosa* and *Staphylococcus epiderm*idis using Polymethyl methacrylate. Results indicated a decrease in bacterial attachment to the rougher surface compared to a smooth surface.

Boulangé-Petermann *et al*. (1997) studied the attachment of *Streptococcus thermophilus B* to industrial-finished AISI 304 stainless steel plates regarding surface topography, roughness, and surface hydrophobicity. The bacteria were isolated from heat exchanger plates in the downstream section of the regenerator of a pasteuriser. The bacterial attachment to stainless steel surfaces did not vary significantly, and no apparent relationship existed between roughness parameters and the number of attached bacteria.

Mueller *et al*. (1992) evaluated bacterial colonisation on solid-water interfaces. This was measured using a flow system equipped with real-time image analysis. Four substrates (copper, silicon, 316 stainless steels, and glass) and two bacterial species (*Pseudomonas aeruginosa* and *Pseudomonas fluorescens*) were used in the experiments. Results indicated an increase in the adsorption of cells with increased roughness for all substrates.

There are reports across various fields of study to reduce bacterial attachment to a surface, presenting inconsistent results. Most authors investigated bacterial attachment with only a selection of bacterial strains not knowing which bacteria within a community would selectively attach to a given substratum. It is known that the bacteria should colonise/attach either to a rough or smooth surface, however, it is rarely proven with a multispecies system. The literature lacks reports on surface modifications and bacterial attachment contributing to corrosion in the industry. Dezelic & Schmidlin (2009) and Park *et al*. (2019) studied multispecies biofilms with contrasting results. The authors used various methods to evaluate bacterial colonisation to a surface. This indicated that the methods used to quantify bacterial attachment must be consistent.

2.14 USING AFM AND SEM ON MODIFIED BACTERIAL SURFACES

Methods to quantify bacterial cells and surface roughness on a surface can be a challenge; however, there are disadvantages associated with certain methods, presented below. Scanning electron microscopy (SEM) can provide three-dimensional imagery of surface structures at multiple resolutions. The disadvantage is that the high-vacuum conditions and non-conductive biological sample forces use physical coating methods of the sample. Procedures are then carefully implemented, which do not destroy complex structures or cause

artefacts on the surface (Bergmans *et al.,* 2005). Samples are fixed with various components and dried using acetone or ethanol. In this way, the water is gradually replaced by organic solvents. This can be a disadvantage when visualising the samples under Raman spectroscopy. It proved challenging to physically dry the sample without destroying the complex structures.

Critical point drying is one method which does not form artefacts. Usually, ethanol is replaced by a fluid containing carbon dioxide. Biological samples are also known to be freeze-dried. Last, samples are well-known to be coated with gold as this is a conductive material (Bergmans *et al.,* 2005, Vitkov *et al.,* 2005). It may be challenging to evaluate bacteria various bacterial species with intricate cocci, rods and filaments using SEM. However, SEM is a suitable device for investigating conditioning films or proteinaceous layers, such as the acquired dental pellicle (Hannig *et al.,* 2007).

Atomic force microscopy (AFM) can reach a high resolution of less than 1 nm, and vacuum conditions are not required, a suitable device for nano microbiology studies as reviewed by Dufrêne (2008). Membrane components and living cells can be evaluated directly in buffer or on solid substrates (Dufrêne, 2008) and real-time monitoring of structural changes (Dufrêne, 2008). Modern microscopic techniques, such as AFM, offer the opportunity to obtain new insights into microorganisms and their extracellular matrix (Dufrene, 2008). Table 2.3 provides a list of methods used to visualise and quantify bacterial attachment on a surface, the advantages and limitations of each method is presented.

Table 2.3: Methods for visualisation and quantification of the attachment of microorganisms regarding their main advantages and limitations (Hannig *et al.*, 2010)

Method	Advantage	Disadvantage
4', 6 – Diamidino-2-phenylindole	A simple method to observe attached microorganisms	This method cannot identify bacterial species and cannot identify live/dead cells
Live/dead staining	It can be a reliable way to evaluate antimicrobial agents and observe viable bacteria	There are questions about the dead cells, and the method cannot identify the species
Fluorescence in *situ* hybridisation	With this method, one can identify strains of bacteria	The bacterial membranes which must be intact can only be stained, and the number of specialised probes is limited
Scanning electron microscope	Good quality evaluation of bacteria on surfaces	Qualitative method and impossible with multispecies studies
Environmental scanning electron microscopy	Bacteria can be observed in their original state with no physical coating methods	Primarily qualitative and cannot determine bacterial species
Transmission electron microscopy	Good insight into the bacterial cell structure and the biofilm layer	Qualitative with physical coating methods
Atomic force microscopy	Evaluation of bacterial cells, biofilm structure, membrane components, and cell-cell interactions with no physical coating	Time-consuming on multispecies surfaces
Culture plate method	The standard for quantification, identification, and cultivation of bacteria	Only 50% of oral bacteria are culturable. Desorption of adherent bacteria is necessary. Specialised experience in identifying bacterial species

Park *et al.* (2019) and Rudney *et al*. (2012) used a conserved sequence in the 16S rRNA gene with qPCR to quantify bacterial levels. These studies did not use AFM to quantify surface roughness.

Dezelic & Schmidlin (2009) studied the multispecies bacterial influence of surface roughness and contact time on forming a multispecies biofilm on dental materials. Surface roughness was determined using a profilometer. Samples were sputter coated with gold and observed under SEM at magnifications 200 x and 1000 x to evaluate bacterial colonisation.

Duarte *et al*. (2009) evaluated the R_a (average roughness) from AFM and averaged scanned areas for each disc. Samples were fixated. The samples were further dehydrated and coated with gold before evaluating under the SEM. At magnification x 10000. Bacteria colonised on rough surfaces rather than the smooth one.

Beech *et al*. (2002) studied biofilms formed in various environments on the field, in laboratory conditions or on natural or modified surfaces studied in various stages of development using a diverse microscope technique. The methods were qualitative and, except for SEM, would not present more information on how the biofilm influences the substratum.

Medilanski *et al*. (2002) quantified attached bacteria using the epifluorescence microscope counting by staining. The attached cells were counted manually by examining 10 fields of vision selected randomly from the centre of the samples. The study used AFM to quantify surface roughness.

Fang *et al*. (2000) used AFM to obtain high-resolution bacteria images and quantify tip-cell interaction forces and surface elasticity. Air drying samples had more stable reproducible force measurement results. The study only observed sulphate-reducing bacteria.

Arnold & Bailey (2000) investigated the kinetics of bacterial growth during surface exposure using UV-visible spectrophotometry. Enumeration of bacteria using SEM was conducted at early biofilm formation. Triplicate counts on 10 fields of observations were conducted. The surface morphology of the samples was analysed using an AFM with the same batch samples used in the SEM studies. SEM results display that the surface types varied in bacterial attachment. Physical and electrochemical treatments improved the resistance of stainless steel to bacterial attachment. Electropolished stainless steel with a smoother surface indicated significantly fewer bacterial cells than other treated surfaces.

Taylor *et al*. (1998) investigated roughened samples of polymethyl methacrylate (PMMA) with and without bovine serum albumin (BSA), and the attached bacteria were rinsed, fixed, and air-dried. Samples were physically coated with gold before SEM analysis. AFM was used to obtain average surface roughness (R_a). Because of the above methods to quantify a

multispecies biofilm, microscopic counting might be impossible. All studies have counted bacteria at the initial stages of attachment (15 min and 15 hours) (Dezelic & Schmidlin, 2009). The visualisation of the cells with bacterial appendages may be challenging when counting the cells under SEM. Park *et al*. (2019) used rDNA sequencing with qPCR to quantify multispecies bacterial attachment on rough and smooth surfaces and this proved to be a good quantitative method for determining cell attachment to the surface. Third-generation sequencing can provide more useful information on bacterial strains selectively colonising a surface. In much of the literature, samples with bacteria are being physically dried without question that the sample could be conductive. Fang *et al*. (2000) reported that an air-dried sample provided reproducible results. AFM was not always applied as a standard method to determine surface roughness. Using AFM is non-destructive and minimally manipulative to the cell surface (Pembrey *et al*.,1999). With the studies conducted, no authors reported the root mean square (RMS) roughness value as a quantitative measurement of surface roughness.

CHAPTER 3 METHODOLOGY

3.1 INTRODUCTION TO METABOLIC ACTIVITY

This study aimed to understand the phases of bacterial growth and present a newly developed multispecies kinetic growth model specifically targeted at the petrochemical industry. 16S rDNA gene sequencing on colony plates revealed the dominant bacterium in the system. The list of instruments used to experiment is presented with a detailed methodology.

3.2 RESEARCH DESIGN

The approach employed in this study involved collecting bacteria from a cooling tower of a petrochemical processing plant in South Africa using a perforated stainless steel mesh coupon. The metabolic activity of the bacteria was evaluated over 15 days using a spectrophotometer. Kuang *et al*. (2007) studied the growth phase of SRB in a sea water system. Kuang *et al*. (2007) described the growing process of SRB (sulphate-reducing bacteria) in three stages growing (one to three days), residual (day 4) and death phase (day 14). A recent study (Wang *et al*., 2020), exhibited the growth of *Bacillus subtilis* with time, and it was observed from this study that the bacteria grew exponentially from day 2-3, then reached a residual phase by day 4.

Kuang *et al*. (2007) and Wang *et al*. (2020) did not investigate the growth process of a mixed culture of bacteria. These standards were chosen because the works are closely related to the corrosion of steel presented later in this work. This experiment was conducted to understand the phases of bacterial growth and to identify the dominant bacteria that play a role in the corrosion of steel. Some bacteria may not grow owing to aerobic conditions. However, it is to be noted that the cooling tower is open to atmosphere. Table 3.1 and Table 3.2 present the instruments used, followed by the conceptual models for this experiment respectively.

Table 3.1: Table of instruments

Design of the research instrument	Purpose of instrument	Reliability and validity
Incubator	Incubation bacteria for optimal growth at 35 °C	The incubator has a thermostat ensuring the temperature is kept constant at 35 °C
Laminar flow hood	Create sterile environment	There was no contamination established in the samples submitted for 16S gene profiling
Hatch DR 6000 Spectrophotometer, United States	Measure absorbance	Widely used in the labs and research laboratories
Autoclave	Sterilise equipment used in the experiment	Widely used research laboratories
Mesh coupon for collecting bacteria. Dimensions: 0.178 mm x 12.7 mm x 76.2 mm. Composition: Appendix A Section 9.1.5.	Collects bacteria	Growth observation
Filters 0.22 μm	Filters out bacteria	The results must be lower than bacteria unfiltered
pH metre	Measures the pH	Widely used in research laboratories and was calibrated before use
PCR machine, Veriti 96 Well Thermal Cycler (AB Applied Biosystems)	DNA amplification	Maintained at the University of Pretoria
DNA Sequencer, Thermo Fisher Scientific, Carlsbad, USA	Species identification	Maintained at the University of Pretoria
Zymoclean Gel DNA Recovery Kit (Zymo Research)	Band purification	Standard kit

Table 3.2: Conceptual model

Conceptual model	Time → Growth	AQUASIM 2.0 simulation software and spectrophotometer measurement

3.2.1 Media preparation: Colony plates and MTT solution preparation

Modified batch mineral medium was prepared from 0.501 g KH_2PO_4, 1.000 g NH_4Cl, 4.502 g Na_2SO_4, 0.050 g $CaCl_2.2H_2O$, 0.062 g $MgSO_4.7H_2O$, 12.012 g 50% solution sodium lactate, 1.001 g yeast extract, 0.004 g $FeSO_4.7H_2O$, 5,002 g $Na_3C_6H_5O_7$ Sodium citrate in 1 L distilled water to simulate the mineral rich water quality of river water fed to the cooling towers with carbon sources. The pH was measured at 6.52 and adjusted to 7 using 5 M NaOH. SRB plate media was prepared using the media above and adding 15 g of bacteriological agar. pH was 6.57 and adjusted to 7 using 5 M NaOH. TSA plate media was prepared using 40 g of Tryptone Soya Agar in 1 L distilled water. The pH meter was calibrated before testing the pH of the media. The adjustment of pH was conducted for consistence with other studies on the impact of metal finish on bacterial attachment (Zhu *et al*., 2003). MTT solution was prepared in the dark using 5 mg of MTT powder in 1 mL distilled water filtered into a 2 mL vial and frozen at -72 ºC. Media, distilled water, and instruments were autoclaved at 121 ºC at a pressure of 1.5 kPa for 20 min. A summary of the cooling water composition is presented in the Appendix Section 9.1.5.

3.2.2 Bacterial cultivation

A stainless-steel perforated mesh coupon (Table 3.1) designed to collect bacteria was inserted in the cooling tower coupon rack for 11 months. Cooling water is directly transported from the cooling tower to the coupon rack at flow conditions of 1 m/s. The coupon rack is designed to hold one biofilm mesh coupon. The coupon was removed from the coupon rack using sterilised tweezers and inserted into a sterile sample bag containing cooling water. Under a laminar flow hood, the mesh coupon was immediately transferred (using sterile tweezers) into the batch reactors containing autoclaved prepared media with sterilised carbon steel alloys and without carbon steel alloys (for the metabolic activity study). The batch reactor was incubated in an incubator equipped with a thermostat and set at a constant temperature of 35 ºC (cooling

water temperature). It is to be noted that the conditions were aerobic, due to the opening and closing of the reactor, similarly, the cooling tower was open to atmosphere.

3.2.3 Metabolic activity

Metabolic activity, which is bacterial growth rate, was evaluated using prepared media in a batch reactor inoculated with a mixed bacterial culture without carbon steel alloys. The batch media was gently mixed from side to side before extracting duplicate 2 mL aliquots of the sample. One sample was filtered, and the other was unfiltered. Vials were diluted with 3 mL of autoclaved distilled water. The diluted samples, including 0.2 mL MTT solution, were added to 2 mL vials. The 2 mL vials were placed in an incubator at 35 °C for 60 min. Dimethyl sulfoxide (DMSO) was added before measuring absorbance using a Hatch DR 6000 Spectrophotometer. Figure 3.1 presents a flow diagram of the process followed to measure absorbance.

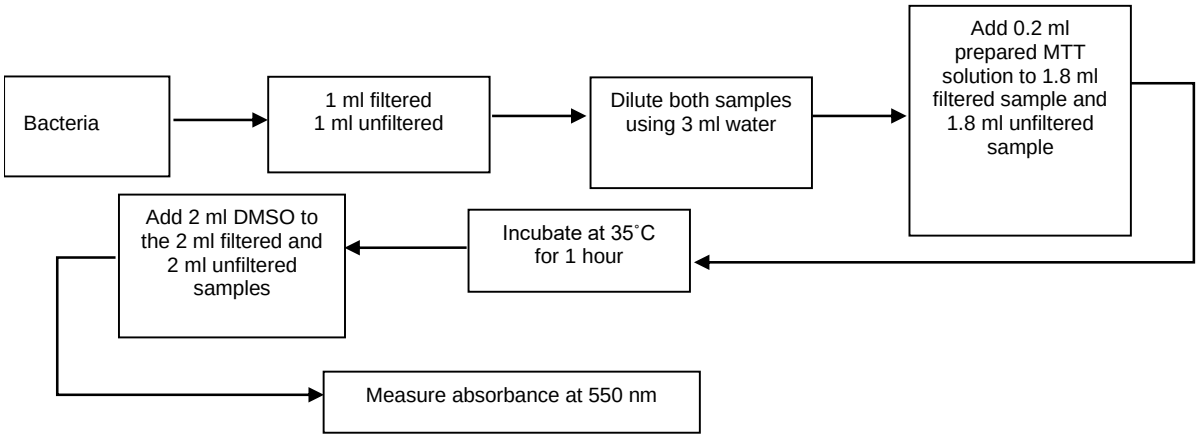

Figure 3.1: Process flow diagram to measure absorbance

3.2.4 Colony-forming units

The number of live heterotrophic bacteria in water was measured using the standard plate count method. The colonies on the plates that appear after incubation were counted; these may result from pairs, clusters, chains, or single cells, all forming part of a colony forming unit (CFU). Six dilutions were conducted. 0.1 mL of straight samples were plated first and kept aside to plate the bacteria, 1 mL of straight bacterial sample was added to the first dilution

bottle, the 1 mL tip was discarded, and a new tip was used to remove 1 mL of sample from the first dilution bottle and insert it into the second bottle, and the sampling procedure was followed for the five bottles. Once dilution was complete, each bottle was gently shaken from side to side; 0.1 mL of the bacterial samples were then plated from dilution 6 to dilution 2 using the same tip. A spreader was dipped in ethanol and ignited using a gas cylinder, the spreader was moved around to cool, and the samples were spread from dilution 6 to dilution 1.

The plates were immediately incubated in an upside-down position. The plating was conducted under sterile conditions under a laminar flow hood. All instruments were autoclaved before use. Surfaces were sterilised using 70% ethanol. TS plates were removed after two days, and SRB plates were removed from incubation after 10 days. Colonies were then counted visually. The plates were immediately wrapped in parafilm and placed in a fridge at -3 °C.

3.2.5 16S gene profiling on colony plates

16S rDNA gene sequencing analysis was conducted on colony plates for days 3, 6, and 13 to identify bacterial strains. The day 3 plates that were submitted included a combination of SRB and TSA, and only TSA plates were submitted for days 6 and 13. The strain identification was based on the plus/minus 600 bp partial sequence of the 16S rDNA gene of the organisms using a Veriti 96 Well Thermal Cycler (AB Applied Biosystems). The sequences were compared against the GenBank of the National Centre for Biotechnology in the United States of America using a basic BLAST search.

The 16S gene profiling was started by purifying all PCR products by adding 2 U/µl of Exonuclease 1 (Thermo Scientific) and 2 U/µl of FastAP (Thermo Scientific). This was followed by incubation on the T100TM Thermal Cycler (BioRad) at 37 °C for 15 minutes to activate the enzymes and a second incubation at 85 °C for 15 minutes. Sometimes a second amplification product remained after cleaning; therefore, a Zymoclean Gel DNA Recovery Kit (Zymo Research) was used to purify the band of the expected size.

The purified products were then sequenced using the BigDye Terminator v3.1 Cycle Sequencing kit (Thermo Fisher Scientific, USA). The AB13100 Automated Capillary DNA sequencer (Thermo Fisher Scientific, Carlsbad, USA) at the DNA Sanger Sequencing Facility, hosted in the Faculty of Natural and Agricultural Sciences of the University of Pretoria, was used to determine DNA sequence chromatograms from the purified sequencing products.

3.3 INTRODUCTION TO SURFACE COLONISATION

This study evaluated differences in bacterial colonisation on rough and smooth-finished surfaces. The dominant bacteria observed on colony plates were compared to the bacterial attachment to steel. A separate batch reactor was used with sterilised carbon steel alloys. Total organic carbon (TOC) and High-Performance Liquid Chromatography (HPLC) analysis were conducted simultaneously with colonisation studies to present insight into metabolites produced and used during attachment. The metabolites identified from this analysis were compared to the growth model to present more information about the bacteria in this system.

Prithiraj *et al*. (2019) demonstrated that a mixed bacterial culture exposed to industry-finished steel affected the corrosion rate. Zhu *et al*. (2003) further challenged that the attachment of certain species to industry steel with their metabolic functioning could influence the corrosion rate. The industrial study by Zhu *et al*. (2003) posited that the possible key role players; *Pseudomonas sp.* and *Clostridium sp.* bacteria could produce organic acids accelerating corrosion rate; however, the study did not prove the preferential attachment of these species to a surface. Table 3.3 presents the test methods of each hypothesis with a conceptual model. A list of instruments used in this experiment is presented in Table 3.4. The experimental design and detailed methodology are then showcased in this section.

Table 3.3: Table of hypothesis

Alternate hypothesis	**H1:There is a time-related difference in colonisation**	
Null hypothesis	**H0:There are no time-related differences in colonisation**	
Conceptual model	Time → colonisation with two surface finishes	Test method: rDNA gene sequencing and Permutational analysis of variance on species abundance (PERMANOVA)
Alternate hypothesis	H1:There is a time-related difference in bacterial levels	
Null hypothesis	**H0:There are no time-related differences in bacterial levels**	
Conceptual model	Time → bacterial levels with two surface finishes	Test method: qPCR (One-way ANOVA)

Alternate hypothesis	**H1:there is a time-related difference in surface roughness**	
Null hypothesis	**H0:there are no time-related differences in surface roughness**	
Conceptual model	Time → Surface roughness	Test method: One-way ANOVA with AFM
Conceptual model	Time → Carbon source	Test method: Reaction kinetics model and simulation, HPLC, and TOC

3.4 RESEARCH DESIGN

The standard research designs selected are works of Fang *et al.* (2000), Park *et al*. (2019), Medilanski *et al*. (2002), and Dezelic & Schmidlin (2009). The study by Fang *et al.* (2000:89) demonstrated that AFM microscopy could obtain high-resolution topographical images of bacteria. Introduced that AFM analysis offered new opportunities in characterising the bacterial surface. The study would evaluate these parameters, as this would present insight into the formation mechanism of biofilm.

Fang *et al*. (2000) studied rod-shaped bacteria; however, authors did not evaluate a mixed culture of bacteria. Basic preparation methods for AFM analysis was provided, which includes information about drying methods that affect the physico-chemical properties of the bacterial cells. It was reported that air drying of the sample surface produced stable and reproducible results. Physical drying methods, such as coating with gold or dehydrating the bacterial surface were not used in this study.

Park *et al*. (2019) investigated changes in multispecies biofilms on composite resins of different roughness. The study provided important information regarding multispecies studies on early colonisers, middle colonisers, and late colonisers and used 16S rDNA sequencing with qPCR to obtain bacterial levels at the surface. The study by Medilanski *et al*. (2002) evaluated the influence of bacterial attachment to five surface finishes. The study investigated a mixture of four bacterial species with a rod (*SRB* and *Pseudomonas sp*.) and coccus shapes. An epifluorescence microscope was used to count bacteria in 10 areas on the steel. No apparent conclusion was made as to which surface the bacteria preferentially attached. The study further emphasised a vital parameter when working with industrial-finished steels, where metals must be prepared to industrial standards. Organic-free steel surfaces are challenging

to obtain and keep and do not represent the state of steel typically subject to bacterial attachment in active installations.

Because of the research designs, microscopic counting might be impossible; therefore, third-generation sequencing with qPCR could give more insight into microbial species colonising a steel surface. This work would provide an avenue of parameters to establish a conclusion on multispecies bacterial attachment to rough and smooth surfaces. The literature indicates inconsistencies in the reported results. Several authors do not use rDNA sequencing methods on multispecies systems and, therefore, select only a few strains which can be counted under the microscope. Park *et al.* (2019) and Dezelic & Schmidlin (2009) evaluated multispecies attachment and did not use the AFM to quantify surface roughness, and rather used instruments such as confocal laser scanning, scanning electron microscopy and a profilometer; however, Medilanski *et al*. (2002) had used the AFM to quantify surface roughness. The learnings from these studies present essential information about inconsistencies reported across various studies. This includes multispecies studies with methods to prepare samples (drying or coating), quantification of surface roughness and evaluation of bacterial colonisation on a surface. A more superficial preliminary investigation was conducted as part of the main study to evaluate the conductivity of the surface without using physical drying methods.

Table 3.4: Table of instruments

Design of the research instrument	Purpose of instrument	Reliability and validity
Incubator	Incubation bacteria for optimal growth at 35 °C	The incubator has a thermostat ensuring the temperature is kept constant at 35 °C
Laminar flow hood	Create sterile environment	No contamination
Autoclave	Sterilise the equipment used in the experiment	Widely used in the labs and research laboratories
Mesh coupon for collecting bacteria	Collects bacteria	Growth observation
Atomic Force Microscopy, Germany	Morphological analysis and obtaining 3D and 2D imagery of biofilm architecture, visual of the cell on the surface, measuring the width of the scratches when metal coupon surface is polished	Maintained at the University of Pretoria
Scanning Electron Microscopy Crossbeam 540 Zeiss Gemini2, Germany	Visual of the surface	Maintained at the University of Pretoria
Struers Tegramin – 30, United States, Cleveland	Automatic rotating polishing machine	Surface finish verified under a Nikon Eclipse MA200 microscope. A polishing machine is used in specialised metallurgical labs
Aminex HPX-87H, United States	High-performance liquid chromatography. Evaluation of specific carbon sources	Maintained at the University of Pretoria
Teledyne Tekmar 14-9600-200, United States	Measuring total organic carbon content (TOC)	Widely used in the University and industry to obtain accurate product information
WITec Alpha 300 micro-Raman confocal microscope, Germany	Amorphous product analysis	Maintained at the University of Pretoria
Spectrum 65, Perkin Elmer-FTIR microscope, Waltham, Massachusetts, US	Study thin films on surfaces	Widely used in universities and industry

Design of the research instrument	Purpose of instrument	Reliability and validity
PCR, Eppendorf Mastercycler Nexus Gradient	DNA amplification	Maintained at Inqaba laboratories, specialising in 16S gene profiling
ZymoBIOMICS DNA Miniprep kit (Zymo Research)	Genomic DNA extraction	Standard kit
Nikon Eclipse MA 200, Tokyo, Japan	To obtain microstructural information of steel	Widely used in metallurgical laboratories
CFX96 Real-Time PCR System (Bio-Rad)	Quantification of bacterial levels on the steel	Maintained at Inqaba laboratories, and efficiency was tested.

3.4.1 Metal polishing

Three carbon steel tube used in this study measured 1 cm by 1 cm and were sourced from the petrochemical plant. The carbon steel tube grade used in this study was A106 GB (alloy A). The steels were mounted in Bakelite and automatically polished to two finishes, 400-grit and 3 µm, using silicon carbide waterproof paper. The coupons were polished using a Struers Tegramin – 30 automatic polishing machine for 3 min, using a force of 35 N at 300 revolutions per minute—polishing to a 400-grit, started by using 220-grit silicon carbide paper for 3 min, then applying the 400-grit silicon carbide paper for 3 min. Once completed, the surface was lightly rinsed with acetone and dried using a hair drier. Polishing to a 3-micron finish, started by using 220-grit silicon carbide paper for 3 min, then applying the 9-micron polish for 3 min, then a 3-micron polish. Once completed, the surface was lightly rinsed with acetone and dried using a hair drier.

3.4.2 Media preparation

Media was prepared in a batch reactor, as discussed in Section 3.1.1. The media were autoclaved and left to cool down. The media was inoculated with the bacterial consortium collected from the cooling tower coupon rack. Bacteria were grown by incubation at 35 °C at a pH of 7. All instruments were autoclaved for this experiment.

3.4.3 Alloy preparation

Carbon steel coupons, measuring 1 cm by 1 cm, were polished to two different finishes. Under a laminar flow hood, the carbon steel alloys were fastened on cable ties, marked using tape, and sterilised using 70% ethanol. The alloys were soaked in 70% ethanol for one hour, then removed and left to dry. The cable ties with the coupons were inserted into the bacterial media. The batch reactor with bacteria and carbon steel alloys was incubated at 35 °C; parafilm was used to seal the opening side of the batch reactor. Conditions were aerobic owing to the opening and closing of the reactor for samples sent for TOC and HPLC analysis.

3.4.4 Surface study

Alloys were removed from the media under the laminar flow hood and gently rinsed with sterile distilled water to remove loosely attached bacteria following the method developed earlier by Fang *et al*. (2000). The morphological properties of the uncoated samples (in a hydrated state) as well the elemental composition and distribution mapping of the bacterial surface in abiotic and biotic conditions were studied using a scanning electron microscope coupled with an energy dispersive X-ray (EDX). Samples were evaluated under the microscope with an accelerating voltage of 5 kV. Alloys were not physically dried or sputtered coated. The hydrated bacterial coupons were dried by placing them on a paper towel (to absorb any excess media dripping from the coupon) on the side that was not scanned and transferred to a platform (stage) for scanning. Dagnall (1980) explains that smooth and rough surfaces are distinguished differently by observers, and visual interpretation and touch are subjective. In this work, the roughness of the surfaces were quantified using AFM and dimensions of nanometres were used (nm). AFM was conducted on smooth and rough surfaces before and after bacterial exposure on the biofilm over 3, 6 and 13 days on alloy A to obtain roughness parameters. AFM was conducted in ScanAssyst mode on the Bruker dimension icon. The RMS roughness value was reported as a statistical measurement of the square root of the measurement.

3.4.5 16S rDNA sequencing with qPCR on the surfaces

Separate alloys (Six coupons) for 16S rDNA analysis were removed under the laminar flow hood; alloys were gently rinsed three times with sterilised distilled water to remove loosely attached bacteria and swabbed on the polished side (middle of the alloy) using a sterile swab.

The sterile swab tube was sealed with parafilm and stored in a freezer. The analysis was conducted to identify the early (day 3), middle (day 6) and late colonisers (day 13) on each surface.

Genomic DNA (gDNA) extraction was conducted using a ZymoBIOMICS DNA miniprep kit (Zymo Research). The extraction protocol was started by adding the swab sample to the 2 mL ZR BashingBead Lysis tube (0.1 and 0.5 mm dry matrix). Then 750 µl of the ZymoBIOMICS Lysis solution was added to the tube and the cap was closed tightly. The bead beater fitted with a 2 mL holder assembly was secured and processed using the optimised beat conditions, for 1 minute 'on' at 9000 rpm and 2 minutes rest. The cycle was repeated 4 times for a total of 4 minutes of bead beating. The ZR BashingBead Lysis tubes was centrifuged in a microcentrifuge at 10000 x g (units of gravity for relative centrifugal force) for 1 minute. Up to 400 µl of supernatant was transferred to the Zymo-Spin III-F filter in a collection tube and centrifuged at 8000 x g for 1 minute. The Zymo-Spin III-F filter was then discarded. An amount of 1200 µl of the ZymoBIOMICS DNA Binding Buffer was added to the filtrate in the collection tube and mixed well. Exactly 800 µl of the mixture was transferred to a Zymo-Spin IICR Column in a collection tube and centrifuged at 10000 x g for 1 minute. The flow-through (unwanted cellular material/contaminants) was discarded and a second amount of 800 µl of the mixture was transferred again to the Zymo-Spin IICR Column in a collection tube and centrifuged at 10000 x for 1 minute. An amount of 400 µl, 700 µl and 200 µl of ZymoBIOMICS DNA wash buffer 1, 2 and 3 was added, respectively, to the Zymo-spin IICR Column in new collection tubes and centrifuged at 10000 x g for 1 minute. The flow-through was discarded. The Zymo-Spin IICR column was transferred to a clean 1.5 mL microcentrifuge tube and 100 µl ZymoBIOMICS DNase free water was added directly to the column matrix and incubated for 1 minute, then centrifuged at 10000 x g for 1 minute to elude the DNA. A Zymo-spin IIIHRC filter and 600 µl ZymoBIOMICS-HRC prep solution was placed in a new collection tube and centrifuged at 8000 x g for 3 minutes. The eluted DNA was now transferred to a prepared Zymo-Spin III-HCR filter, in a clean 1.5 mL microcentrifuge tube at exactly 16000 x g for 3 minutes. The extracted gDNA was amplified in an Eppendorf Mastercycler Nexus Gradient PCR machine using a universal primer pair 27F and 1492R (Zhao *et al*., 2022). This was conducted to target the V1 and V9 regions of the bacterial 16S rRNA gene. The resulting amplicons were barcoded with PacBio M13 barcodes for multiplexing through limited cycle PCR. The resulting barcoded amplicons were quantified, and a pooled equimolar and AMPure PB bead-based purification step was performed.

The PacBio SMRTbell library was prepared from the pooled amplicons following the manufacturer's protocol. Sequencing primer annealing and Polymerase binding were conducted following the SMRTlink Link software protocol to prepare the library for sequencing on the PacBio Sequel LLE system. Samples were sequenced on the Sequel system by PacBio software. Raw subreads were processed through the SMRTlink (v9.0) software and usearch. The taxanomic information was determined based on the Ribosomal database project's 16S database v16. The taxa classification percentage abundance reports were created using an inhouse python script. Highly accurate reads were processed through Circular Consensus Sequences (CCS) and Vsearch software to produce a metagenomic report with species read count and percentage abundance.

Another set of six coupons were gently rinsed and swabbed under sterile conditions and used to obtain bacterial levels on the surface using quantitative polymerase chain reaction (qPCR). The standard curve was generated using a serial dilution of the pGEM-T plasmid from 0.1 ng to 0.1 fg.

The qPCR was then performed in 96 well plates with Luna Universal qPCR Master Mix (New England Biolabs, Ipswich, MA, USA) using dye-based qPCR assay. Each reaction contained 1 µl of DNA template, 0.25 µm forward and reverse primers (Park *et al*., 2019:493) and 1 X Luna Universal qPCR Master mix. The reactions were run on CFX96 Real-Time PCR System (Bio-Rad) following a three-step PCR program. The cycling conditions were 1 X (95 °C for 5 min), 40 X (95 °C for 10 s; 60 °C for 15 s and 72 °C for 20 s) followed by a melt curve analysis (Appendix A Section 9.1.6) from 60 °C to 95 °C in 0.2 °C increments. Three technical replicates were run for each DNA sample. Amplification of different input templates were evaluated based on the quantification cycle (Cq) value. The absolute copy number was calculated using the formulas in Appendix A Section 9.1.6. The average Cq values were plotted against the absolute copy number of standards and standard curves which were generated by a linear regression of the plotted points (Appendix A Section 9.1.6). The absolute copy number for the bacterial strains was calculated based on the standard curve.

3.4.6 Total organic carbon analysis (TOC)

Total organic carbon analysis was conducted using a Total Organic Carbon non-purgeable organic technique to evaluate the carbon content over 15 days. Bacterial samples were filtered using a 0.45 µm syringe filter under sterile conditions, then diluted to 1000 for TOC analysis.

The Teledyne Tekmar 14-9600-200, United States, machine uses a voltage of 230 and 2.50 Amps and conforms to UL STD 61010A-1 certified to CSA Standard C22.2 N0.1010.1 and based on the Standard Method 5310C.

Organic carbon was measured a with UV-persulphate-ultraviolet oxidation analyser, equipped with a Non-Dispersive Infrared (NDIR) detector. The instrument converts the organic carbon in a sample to CO_2 by ultraviolet oxidation, after the removal of the inorganic carbon by acid treatment. The CO_2 formed, which is directly proportional to the concentration of the organic carbonaceous material in the sample, is detected using the infrared detector.

The filtered sample was shaken gently, and 30 mL of the sample was transferred into a 40 mL Volatile Organic Analysis (VOA) vial. The vial was closed with a screw cap. The sample was diluted to 1000 using double deionised water. This was done in order to adhere to the calibration range of 0-20 mg C/L. The instrument was then configured and stabilised by switching on the TOC instrument and computer and the software was opened. Thereafter, the nitrogen pure gas supply was opened to deliver a maximum pressure of 200 kPa to the instrument. The samples were then positioned appropriately on the auto-sampler. In the software, inputs such as “sample name”, “TOC range” must be entered. Once the instrument was started the control standard was run. The TOC results were shown on the computer screen once the analysis was complete. The results were calculated by the instrument by the software, using the applicable calibration range.

3.4.7 High-performance liquid chromatography analysis (HPLC)

HPLC analysis was conducted to evaluate the degradation of the specific carbon sources (lactic acid and citric acid) in the batch reactor. A chromatographic system equipped with a UV/Vis detector and a BioRad Aminex HPX-87H column was used. The detector was set at 210 nm. Sulphuric acid was the mobile phase at a flow rate of 10 µl/min with a column temperature of 35 °C. Simulated concentration models of lactate and citrate were generated using AQUASIM 2.0, and sensitivity analysis was performed. Experimental measurements from the HPLC analysis were included in the model using first-order kinetics in a batch reactor (Table 3.5-3.7). To develop a calibration curve, various concentrations of certified organic acid standards and by-products of the rTCA metabolic pathway of the microbes were used.

The standards used were citric acid and lactic acid. Serial dilution was performed for liquid standards to create the concentrations. Solid standards were first weighed to create a liquid

stock solution, and then the analysis samples were prepared through serial dilution. A chromatographic system equipped with a UV/Vis detector and a BioRad Aminex HPX-87H column was used. The detector was set at 210 nm, the flow rate of the 0.5 mM sulphuric acid mobile phase was set at 10 µl/min, using 10 µl injection volume of the samples, and the column temperature was set at 35 °C.

Table 3.5: HPLC column specifications

Parameters	**Conditions**
HPLC Detector	UV/Vis
Column	Aminex HPX-87H, 300 mm x 7.8 mm
Temperature	35 °C
Injection Volume	10 µl
Flow rate	10 µl/min
Mobile phase	5 mM Sulphuric acid
Wavelength	210 nm

Table 3.6: Lactic acid programme parameters

Variables (dA/dt = k*C**)**	**Description of variable**
C	Concentration state variable
Cmeas	Concentration real list variable
k	Constant variable
t	Time programme variable
Volume	Constant volume batch (initial condition C = 6 g/l)
Stoichiometric coefficient	C = -1

Table 3.7: Citric acid programme parameters

Variables (dA/dt = k*C)	**Description of variable**
C	Concentration state variable

Cmeas	Concentration real list variable
k	Constant variable
t	Time programme variable
Volume	Constant volume batch (initial condition C = 6 g/l)
Stoichiometric coefficient	C = -1

3.4.8 Statistical analysis

Mean values and 95% confidence intervals were calculated to determine the difference between rough and smooth surfaces at respective bacterial colonisation times. Time-related differences in roughness values were determined with a paired t-test. One-way ANOVA was performed on the surface finishes and corrosion rates to establish differences among the differently finished alloys. Significance was set at 95%. The bacterial species abundance was evaluated using PERMANOVA (Permutational analysis of variance) analysis in PRIMER 7. The analysis was conducted to determine the differences in species abundance between sample surfaces. Percentage data was transformed using the square-root. The resemblance and PERMANOVA design was conducted using the Bray-Curtis similarity, unrestricted permutation method. The linear relationship between species abundance and corrosion rate was evaluated using Pearson's correlation and regression to obtain significance. Significance was set at 95%. One-way Anova was performed on the absolute copy number to obtain the difference in bacterial levels between the rough and smooth surfaces.

3.4.9 Kinetic modelling using AQUASIM 2.0

AQUASIM version 2.0 is a computer program for the identification and simulation of aquatic systems, it was developed by Peter Reinchert, Jürg Ruchti and Werner Simon, Switzerland. In this study AQUASIM 2.0 was used to develop the kinetic model for a multispecies batch system.

AQUASIM was downloaded on a windows operating system. Once the program was downloaded, the parameters were defined. In the AQUASIM program, the "Edit variable" box was opened. To add a variable the "New" button was selected, and it was required to define this variable. The variables in this work were defined and edited in the programme as follows and a lis.text file is provided in the Appendix section 9.1.7:

Name of variable: Ks (constant variable). The constant variable was edited, Description: concentration for ½ mumax, Unit: g/L, Value: 0.22, Standard deviation: 1, Minimum: 0. Maximum: 10. The buttons for sensitivity analysis and parameter estimation were selected.

Name of variable: mumaxmeas (Real list variable). The real list variable was edited, Description: measured growth, Unit: 1/d, Argument: t, Standard deviation: global, read in the measured data from a text file. Interpolation: linear. The button for sensitivity analysis was selected.

Name of variable: S (Dynamic volume state variable). The dynamic variable was edited, Description: concentration of limiting nutrient. Unit: g/l, Type: The buttons for dynamic and volume were selected.

Name of variable: t (Program variable). The program variable was edited, Description: time, unit: days, reference to: time.

The next step was to open the “Edit processes” box. To add a process, the “New” button was selected, then the “Dynamic Process” type was selected. It was required to edit the dynamic process, by selecting the “edit” button. The dynamic process was edited as follows:

Name: growth_rate_of_cells. Description: Specific growth rate of cells. Rate: mumax*S/(Ks+S), Stoichiometric Coefficient: S: -1.

The next step was to open the “Edit compartments” box. To add a compartment, the “New” button was selected, then the “Mixed reactor compartment” was selected. It was required to edit the mixed reactor compartment, by selecting the “edit” button. The mixed reactor process was edited as follows:

Name: Growth_rate. Description: growth. Reactor type: constant volume. Volume: 1. The active for calculation button was selected.

In the tool bar, the simulation button was selected, where there are two columns for calculation definitions. To add a calculation definition, the “New” button was selected. The name of the calculation definition was specified, Name: calc1. Initial state: given, made consistent. Status: active for simulation. It was required to edit the calculation definition by selecting the “edit” button. The calculation definition was edited as follows:

Name: calc1. Description: growth. Calculation number: 0. Initial time: 0. Initial state: given, made consistent. Output steps: step size: 0.1, number of steps: 300. Status: active for simulation. At the main simulation box with the two columns, select the “Initialise” button and “Start/Continue button”.

In the tool bar, the button with a graph seen as “View results” was selected. To add a plot definition, the “New” button was selected. The plot definition was edited as follows:

Name: Specific_growth_rate. Description: specific growth rate. Title: specific growth rate. Abscissa: time, Label: Time (days). Ordinate: Label: Specific growth rate (1/d). The curves were required to be added: the first value was S, and the curve was then edited by selecting the “Edit” button. The curve definition for the variable “S” was edited as follows: Type: Value, Variable: S, Calculation number: S. Time/space: 0. Line: active. The style of the graph was then defined. Variables: t, and mumaxmeas were added to the curves and edited in the same manner.

Then, in the view results box, the “Plot to screen” button was selected. A graph then appeared.

In the tool bar, the parameter estimation button was selected and the mumax and Ks variables were activated. In the calculations the “New” button was selected, to edit the calculation for parameter estimation. The calculation was edited as follows:

Name: fit1. Initial state: given, made consistent. Status: Active for parameter estimation. The “Add” button was selected. It was then required to edit the Fit target. The fit target was edited as follows: Data: mumaxmeas. Variables: Ks, mumax, mumaxmeas, S and t were added to the Fit targets. Method: secant. Number of iterations: 100. The “Start” button was selected. A file named: “fit” was saved. A pop status was created: convergence criterion met. Number of iterations performed: 3. Parameter: Start to End (maximum, minmum). Ks: 0.22 to 0.20023873 (0,10), mumax: 0.455 to 0.31257422. Initial Chi^2: 1178.0353 Final Chi^2:1177.6268.

The “View results button” was selected. The “Specific_growth_rate” was selected. The “Plot to screen” button was selected.

A sensitivity analysis lastly was performed. By selecting the “Sensitivity” button in the tool bar. In parameters growth, Ks, mumax and mumaxmeas was activated. In calculation definitions, “calc1” was activated. Then the calculation definition was edited by adding Name: calc1. Initial

state: given, made consistent. Output steps: 0.1 to 300. Then Select the “Add” button. The sensitivity analysis button was selected.

The “Start” button was selected. A text file “sen” was saved. A prompt then indicated that the sensitivity analysis was successfully completed.

3.5 INTRODUCTION TO CORROSION RATE

The study evaluated corrosion because of bacterial colonisation and metabolic activity. Based on the findings, a surface finish was recommended. Kim *et al*. (2013) indicate that surface roughness alone influenced the corrosion rate and suggested that increased roughness was directly proportional to the corrosion rate. In this section, a table of hypotheses (Table 3.8) is presented, and after that, standard corrosion test methods are presented with a discussion on selected analysis methods to characterise alloy surfaces. The section also includes a hazard description and preparation of media involved in this experiment.

Table 3.8: Conceptual model

Conceptual model	Time → Corrosion rate	Test method: Weight loss method and One-way ANOVA
Conceptual model	RMS roughness → Corrosion rate	Test method: correlation and regression analysis

Duplicate batch systems were used to evaluate the corrosion of carbon steel A 106 GB. One system was inoculated with bacteria and the other a control without bacteria. Equation 1 was used to determine corrosion rate (mm/y) using NACE standards 169-2000 Item no.21200, ASTM G1-72 (Kadaifciler *et al*., 2023) and ASTM D2688-70 (Kumar *et al*., 2022). These laboratory methods and standards are used for preparing, cleaning, and evaluating corrosion test specimens, and testing for corrosivity of water absent heat transfer (weight loss methods)

$$\boldsymbol{Cr} = \frac{(\boldsymbol{W_1} - \boldsymbol{W_4}) \times \mathbf{365} \times \mathbf{100}}{\boldsymbol{\rho_c}.\boldsymbol{A}.\boldsymbol{t}} \quad (1)$$

Where *Cr* = corrosion rate (mm/y), W_1 = initial weight of coupon (g), W_4 = final weight of coupon (g), ρ_c = coupon density (g/dm^3), *A* = surface area (dm^2) and *t* = time in days. Carbon steel alloys were initially weighed and placed in the batch reactors. The cleaning and weighing

process after media exposure was conducted by placing the alloys in 32% HCl solution for 25 min with 0.34 mL Armohib corrosion inhibitor as well as 10% caustic solution to obtain the final weight. Coupons were further soaked in acetone and brushed lightly with a soft brush under flowing water after every treatment and dried at 105 ºC before weighing. The soft brush was used to remove any visible biofilm or corrosion product on the surface.

3.5.1 Etching and elemental analysis of carbon steels

Microstructures and elemental analysis of alloy A: A 106 GB, used in this study were obtained conforming to ASTM 407, ASTM E3 and ASTM E415 standards. The specimens were mounted with a multifast Phenolic hot mount resin using a Struers mounting press (CitoPress – 15, Ballerup, Denmark) set at 180 °C. The mounted carbon steel alloys were polished with a polish disc from 220 grit to 1200 grit and cleaned with acetone. To reveal the microstructures of the alloys, the alloys were etched by immersing in nital (2 mL HNO_3 and 98 mL ethyl alcohol) for 15 seconds, then cleaned with water and acetone and observed under an optical microscope (Nikon Eclipse MA 200, Tokyo, Japan).

3.5.2 Corrosion products analysis and crucial functional groups

FTIR has been used to study films on alloy surfaces by the absorption and transmission of infrared radiation, molecular fingerprints can be obtained. In this study the transmission mode was used to obtain the spectra. The higher energy region (higher than 1500 cm^{-1}), can be used to determine then presence of functional groups in a molecule. Samples were placed directly under the probe to obtain the spectra, without coating the sample.

Raman spectroscopy can be used for amorphous product analysis, whereas XRD can be difficult to analyse. A Raman machine with a laser of 532 nm and laser power of 0.102 mW with an integration time of 15 min was used. It is essential for surface characterisation in corrosion studies and can be used for single or multi-layer surface characteristics evaluation. Raman provides information about surface bonds. It can also evaluate the phase transformation of corrosion products (Dwivedi *et al.,* 2017). A Raman Confocal Microscope was used in this study to determine the corrosion products on the carbon steel alloy surface (with biofilm). This would present insight into multispecies bacteria's function in forming iron oxides.

3.6 CORROSION RATE

Hazards associated with the experiment included hydrochloric acid and sodium hydroxide, which could cause burns; therefore, it was imperative to wear suitable protective clothing, such as gloves and eye protection. An exothermic reaction was initiated when sodium hydroxide was in contact with water. Acetone was kept away from sources of ignition.

3.6.1 Preparation of 10% sodium hydroxide solution

To prepare 10% NaOH, 100 g of NaOH pellets were dissolved in 1000 mL of deionised water using a mixing plate.

3.6.2 Preparation of 32% hydrochloric acid

To prepare 32% HCl, 62.5 mL of HCl solution with 0.34 mL corrosion inhibitor was added to 2000 mL of deionised water. Carbon steel alloys were placed in the batch reactor (Weight 1) and removed on days 3, 6, and 13. The cleaning and weighing process after bacterial media exposure was conducted by placing the alloys in 32% HCl solution for 25 min with 0.34 mL Armohib corrosion inhibitor as well as 10% caustic solution to obtain the final weight. Coupons were further soaked in acetone and brushed lightly with a soft brush to remove any visible biofilm or corrosion product on the surface.

CHAPTER 4 METABOLIC ACTIVITY

4.1 INTRODUCTION

This chapter presents a newly developed kinetic model and metabolic growth curve for multispecies bacteria. Section 4.2 introduces the growth curve. Section 4.3 presents the kinetic growth model. Section 4.4 presents the colony-forming units indicating that bacterial growth is still observed beyond 13 days. Section 4.5 presents the TOC and HPLC results, which provide more information on bacterial growth. Section 4.6 provides the method for developing a kinetic growth model for a multispecies batch system using AQUASIM. The chapter then concludes all sections. The method used to collect a mixed bacterial culture from a cooling tower in a petrochemical processing plant succeeded, as the results indicated bacterial growth (Figure 4.1). The spectrophotometric results confirmed that the growth of the bacterial consortia (Gram-negative) was slower than that of pure strains SRB and *Bacillus subtilis* as observed by Kuang *et al*. (2007) and Wang *et al*. (2020).

4.2 METABOLIC GROWTH CURVE

Figure 4.1 presents the various growth phases of multispecies bacteria collected from a cooling tower in a petrochemical processing plant.

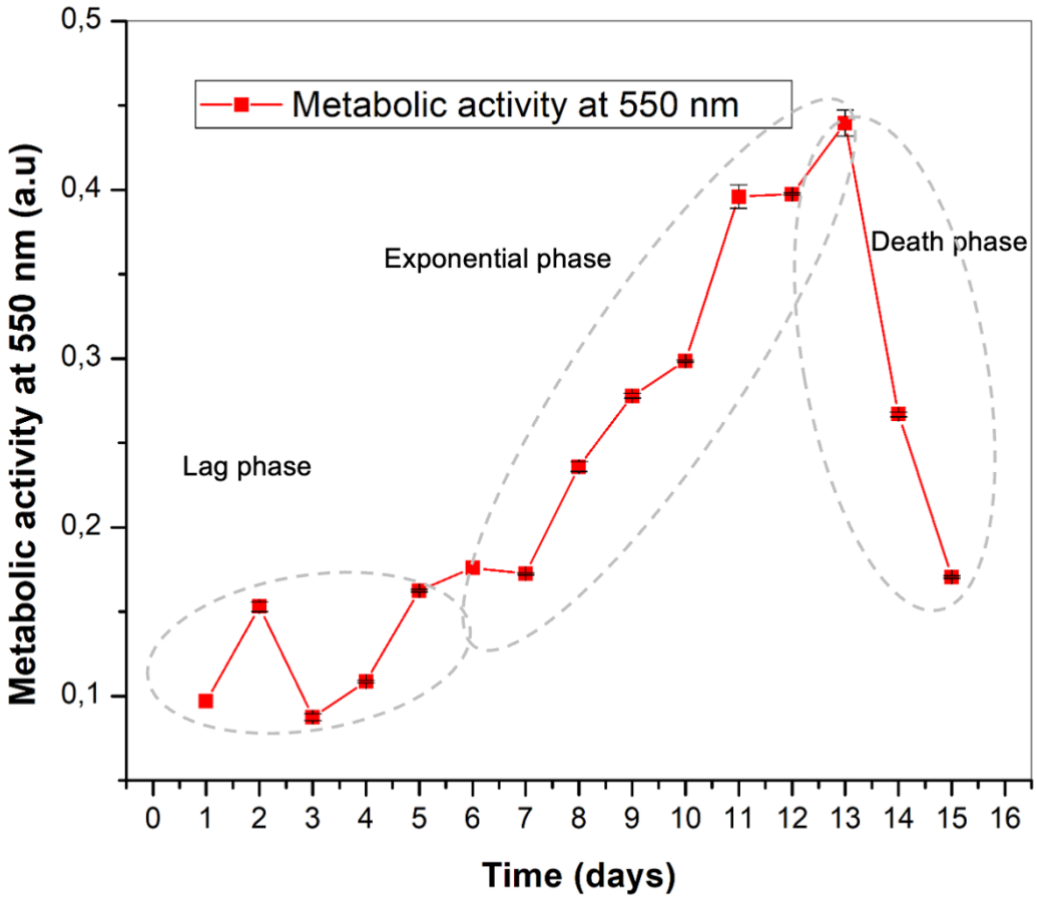

Figure 4.1: Bacterial growth curve (metabolic activity at 550 nm). Growth phases are indicated with a grey dotted line, media was incubated at 35°C, aerobic conditions.

In Figure 4.1, the lag phase was observed from days 1 to 6. The lag phase is the most poorly understood growth phase, primarily because of a lack of data describing the underlying physiological and molecular processes (Rolfe *et al.,* 2012). It has been assumed that the lag phase allows acclimation of the bacterial cells and exploration of the new environment (Madigan *et al.*, 2000). The exponential phase was observed from day 7. No stationary phase was observed, this was possibly due to high substrate utilisation rate by the bacteria, resulting in quicker growth and death phase. This hypothesis is guided by the fact that the bacteria originate from the petrochemical environment which tends to have concentrations of hydrocarbons as their food source in continuous supply and utilised the limited carbon sources at a high rate (Rajasekar *et al.,* 2005). Hydrocarbon content is presented in Appendix A Section 9.1.5. The composition in the cooling tower will always vary due to operational

demands, therefore it was impossible to prepare a batch media to the exact composition as the cooling water. For future work it would be worthwhile investigating bacterial growth using industry hydrocarbons (eg. diesel and jet fuel) in the media. The peak in growth was reached on day 13, where Gram-negative bacteria entered the death phase. In the death phase, the Gram-negative bacteria started to lose viability; however, there were viable Gram-positive bacteria, which could not be quantified by the spectrophotometer analysis, and will be discussed in the sections below.

4.3 KINETIC GROWTH MODEL

For bacterial growth, Monod formulated an equation presented by Equation 2, which has the same form as the Michaelis-Menten equation but differs because it is empirical, whereas the latter is based on theoretical consideration. A combination of mathematical modelling and experimental data presents a meaningful and quantitative interpretation of the experimental results that reveal new aspects of microbiology physiology (Mahanta *et al*., 2014).

$$\mu = (\mu maxS)/(Ks + S) \quad (2)$$

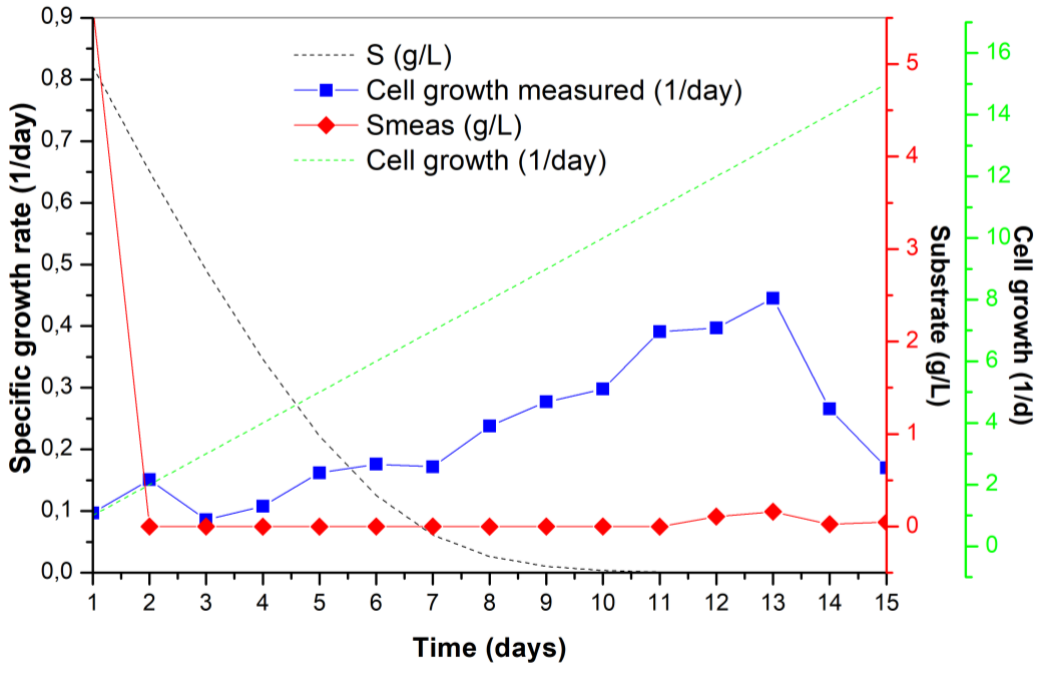

Figure 4.2: Monod model with lactate as the substrate

The green and black lines indicate the simulated curves, and the blue and red line indicates the measured values.

The growth characteristic typically established in batch flask systems are revealed in Figure 4.2. This is also the growth that would be expected under conditions in a natural environment where substrate and nutrients are limiting factors (Maier & Pepper, 2015). There was a fast and sharp decrease in the substrate concentration, with most of it being consumed within the first day of the growth process. This came with a gradual increase in the specific growth rate, with a maximum rate of 0.45 1/day observed on day 13. The specific growth rate is independent of the substrate concentration, this means that if the substrate concentration where to be increased in the system , there would be no further effect on the specific growth rate. The model supports this statement that an increase in lactate concentration was observed on days 12 to 15 and the specific growth rate did not change.

In the presented model, the lag phase, exponential and death phase were seen, with the absence of the stationary and long-term stationary phase. In the simulated curve, only the exponential growth phase was observed, where the maximum specific growth rate was reached much faster, with a value of 0.22 1/day on day 5. The Gram-negative species in this system performed better under low substrate conditions than the simulated model, especially during starved conditions (0 g/L). From the model, a specific growth rate (μ) can be determined at various phases of the growth curve (Table 4.1). This provides insight into the microorganisms in the system.

Table 4.1: Specific growth rate at various phases of growth

Experimental-specific growth rate	**1/d**	**Simulation-specific growth rate**	**1/d**
μ (lag)	0	μ (lag)	0
μ (log) = maximum specific growth rate	0.22	μ (log) = maximum specific growth rate	0.45
μ (stationary)	0	μ (stationary)	0
μ (death)	<0	μ (death)	<0

4.4 COLONY-FORMING UNITS

The CFU graph (Figure 4.3) presents data from TSA plates from day 3 (lag phase). The number of bacteria in the TSA plates peaked on days 7 and 9, with the highest peak observed

on day 13. These days are supported by the growth curve (Figure 4.1); however, the CFU results indicated there was still bacterial growth on day 15. This may be owing to the nutrients in the plate agar which allowed for bacterial growth, therefore, the death phase may take longer to appear in the CFU graph (Maier *et al*., 2015). This method evaluated live bacterial cells, whereas the spectrophotometric analysis measured both live and dead cells.

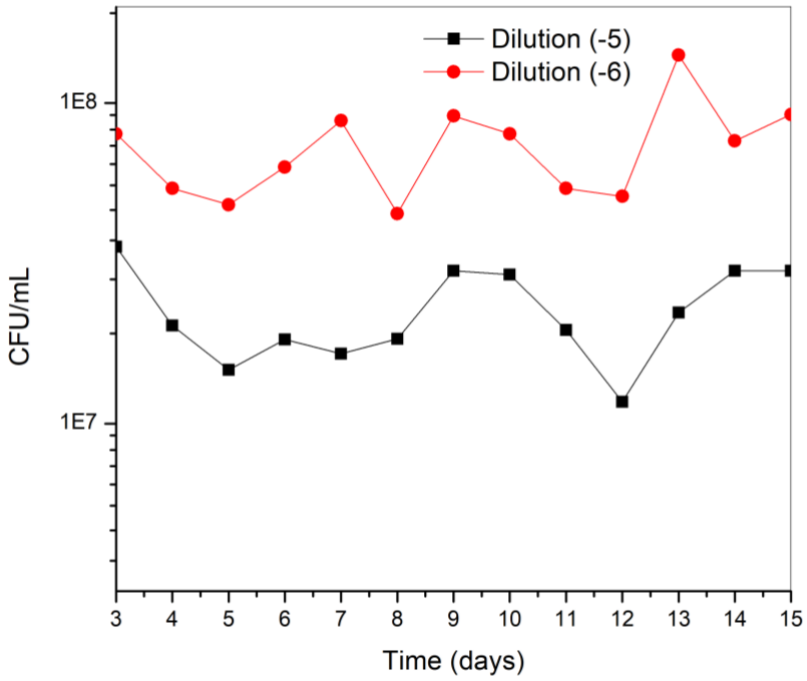

Figure 4.3: CFU from days 3 to 15 at 35 °C

4.4.1 Gene sequencing (16S rDNA)

Gene sequence on colony plates (16S rDNA) revealed that the dominant bacterial strain was the Gram-negative P*seudomonas aeruginosa* motile bacterium (Li *et al.,* 2016) on days 3, 6, and 13 (Table 4.2). This bacterium is prevalent in marine environments (Little *et al*., 2008) and has also been reported in the petrochemical wastewater environment. It is an aerobic slime-forming bacteria which can accelerate the corrosion process (Liang *et al*., 2014).

Table 4.2: 16S rDNA gene sequencing results on selected colony plates emphasising the dominant bacteria

	Isolate	Result	% Sequence identity	Gram-negative or Gram-positive
1	3S1 (Day3/SRB)	*Pseudomonas aeruginosa*	99.7	Gram-negative
2	3T1 (Day3/TSA)	*Plesiomonas shigelloides*	99.3	Gram-negative
3	3T2 (Day3/TSA)	*Enterococcus faecalis*	99.9	Gram-positive
4	3T3 (Day3/TSA)	*Bacillus thuringiensis*	100	Gram-positive
5	6T1 (Day6/TSA)	*Acinetobacter junii*	100	Gram-negative
6	6T2 (Day6/TSA)	*Shewanella xiamenensis*	99.3	Gram-negative
7	6T3 (Day6/TSA)	*Morganella morganii*	98.6	Gram-negative
8	6T4 (Day6/TSA)	*Bacillus wiedmannii*	99.7	Gram-positive
9	6T5 (Day6/TSA) Black	*Pseudomonas aeruginosa*	100	Gram-negative
10	13T1 (Day13/TSA)	*Acinetobacter guillouiae*	99.0	Gram-negative
11	13T2 (Day13/TSA)	*Bacillus thuringiensis*	99.8	Gram-positive

	Isolate	Result	% Sequence identity	Gram-negative or Gram-positive
12	13T3 (Day13/TSA)	*Pseudomonas aeruginosa*	100	Gram-negative

4.5 SUBSTRATE ANALYSIS

In Figure 4.4, the lactate and citrate added to the system were depleted after day 1; however, carbon content was observed during the 15 days, suggesting that bacteria produced carbon sources (lactate and acetate) to adapt and survive to grow (Navarro *et al*., 2010). The bacteria may have utilised the carbon source (lactate) through the lactate dehydrogenase metabolic pathway. The carbon was then converted to molecules of acetate (Detman *et al*., 2019) and lactate. The conversions of these metabolites to other important molecules, for example, butyrate should be investigated in future work.

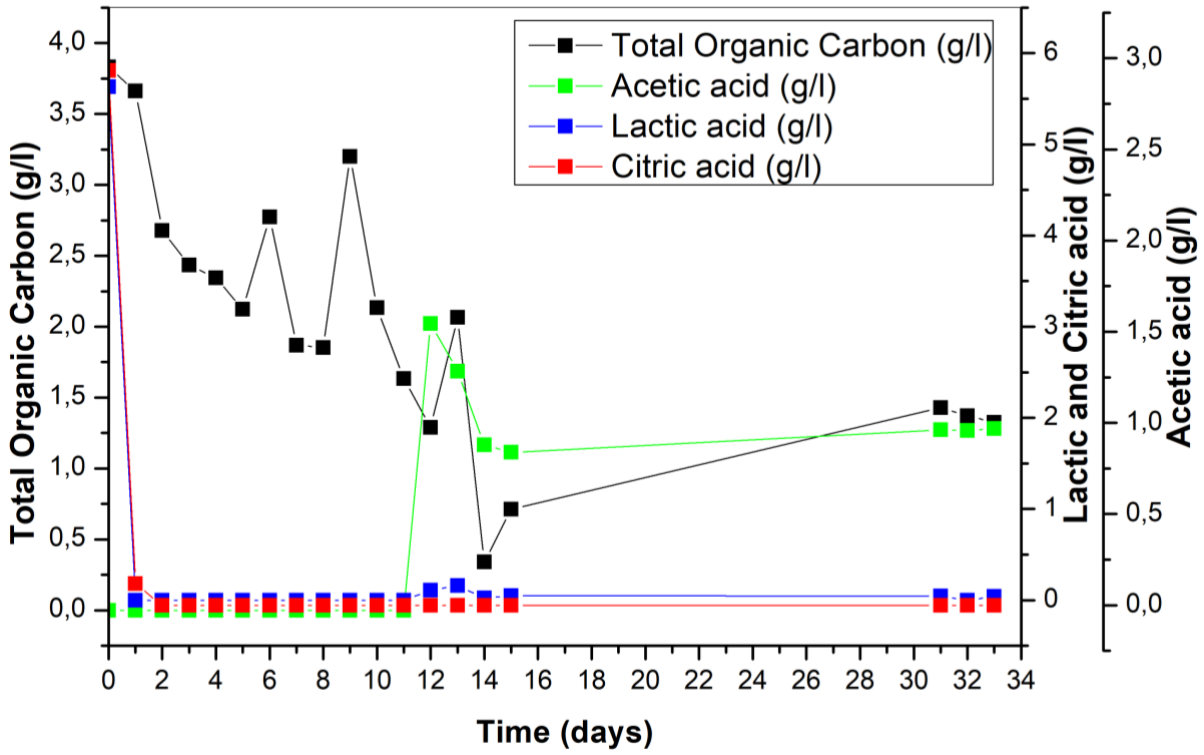

Figure 4.4: Carbon sources and total organic carbon content

The media was incubated at 35 °C, aerobic conditions.

4.5.1 Carbon sources

From the data in Figure 4.4, bacteria started producing lactic acid from day 12 (0.09 g/l). Other organic acids are also produced from the bacteria, such as acetic acid (Douglas, 2004). Acetic acid was discovered at later growth stages on day 12 (Table 4.3). The detection of acetate and elevated TOC values from day 1 was observed despite the rapid depletion of lactic acid and citric acid.

Acetic acid is considered to be one of the most common low-carbon chain fatty acids and is highly corrosive to carbon steel (Wang *et al.,* 2020). Acetate is produced by the homofermentative conversion of glucose by *Clostridium* bacteria identified as 'Acetogenic' (Douglas, 2004). The TOC results revealed that carbon sources were gradually depleting from day 1 to 5, and a slight increase in carbon content was observed on day 6. The carbon content decreased from days 7 and 8, and a sudden increase of 3.1 g/l was observed on day 9. The carbon source gradually decreased again until day 13, when a sudden spike was noticed at 2.1 g/l. After that, a gradual decline in carbon sources occurred. The carbon value then increased to 0.71 g/l after day 14.

The findings are supported by the growth curve (Figure 4.1), although these graphs are different from each other. Both graphs can be compared. When evaluating the TOC graph with the growth of bacteria, it was seen that the spikes in carbon values were also observed around the exponential phases (day 6-13) of bacterial growth. This suggested that the bacteria were producing an unidentified carbon in the exponential phase of growth. However, after day 14, bacterial activity was still evident owing to carbon production, as observed in Figure 4.4; and a decline in bacterial activity was observed in the growth curve after day 14. The media was left for 15 more days, and TOC was evaluated on days 31 to 33. There was still significant carbon content in the media at 1.43 g/l and no decrease, which further supports that the long-term stationary phase of bacterial growth exists.

During prolonged starvation, certain bacterial species enter a continuous cycle of growth and death until there is a renewal of favourable growth conditions, indicating that Gram-positive bacteria produce dormant spores in nutrient-depleted conditions and the Gram-negative bacteria acquire resistance (Navarro *et al*., 2010). This may also explain the irregular TOC pattern (Figure 4.4) observed on day 9, 13 and 15-31.

4.6 KINETIC MODELS FOR LACTIC AND CITRIC ACID DEGRADATION

Concentration degradation models (Figure 4.5 and Figure 4.6) were conducted using AQUASIM 2.0 software, where the black trend line indicates the measured concentration. The error was within range, as indicated by the blue dotted line. Carbon sources were depleted over the 15 days. A general observation was that bacteria used citric acid at a lower rate than lactic acid.

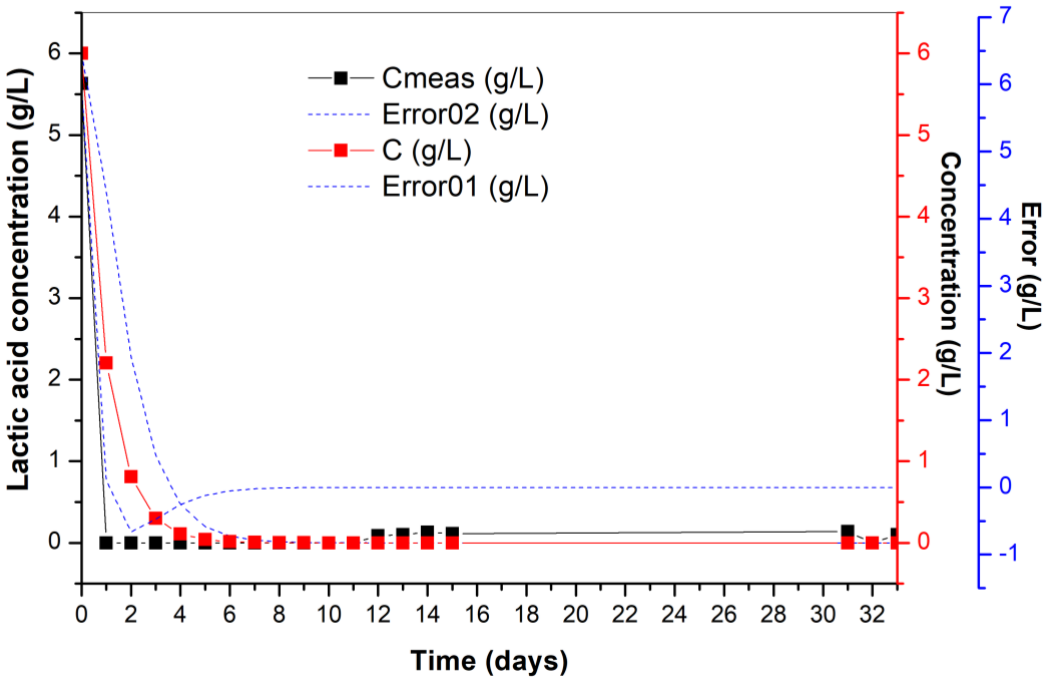

Figure 4.5: AQUASIM sensitivity model of the degradation of lactic acid concentration

The black curve represents the experimental results.

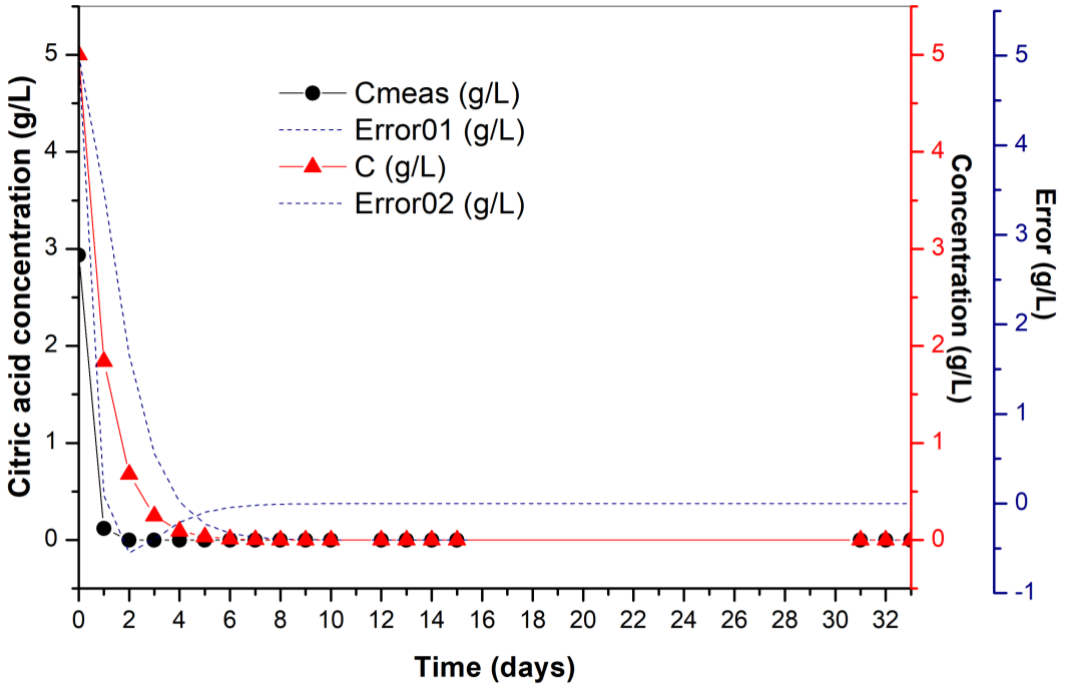

Figure 4.6: AQUASIM sensitivity model of the degradation of citric acid concentration

The black curve represents the experimental results.

4.7 LACTATE AND ACETATE

Lactate and acetate are required for bacterial growth of *Clostridium butyricum* (Detman *et al.,* 2019). Research adapted from bacteria using lactate was used to present pathways identified for lactate in this system (Figure 4.7), which includes lactic acid and acetic acid transformation to possible butyrate and other products by *Clostridium butyricum*. Butyrate production as a metabolite will be further investigated in future studies. It was not investigated in this study. LAB performs an essential function as competitors and hydrogen producers, assisting in balancing bacterial diversity in bioreactors (Douglas, 2004, Sikora *et al.,* 2013).

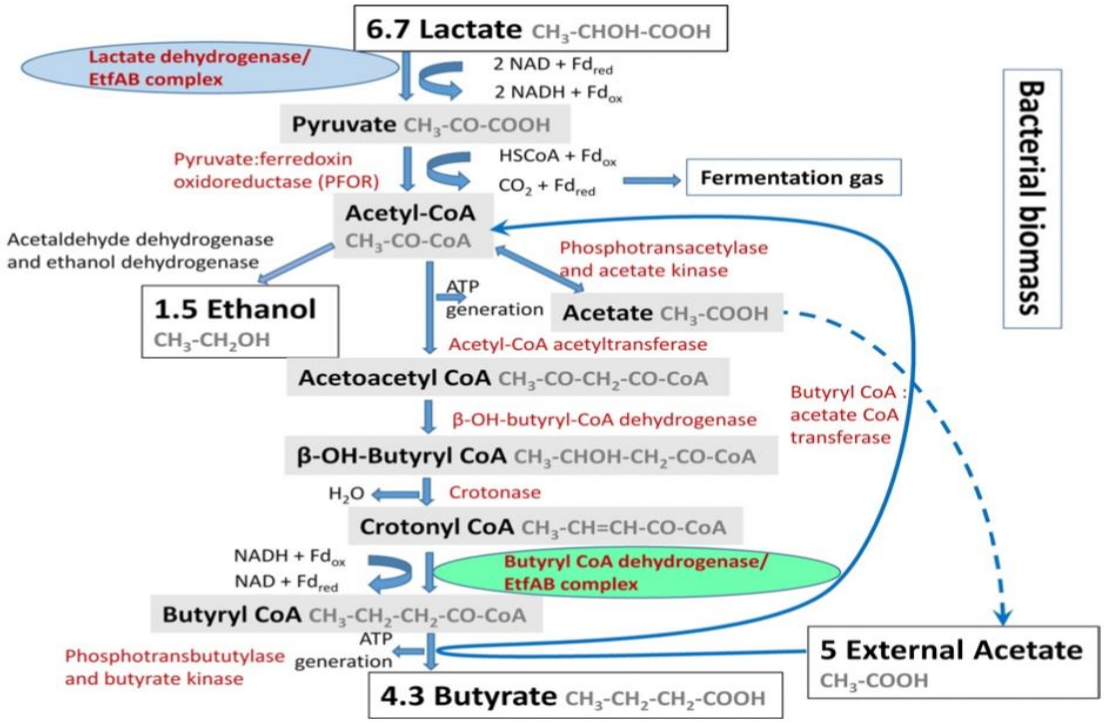

Figure 4.7: Metabolic pathway by Detman *et al.* (2019)

Showing the initial concentration of lactate being depleted by Clostridium butyricum (dehydrogenase process) to form acetic acid and converted to butyrate. The model does not account for producing of lactate and possibly acetoin as metabolites.

4.7.1 Citrate

Citrate is also known to influence the metabolism bacteria (Jung *et al*., 2022). Earlier literature reported that heterofermentative and homofermentative bacteria utilise citrate to produce Acetylmethylcarbinol (acetoin) (Drinan *et al*., 1976), this metabolite was not evaluated in this study. The metabolic by-products of a variety of bacterial species found in nature, can support the growth of another while the attachment of another could provide ligands allowing attachment of others. The competition for substrate and waste may be generated by the initial colonisers, which limit the diversity of the bacterial species (Leung *et al*., 1998, Wimpenny, 2000).

Because of the aforementioned results, *Pseudomonas aeruginosa are* dominant in the marine environment and the reason for corrosion problems. Spectrophotometric results suggest that dominant Gram-negative bacteria (*Pseudomonas aeruginosa)* and Gram-positive spore forming bacteria were growing at an exponential rate, as observed from days 6, 9, and 13. However, according to the CFU results, growth was still observed after day 13, owing to the nutrients in the plate agar, thereby, slowing down the death phase.

There was no stationary phase/residual phase observed with this consortium of bacteria. TOC, and HPLC results support the long-term stationary phase. In the TOC and HPLC results it was observed that there was still total organic carbon, acetate and lactic acid produced beyond 15 days. Further studies on the growth of Gram-positive bacteria in this system could be worthwhile. The spikes in TOC values were perceived in the exponential phase of the bacterial growth curve. Acetic acid and lactic acid by Gram-positive bacteria were produced from day 12 and were also established on days 31 to 33. Metabolites, such as butyrate and acetate, with their corrosion-related properties, can be investigated further. A general finding was that citric acid was utilised at a lower rate than lactic acid. The next chapter further reveals the attachment of the dominant bacteria to rough and smooth-finished surfaces.

CHAPTER 5 SURFACE STUDY

5.1 INTRODUCTION

This study evaluated time differences in bacterial colonisation with surface roughness to understand if these two parameters are proportional to each other. The bacteria cultivated for attachment studies are from the same cooling water system mentioned in CHAPTER 4. CHAPTER 5 comprises three sections. The chapter introduces the reactor set-up on day 1 and provides the microscopy results with a discussion on spatial patterns. Section 5.3 provides the statistical results of colonisation because of surface roughness. Section 5.3 presents the surface roughness parameters obtained before and after bacterial exposure. Section 5.4 presents the microscopy images using SEM and AFM. The chapter then concludes on surface roughness and colonisation.

Figure 5.1: Batch reactor set-up

Alloys as depicted in Figure 5.2(a) were removed from the batch reactor (Figure 5.1) on days 3, 6, and 13. On day 3, spatial patterns were observed on the alloys (rough and smooth finish). Patterns were also evident on day 6; however, these patterns were no longer visible on day

13 alloys. Xavier *et al*. (2009) presented a mechanistic model of cell growth at the surface and indicated that the tension between growth and competition for nutrients explained how patterns emerge in biofilms. The interacting units are vital features which form higher-order structures. The evolutionary competition among microorganisms is poorly understood, which could affect the biological organisation (Xavier *et al.,* 2005). Surface-associated growth helps form biofilms, including a consortium of bacteria in a polymer matrix (Marshall, 1992).

Attachment to a surface was postulated to initiate physiological changes in the cells, which may lead to the overproduction of exopolymers (Davies & Geesey 1995). The exopolymers prevent the movement of the cells on the colonised surface and facilitate the spatial arrangement of the various species with a biofilm (Costerton *et al.,* 1994). The interactions provide the biofilm community with metabolic and physiological capabilities impossible for individual unattached cells (Gilbert *et al*., 1997). Spatial patterns were not evaluated in this study and should be conducted in future work.

Figure 5.2: An example of the smooth and rough alloy exposed to bacteria

Removed on (a) Day 3, day 6, and day 13.

5.2 SURFACE COLONISATION

Bacterial cell counting could not be effectively conducted on smooth and rough-finished surfaces using a SEM microscope. The bacteria could only be visualised by SEM on day 3, discussed in the section below. Table 5.1 presents the surface assessment of the bacterial species abundance using rDNA gene sequencing. The early, middle and late colonisers are presented for rough and smooth surfaces. In this study there were no significant time-related differences in colonisation (Table 5.2) and bacterial levels (Table 5.3) for both surfaces finish p(perm)>0.05 and p>0.05 respectively. The species details can be observed in Appendix A Section 9.1.1.

During the preliminary stages of attachment (Table 5.1), abundant *Clostridium sp*. favoured the rougher finished surfaces with a species abundance of 80.25% compared to the smooth surfaces with a species abundance of 77.76%. *Clostridium sp*. attachment may be higher on the rough finished surface due to friction at the surface and larger surface area. Scratches and grooves observed on the rough surface range from about 1-1.5 µm, the bacteria generally have a width of about 0.5 µm, this then would enhance the attachment of cells to the surface (Park *et al*., 2019, Nouri *et al*., 2023). *Clostridium sp*. contributes to biofilm development and possess metal-related metabolic activities, initiating attachment to the steel surface at early attachment stages (Jeong *et al*., 2023). Frequently ascertained bacteria on the surfaces were *Clostridium sp*; however, *Pseudomonas sp*. were observed during days 3 and 6 and favoured the rough-finished surface (400 grit). *Pseudomonas sp*. were observed only in the later attachment stages of the smooth surface. The bacterium was observed in colony results (Table 4.2), affirming this bacterium was present in both prepared batch media.

The abundant lactic acid and hydrogen-producing bacterium, *Clostridium sp*. was reported to produce organic acids (Wang & Yin 2021) and were associated with corroding metals. The bacterium was not observed on colony plates, possibly owing to the metal substrate absence. To track bacterial species in the cooling water systems and industries, colony plating is regularly conducted. Here, the detection of *Clostridium sp.* could be missed, leading to incorrect dosing strategies. A large number of unknown species (42.72%) were observed on the smooth surface during middle colonisation.

From this study it can be generally stated that a significant proportion of the microbial diversity in the petrochemical industry have not been cultivated and identified owing to the number of unknown bacteria that was observed (Mignard & Flandrois 2006). The Vaal River supplied water to a Vaal reservoir by the use of a pumping abstraction system, which pumped water to a main reservoir. Water was then diverted to a third reservoir which supplied the petrochemical cooling towers. Water quality caused by a change in physical environment, storage capacity and hydraulic conditions, has been reported to affect the microbial communities and microbial growth in water distribution systems (Cheng *et al*., 2019, Guo *et al*., 2021). At the current pace of discovery and characterisation it would take some years to describe the remaining unknown species, relying mainly on research scientists (Bouchet *et al*., 2023). *Comamonas* species were evident only on day 13 rough surface and colonised the surface (91.26%). *Comamonas sp*. were seen in the petrochemical wastewater in Iran (Shokrollahzadeh *et al.,* 2008) and in the gas and pipelines industry, observed with other microbial communities and was not

reported to be associated with corrosion (Zhu *et al.,* 2003). This species of bacteria was observed during the late stages of attachment on the rough surface, indicating cell attachment to the already present (day 3 and day 6) bacteria and biofilm.

As the biofilm develops, the diverse organisms living in the EPS matrix interact according to the organisations of the biofilms. This enables the exchange of metabolites, signalling molecules, genetic material, and defensive compounds, organising interactions among organisms. There is competition among cells in biofilms which involve killing mechanisms or strategies that compromise growth, such as nutrient depletion or quorum sensing (Flemming *et al*., 2016, Smith *et al*., 2023), which have an influence on the biofilm composition. Moreover, incubation time has shown to influence the biofilm composition as seen in Table 5.1, similar findings were observed in the study by Park *et al.* (2019).

The presence of bacterial species *Desulfotomaculum aeronauticum* and *Delftia* at the later stages, infers that their presence may not directly impact steel corrosion at early stages. However, these bacterial species were observed in industrial systems and associated with corrosion (Critchley & Javaherdashti, 2004). *Streptococcus* bacteria observed on day 3 was commonly reported to influence dental materials. There are limited reports on the corrosive effects of this species on industrial grade steels. However, this species of bacteria was reported to produce thin biofilms of about 11 µm on surfaces during early attachment stages (Rozen *et al*., 2001), this is in agreement with the findings in Table 5.1.

Table 5.1: rDNA gene sequencing on the smooth and rough alloy surface with the top five species

Smooth surface (a)	**Species read count**	**% (b)**	**Smooth surface** (a)	**Species read count**	**% (b)**	**Smooth surface** (a)	**Species read count**	**% (b)**
Total early colonisers (Day 3)	1425	100	Total middle colonisers (Day 6)	9315	100	Total late colonisers (Day 13)	9522	100
Clostridium intestinale	804	56.42	*Unknown*	3979	42.72	*Desulfotomaculum aeronauticum*	4548	47.76

Clostridium butyricum	155	10.88	*Clostridium butyricum*	2427	26.05	*Pseudomonas*	3293	34.58
Clostridium metallolevans	149	10.46	*Clostridium metallolevans*	1219	13.09	*Unknown*	473	4.97
Unknown	123	8.63	*Clostridium intestinale*	489	5.25	*Clostridium butyricum*	338	3.55
Streptococcus	50	3.51	*Methylobacterium adhaesivum*	187	2.01	*Sedimentibacter*	233	2.45
Other species [c]	144	10.1	*Other species* [c]	1014	10.88	*Other species* [c]	637	6.69
Rough surface (a)	**Species read count**	**%** [b]	**Rough surface** (a)	**Species read count**	**%** [b]	**Rough surface** [a]	**Species read count**	**%** [b]
Total early colonisers (Day 3)	2486	100	Total middle colonisers (Day 6)	9002	100	Total late colonisers (Day 13)	9767	100
Clostridium metallolevans	986	39.66	*Pseudomonas*	2816	31.28	*Comamonas*	8913	91.26
Clostridium intestinale	702	28.24	*Unknown*	1975	21.94	*Desulfotomaculum aeronauticum*	161	1.65
Clostridium butyricum	307	12.35	*Clostridium butyricum*	1830	20.33	*Unknown*	159	1.63

Unknown	229	9.21	*Clostridium metallolevans*	854	9.49	*Delftia*	98	1.00
Pseudomonas	71	2.86	*Clostridium intestinale*	422	4.69	*Psuedomonas*	55	0.56
Other species [c]	191	7.68	*Other species* [c]	1105	12.27	*Other species* [c]	381	3.90

(a) The P-value among both groups were determined to be >0.05. (b) Species percentage abundance. (c) Other individual bacterial species amounting to less than 1% and attached to the alloy surface.

Table 5.2: Summary of PERMANOVA results

Source	Degrees of freedom (df)	Sum of squares (SS)	Mean squares (MS)	Pseudo-F	P(perm)	Unique perms
Sample group	1	1068	1068	0.56007	0.758	35
Resemblance	5	9534.4	1906.9	0	0	0
Total	6	10602	0	0	0	0

Table 5.3: Quantitative assessment of bacterial levels on rough and smooth surfaces

Days	Absolute copy number (smooth surface)	Absolute copy number (Rough surface)
3	88524.41	1062.1
6	1368.399	2412.291
13	1633.688	8127.978

Table 5.4: Summary of ANOVA results of bacterial levels on the rough and smooth surfaces

SUMMARY	Count	Sum	Average	Variance		
Groups						
Smooth	3	91526.50	30508.83	2524373034		
Rough	3	11602.37	3867.46	14069787.6		
Source of Variation	**SS**	**df**	**MS**	**F**	**P-value**	**F crit**
Between Groups	1064644373	1	1064644373	0.84	0.41	7.71
Within Groups	5076885642	4	1269221411			
Total	6141530015	5				

Results failed to reject the null hypothesis where p(perm)>0.05 (Table 5.2); therefore, there were no significant time-related differences in colonisation on rough and smooth finishes. Moreover, bacterial levels (Table 5.3) on both surface finishes showed no significant differences (p>0.5 in Table 5.4) (Dezelic & Schmidlin, 2009). The results highlighted the importance of conducting third-generation sequencing, identifying the key role players at early stages which preferentially attached to the steel surface. During the initial colonisation (day 3), surface roughness influenced bacterial colonisation. The abundant *Clostridium sp.* bacteria was more prevalent on the rough finished surface. This suggested that during initial colonisation, bacteria attached to the substrate. Middle and late-colonising bacteria may attach to the already present biofilm and bacteria. Surface finish no longer becomes the influencing factor, owing to the growth and maturation of the biofilm formed rapidly (Dezelic & Schmidlin, 2009). Because of the results, this study can be observed in the general context as similar findings were observed in a multispecies study in medical dentistry.

5.3 QUANTITATIVE ASSESSMENT OF THE SURFACE

Table 5.5 presents the root mean square (RMS) roughness values of alloy A before and after bacterial exposure in the batch reactor media. One-way ANOVA was conducted over 3, 6 and 13 days to determine time-related differences among the groups. Generally, on the smooth

surface an increase in surface roughness was observed from a value of 8.68 nm (before bacterial exposure) to 114.67 nm (after bacterial exposure); however, on the rough surface during initial colonisation, the RMS roughness value was lower than the smooth surface with a value of 70.7 nm. This indicated that bacteria had formed biofilm rapidly on the rough surface compared to the smooth surface and produced a smoother surface initially; this was visually supported by the SEM images in Figure 5.5(b). The presence of the bacteria on a surface gives a more irregular surface finish, as the spaces between them would not be filled. This gives more insight into the stages of biofilm formation on a particular surface and future work on biofilm structures may be evaluated. The ANOVA test provided a p-value of $p<0.05$ which rejected the null hypothesis, suggesting there was a significant time-related difference in roughness parameters on the smooth and rough-finished surfaces (Table 5.6). A student t-test (Table 5.7) further confirmed these significant differences among groups. This is due to the amorphous nature of the biofilm. This concluded that multispecies bacterial colonisation was not proportional to surface roughness with a p value of $P<0.05$. Similar observations were reported in a multispecies study by Park *et al.* (2019).

Table 5.5: Mean surface roughness parameters before and after bacterial exposure

Smooth finish [(a)]	**After exposure RMS Rq (nm)**	**Rough finish [(a)]**	**After exposure RMS Rq (nm)**
Day 0	8.68 ± 1.24	Day 0	39.16 ± 15.87
Day 3	114.67 ± 10.69	Day 3	70.70 ± 2.1
Day 6	55.81 ± 11.70	Day 6	260.83 ± 31.35
Day 13	31.25 ± 4.61	Day 13	490.33 ± 121.32

(a) *The p-value among rough and smooth groups were determined to be <0.05 and student t-test showed significant differences. (N=3/group). Scan size of 10 µm.*

Table 5.6: Summary of ANOVA results of surface roughness on rough and smooth surfaces

SUMMARY	**Count**	**Sum**	**Average**	**Variance**		
Groups						
Smooth	15	907	60.47	976.17		
Rough	15	3909.1	260.61	22102.11		
Source of Variation	**SS**	**df**	**MS**	**F**	**P-value**	**F crit**

SUMMARY	Count	Sum	Average	Variance		
Between Groups	300420.15	1	300420.15	26.03	0.000021	4.20
Within Groups	323095.96	28	11539.14			
Total	623516.11	29				

Table 5.7: Student T-test

	Smooth	Rough
Mean	60.47	260.61
Variance	976.17	22102.11
Observations	15	15
Pearson correlation	-0.46	
Hypothesised mean difference	0	
df	14	
t stat	-4.69	
P(T<=t) one-tail	0.00018	
t Critical one-tail	1.76	
P(T<=t) two-tail	0.00035	
t Critical two-tail	2.14	

For the smooth finish, a general increase in surface roughness was observed. The increase in surface roughness may be attributed to decreased bacterial attachment. The biofilm on the smooth surface had not covered the entire surface; this was visually observed in Figure 5.5(a). Bacterial attachment and the presence of *Pseudomonas sp*. may be higher on the rougher surface, inferring that the biofilm was produced at an accelerated rate owing to friction at the surface and larger surface area (Medilanski *et al.,* 2002). This resulted in a smooth textured biofilm layer developing initially, rather than in the later stages of biofilm maturation. More insight into the qualitative assessment of surface roughness and the biofilm is discussed in the next section.

5.4 MORPHOLOGY OF THE ROUGH AND SMOOTH SURFACE

Figures 5.3(a) and (b) depict the AFM three-dimensional images of the rough and smooth-finished alloys before bacterial exposure. SEM images of the alloy before bacterial exposure are depicted in Figures 5.4(a) and (b). Figure 5.5 depicts the SEM images of alloys after

exposure to bacterial media. SEM images on the bacteria and biofilm structures can be observed in Appendix A Section 9.1.4. On day 3 after bacterial exposure, the smooth-finished alloy showed a significant increase in surface roughness, where bacteria were observed on the surface by qualitative assessment (Figure 5.5(a)). The attached bacterial cells were randomly oriented on the surface and not parallel to the polishing scratches. For the rough surface on day 3, the RMS roughness was found to have increased from the unexposed value of ~39.16 nm to 70.70 nm. Visually, the SEM images showed a smoother surface where few bacteria could be observed.

On days 6 and 13, rough surfaces exhibited a further an increase in RMS roughness values (Table 5.5), which may be attributed to the complex biofilm structures, including motile bacteria dispersed on the biofilm surface. This was evidenced by SEM images (Figure 5.5(f)). The lower RMS roughness values observed on these days on the smooth surfaces (Figure 5.5(c) and (e)) did not show presence of the motile bacterium, inferring a smoother surface.

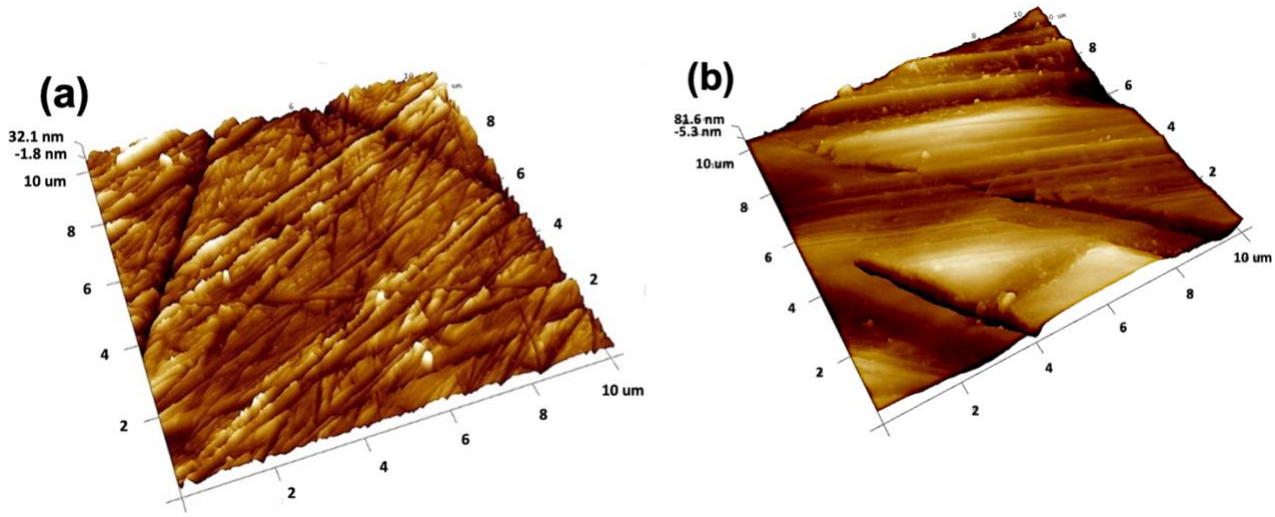

Figure 5.3: Three-dimensional representation of the atomic force micrographs of mechanically polished (a) three-micron and (b) 400-grit finished surfaces

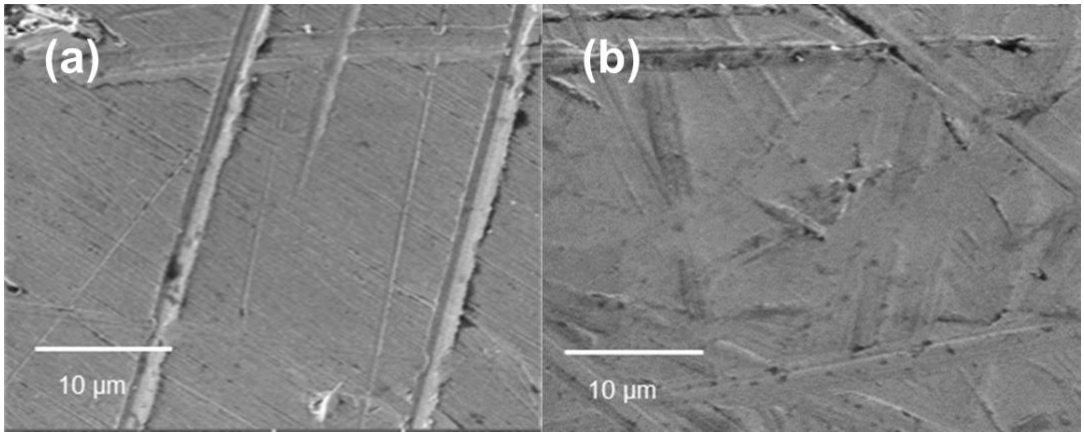

Figure 5.4: Representative SEM images of smooth (a) and rough (b) alloy surfaces

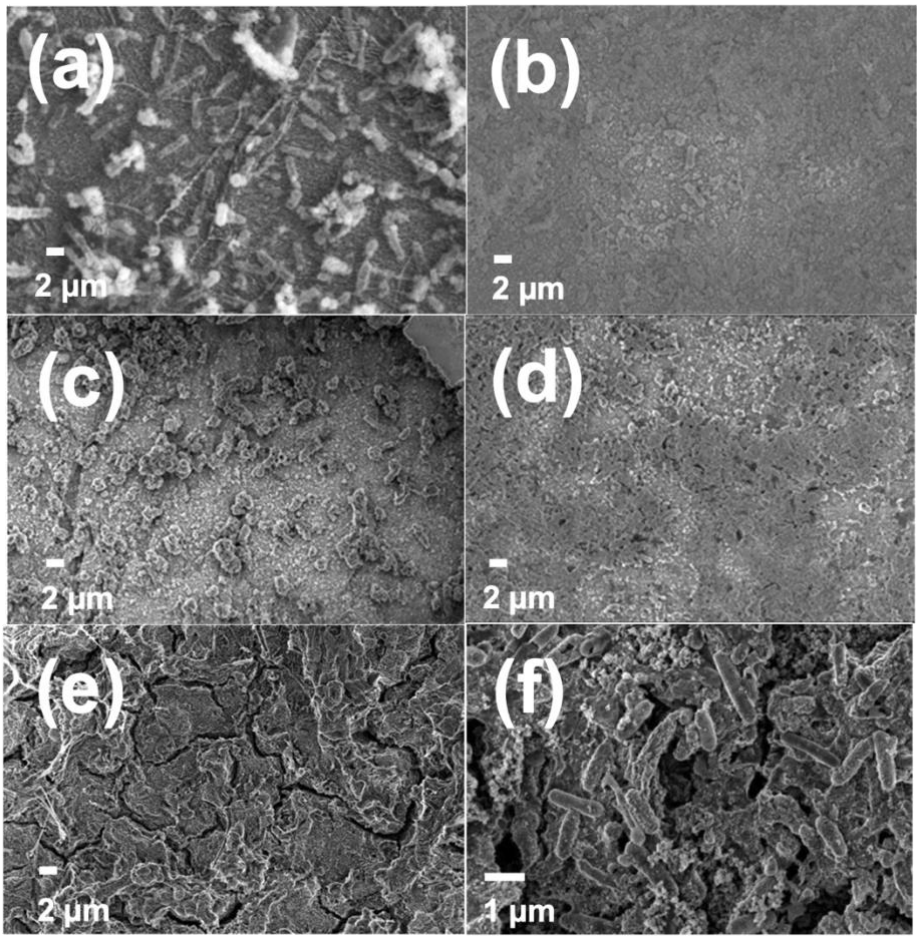

Figure 5.5: Scanning electron micrographs

Depicting biofilm formation, the smooth surface on Days 3(a), 6(c,) and 13(e) and the rough surface on Days 3(b), 6(d) and 13(f).

The microstructure of the unexposed alloy A (Figure 5.6) was compared to the SEM images in Figures 5.7, where the bacterial biofilm and corrosion products were cleaned from the rough and smooth surfaces and revealed intergranular and uniform corrosion. Figure 5.8 depicts the abiotic sample after the surface was cleaned. Figures 5.7(a), (c) and (e) depicts the smooth surface where it was seen that the initial attachment of the bacteria, started the process of intergranular corrosion. This can be visually observed along the grain boundaries (Prithiraj *et al*., 2019). This was seen on day 3 with some damage to the grains. When compared to the abiotic system intergranular corrosion was not observed on day 3, the lamellae were clearly visible in the perlite (Figure 5.8(a)). On day 6, the grains and grain boundaries were visible in some areas of the bacteria exposed samples, and intergranular attack could be observed (Figure 5.7(c)). In the abiotic system there was no damage observed on the surface and the lamellae was still visible on day 6 and day 13. In the biotic system on day 13, the grain boundaries were more visible in comparison to day 6, with certain areas of localised attack to the grain. On the rough finished surfaces (Figures 5.7(b), (d), (f)), uniform corrosion was observed from day 3 and intergranular corrosion was observed with attack to the grain in a localised area (Figures 5.7(b) and (f)). This coincided with the colonisation data on day 3 in Table 5.1 and SEM images in Figures 5.5(a) and (b). On the rough finished surfaces day 3, 6 and 13 in Figures 5.8(b), (d), (e), a more uniform type of corrosion was seen over the entire surface. On day 13 the lamellae in the perlite could still be observed with some damage.

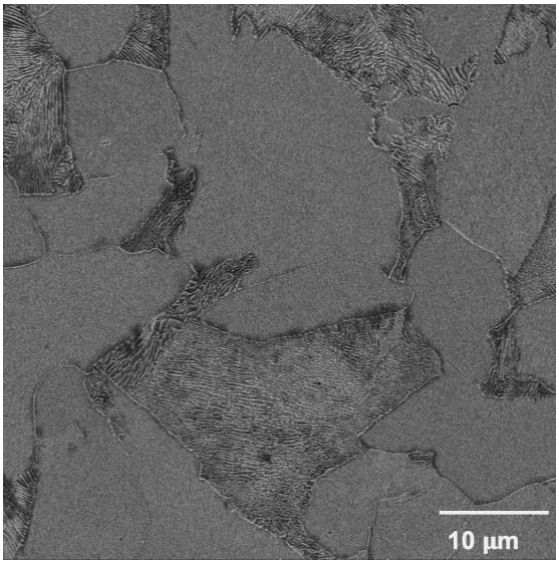

Figure 5.6: Scanning Electron Micrographs of alloy A, etched with nital.

Alloy A (a) showing the perlite (dark area) and ferrite (light area) phases. The lamellae can be seen in the perlite.

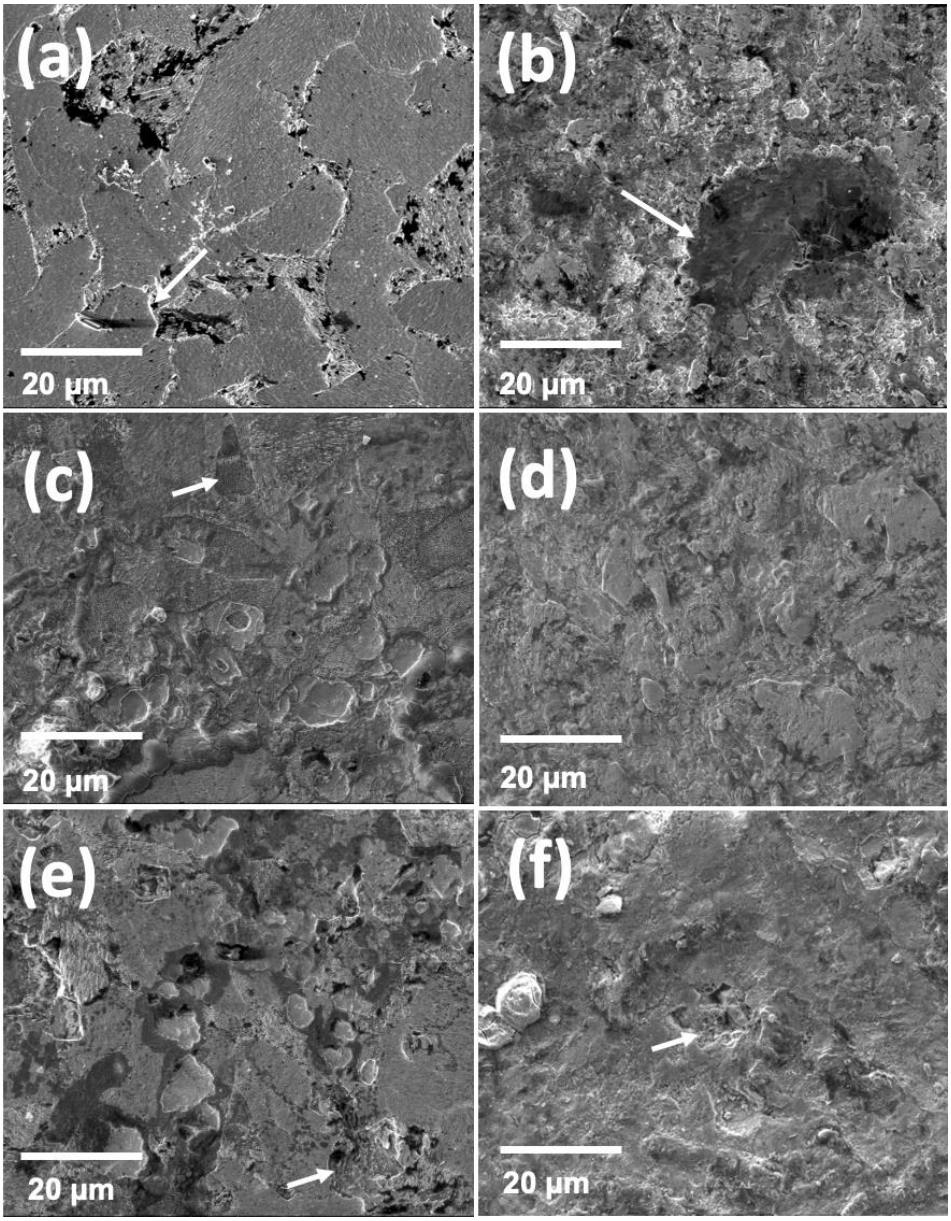

Figure 5.7: Scanning Electron Micrographs of alloy A after cleaning the biofilm and bacteria on the surfaces

Depicting the smooth surface on Days 3 (a), 6 (c) and 13 (e) and rough surfaces on Day 3 (b), 6 (d) and 13 (f). Intergranular corrosion is indicated by the white arrow.

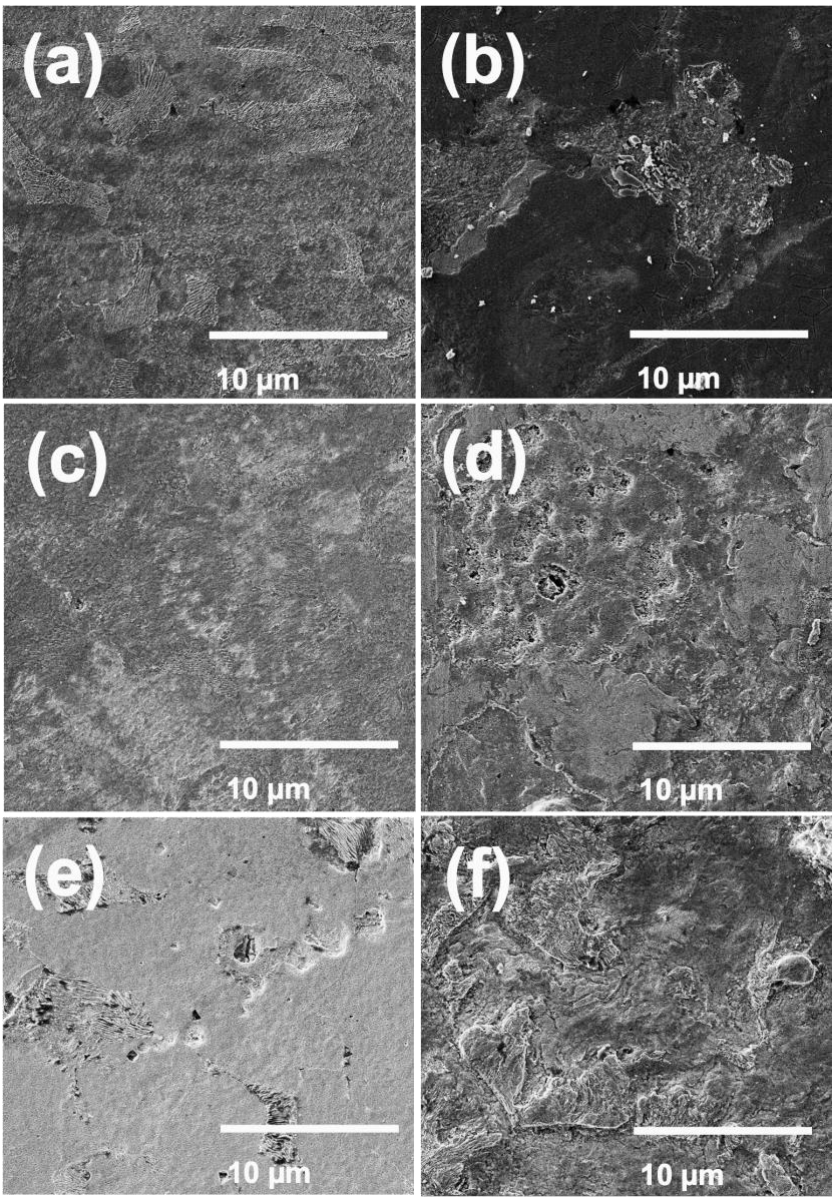

Figure 5.8: Scanning Electron Micrographs after cleaning the corrosion products on the control (abiotic) surfaces, depicting the smooth surface on days 3 (a), 6 (c) and 13 (e) and rough surfaces on days 3 (b), 6 (d) and 13 (f).

It was observed that *Clostridium sp*. may be the reason for the intergranular corrosion attack owing to the fact that this species was seen to dominate the smooth finish (Table 5.1). Preferential attachment and synergistic behaviour of both bacterial strains (*Clostridium sp. and Pseudomonas sp*.) facilitated a more severe combination of intergranular and uniform corrosion attack on visual observation. This was supported by the relative abundance of this species on the rough surface during initial colonisation stages (Table 5.1), evaluation of

corrosion rates may give more insight on the extent of corrosion. Correlation analysis together with regression analysis was conducted on the species abundance and corrosion rates. Moreover, the formation organic acids may affect the corrosion rate of steel (Xi *et al.,* 2020). Routine colony plate analysis conducted by the industry could fail to detect *Clostridium sp.* The bacteria also produced key elements known as corrosion initiators, which can further decrease the iron content. This will be discussed in the next Chapter.

CHAPTER 6 STEEL CORROSION

6.1 INTRODUCTION

The study evaluated corrosion because of bacterial attachment and metabolic activity. Section 6.2 comprises elemental mapping and spectra of alloy A after bacterial exposure. Section 6.3 includes the corrosion rates obtained for alloy grades A rough and smooth-finished surfaces to recommend the best candidate surface finish in preventing biofilm facilitated corrosion. Section 6.4 explicates the Raman spectroscopy results of alloy A with corrosion products which could provide more insight into the corrosion rates obtained. Last, Section 6.5 includes a detailed discussion of the results obtained from FTIR on alloy A to evaluate the functional groups involved in the corrosion process.

6.2 ELEMENTAL MAPPING

The elemental analysis of alloy A before bacterial exposure was used in this study and were obtained conforming to ASTM E415 standards (Table 6.1). A general observation was made on the carbon content. Before bacterial exposure, carbon values for alloy A, in weight percent were determined to be; 0.19%, with iron being 98.29%. After bacterial exposure with biofilm, elemental analysis using EDX on the SEM was used and carbon values for alloy A were observed to be; 7.23% on day 3, 12.18% on day 6 and 8.52% on day 13 (Table 6.1 and Appendix A Section 9.1.2). After removing the biofilm from the surface, EDX detected carbon about 10% on day 6 (Table 6.2). In the abiotic system carbon was seen to be 7.10% on day 6. The presence of the high carbon element detected by EDX analysis is commonly detected in biofilms is a principal component of the bacterial cells. Moreover, metals are able to adsorb organic molecules such as yeast extract. The original iron content in Table 6.1 (before exposure 98.29%) was compared to the iron content after bacterial exposure (Table 6.2). It was seen that the iron had depleted to a value as low as 46.91% on day 13. When compared to the abiotic (control) system iron was observed to be 90.06%. Balamurugan *et al*. (2016) reported a similar minimum value for iron in the firewater system containing Iron reducing bacteria (IRB), also known as *Pseudomonas sp.* Elements in the biofilm, such as sulphur, were observed at the highest value of 1.9% on day 13, phosphorus at 0.33% on day 3, and then further depleted to 0.11% on day 13. The presence of elements such as phosphorus,

sulphur, and chloride with organic acids are corrosion initiators. The sections below discuss how bacterial attachment at preliminary stages affects the corrosion rate of the steel aforementioned.

Table 6.1: Elemental composition of smooth alloy A before and after bacterial exposure with biofilm on days 3, 6, and 13

Elements	Alloy A before exposure [a]	Alloy A after exposure on day 3 [a]	Alloy A after exposure on day 6 [a]	Alloy A after exposure on day 13 [a]
C	0.19	7.23	12.18	8.52
Fe	98.29	74.60	57.15	58.51
Si	0.26	0.22	0.21	0.17
Mn	0.87	0.00	0.00	0.93
P	0.00	0.33	0.56	0.11
S	0.00	0.24	0.33	1.89
Cr	0.10	0.00	0.00	0.00
Mo	0.10	0.00	0.00	0.00
Ni	0.02	0.24	0.27	0.27
Al	0.03	0.00	0.00	0.00
Cu	0.01	0.00	0.00	0.00
Nb	0.02	0.00	0.00	0.00
Ti	0.01	0.00	0.00	0.00
V	0.03	0.00	0.00	0.00
Cl	0.00	0.02	0.01	0.00
K	0.00	0.03	0.11	0.00
W	0.05	0.00	0.00	0.00
Na	0.02	0.47	0.78	0.00
O	0.00	16.60	28.27	29.60
Ca	0.00	0.03	0.14	0.00
Total	100	100	100	100

(a) Units stated in Weight%.

Table 6.2: Elemental composition of the smooth alloy A in the abiotic system and after bacterial exposure (without biofilm).

Elements	Alloy A abiotic system on day 3 (cleaned) [a]	Alloy A abiotic system on day 6 (cleaned) [a]	Alloy A abiotic system on day 13 (cleaned) [a]	Alloy A after exposure on day 3 (without biofilm) [a]	Alloy A after exposure on day 6 (without biofilm) [a]	Alloy A after exposure on day 13 (without biofilm) [a]

C	7.19	7.10	5.95	8.08	9.94	9.05
Fe	84.66	86.71	90.06	84.65	60.2	46.91
Mn	0.83	0.85	0.97	0.82	0.67	0.61
O	7.32	5.35	3.02	6.45	29.1	43.4
Total	100	100	100	100	100	100

(a) Units in weight%

6.3 CORROSION RATE

A best performance steel finish is recommended based on corrosion evaluation in this section. The corrosion rate was observed to have started in the lag phase (day 3) and exponential phases (day 6) of bacterial growth (Figure 4.1). Corrosion rate data (Table 6.3) revealed high corrosion rates when alloys were exposed to bacteria. Smooth surfaces of alloy A were seen to perform best in this system when exposed to the bacteria. It was observed overall that there were reduced corrosion rates on day 13. Although *Clostridium sp*. was more prevalent on all surfaces, *Pseudomonas sp*. were observed on the rough surfaces on day 3 and 6 (Table 5.1). Preferential attachment of the bacterial species on these days affected the corrosion rate, thereby changing the corrosion kinetics of the steel. No significant differences in corrosion rates were observed on both rough and smooth groups. However, when conducting ANOVA only on day 6 rough and smooth surfaces, there was a significant difference observed ($p<0.05$) in Appendix Section 9.2. This gave indication that the increased or decreased biofilm RMS roughness does not necessarily result in high corrosion rates of steel at different periods of exposure. This was evidenced by the RMS roughness values in Table 5.5. Where a high RMS roughness value of 490.33 nm on the rough surface on day 13, showed lower corrosion rates (1.20 mm/y) as seen in Table 6.3. The RMS roughness value (260.83 nm) on day 6 gave a higher corrosion rate (38.72 mm/y) on the rough surface when compared to day 13. For the smooth surface on day 3 the RMS value was 114.67 nm with a corrosion rate of 2.25 mm/y however, on day 13 the RMS roughness observed (31.25 nm) gave a lower corrosion rate (0.24 mm/y). The correlation and regression analysis of the species abundance and corrosion rate proved there was no significant ($p>0.05$) linear relationship between smooth and rough surfaces.

Table 6.3: Summary of corrosion rates of the rough and smooth alloys

Alloy A	Without bacterial exposure (smooth) [(a)]	With bacterial exposure (smooth) [(a)]	Without bacterial exposure (rough) [(a)]	With bacterial exposure (rough) [(a)]
Day 3	0.31 ± 0.04	2.25 ± 0.13	1.02 ± 0.05	1.72 ± 0.02
Day 6	0.32 ± 0.15	-96.54 ± 0.17	0.40 ± 0.02	38.72 ± 0.15
Day 13	0.29 ± 0.03	0.36 ± 0.13	0.24 ± 0.02	1.20 ± 0.05

(a) Units stated in mm/y. p>0.05

A general increase in the corrosion rates was observed for smooth and rough-finished surfaces when exposed to bacteria on days 3, 6, and 13 (Table 6.3) compared to the control system. In the control system the rough alloy on day 3 exhibited higher corrosion rates when compared to the control smooth alloy on day 3. This occurrence was reported in a study by Kim *et al*. (2013), where it was evidenced that the increased surface roughness without microbial influence may also have an effect on the corrosion of steel. However, not as substantial as in a system with bacteria. On the contrary, in the presence of bacteria, the smooth surface on day 3 indicated higher corrosion rates when compared to the rough finished surface on day 3. This indicated that there was corrosion resistance and was observed to be the attachment and formation of biofilm by *Pseudomonas sp*. on day 3 (Table 5.1). Whereas *Pseudomonas sp*. was not observed on the smooth surface. Bacterial biofilm formation on the rough finished surface was supported by the SEM images on day 3 (Figure 5.5(b)). There was an instance of mass increase rather than the expected mass decrease observed on smooth alloy A on day 6 (-96.54 mm/y), this behaviour was not observed in the control system and showed stable corrosion rates of 0.32 mm/y. The mass increase (approximately 1.24 g carbon) observed may be owing to carbon-metal bonding by acetogenic and hydrogen-producing species (*Clostridium sp*.) forming covalent bonds with iron. The elemental carbon map can be observed in Table 6.1 and Appendix A Section 9.1.2.

Enzymes may direct the hydrogen and carbon dioxide produced by the bacteria into the acetogen metabolism, where their active sites share carbon-metal bonds. Douglas (2004) and Martin (2019) reported carbon-metal bonding in steel. It is to be noted that in addition the carbon-metal bonding phenomenon, surface sensitive IR such as FTIR may be used to detect C-Fe bonds to further prove the presence of these bonds, this is discussed in the subsequent section.

For rough alloy A exposed to bacteria on day 6, the highest corrosion rate was observed with a value of 38.72 mm/y. This was a significant increase in corrosion rate compared to the low corrosion rate of 0.40 mm/y observed in the system without bacteria. This then supported the SEM images in Figure 5.7(d), where a combination of uniform and intergranular corrosion was observed over the entire surface. Alloy A smooth finished steel had shown to perform better than the rough finished surfaces.

In light of the results, alloy A smooth finished steel was recommended in this bacterial system. It is to be noted that this specific material is susceptible to pitting corrosion when exposed to bacteria using rough industry standard surface finishes and was reported in a study using accelerated corrosion methods (Prithiraj *et al*., 2019). Pitting corrosion was not observed after cleaning the surfaces (Figure 5.7). This may be due to the type of bacteria which attached to the specific steel grade. Instances of high corrosion rates and mass increase on day 3 and day 6 rough surfaces specifically, may be owing to the synergistic behaviour of *Pseudomonas sp*. and *Clostridium sp*., which attached to the rough surface on day 3 and 6 (Table 5.1). The results in Table 5.1 agree with the findings from Xi *et al*. (2020) and Douglas (2004). In the current study, *Pseudomonas sp*. was revealed to grow rapidly from day 3 and are capable of producing organic acids from as early as day 1 of growth (Xi *et al.,* 2020). The decrease in corrosion rates observed after long-term exposure (day 13) is likely due to the formation of a biofilm layer by *Pseudomonas sp.* that alleviated the corrosion rate (Xi *et al.,* 2020). However, *Clostridium sp.* and *Pseudomonas sp.* together play an essential role in the protection of steel during long-term exposure by formation of a magnetite layer. The formation of the magnetite layer is discussed in the subsequent section.

6.4 CORROSION PRODUCTS ANALYSIS

The evaluation of corrosion products on a carbon steel surface, gives insight on how bacterial attachment and excretion of organic acids play an essential role in the corrosion process. Table 6.5 and Figure 6.1 below present the Raman spectroscopy results of the alloy surface, which indicates three corrosion products, including the possible corrosion product mackinawite with the respective spectral peaks. The alloy surface analysis revealed areas of yellow, reddish brown, and black (Appendix A Section 9.1.3.1). The three corrosion products observed by the Raman spectra were lepidocrocite, goethite, and magnetite. Similar corrosion products on carbon steel were reported in a study by Refait *et al*. (2020).

Lepidocrocite is usually formed at the preliminary stages of the corrosion process, and an increase in exposure time can induce the phase transformation to goethite (Balamurugan *et al.,* 2016). This particular phase transformation was observed in this study on day 3 at 250 cm^{-1}. Lepidocrocite was not easily evident on day 3 from the Raman spectra and rather from Figures 6.2-6.3. Figure 6.3 revealed lepidocrocite on the surface, which was characterised as sharp flower-like structures protruding from the surface. On day 13, lepidocrocite could be observed at intense peaks of 375 and 1308 cm^{-1} and on day 6 at 385 cm^{-1}; however, the peaks were not intense. It can be deduced that mixture of lepidocrocite and goethite was observed on day 13, owing to the phase transformation.

Magnetite was more intense on day 13 (Figure 6.4), taking the shape of dark and flattened discs; this was observed by the Raman shift of 660 cm^{-1} (Antunes *et al.,* 2014). The long-term exposure of the alloy suggests that the magnetite iron oxide formation was owing to microbial activity (Balamurugan *et al.,* 2016). Magnetite peaks only formed from day 6 and were observed as intense peaks on day 13. This was further supported by the day 13 SEM results in Figures 5.7(e) smooth surfaces, where intergranular attack was alleviated on the smooth surfaces (day 13) and some grain boundaries were still visible. This means that the magnetite layer protected the steel surface from further corrosion. There were no magnetite peaks observed on day 3, which further infers that higher corrosion rates could be expected from days 3 and 6 and was evidenced in the corrosion rate results (Table 6.3).

Iron-reduction by *Clostridium sp*. and *Pseudomonas sp*. were involved in the formation of Fe_3O_4 (Magnetite). Organic acids play an important role and are described by Equation 3 (Sun *et al.,* 2014). The presence of the acid can be confirmed by the Fourier transform infrared spectroscopy. However, the presence of the acid was confirmed in the HPLC results in Figure 4.4.

$$CH_3COO^- + 8Fe(OH)_3 \rightarrow 8Fe^{2+} + 15OH^- + 2HCO_3^- + 5H_2O \quad (3)$$

A summary of the Raman spectral peaks on days 3, 6, and 13 is shown in Table 6.4, highlighting the three corrosion products and possible mackinawite. Details on reported values can be observed in the Appendix A Section 9.3.1.

Table 6.4: Corrosion products formation of alloy A after bacterial exposure

Corrosion product	Exposure time in Days	Wavenumber (cm^{-1}) observed in this study	Values close to the reference below	Notes
Lepidocrocite (γ- FeOOH)	Day 3 (no Raman peak, deduced SEM Figure 6.2-6.3), and day 6, day 13 (most intense bands)	375 cm^{-1}, 1308 cm^{-1}	Antunes *et al*. (2014:2014)	Kartsonakis & Charitidis (2020) reported values of 393 cm^{-1}. Boucherit *et al*. (1989) reported a value of 1307 (intense peaks).
Goethite (α - FeOOH) Mackinawite	Day 13 (Sharp intense peak) and day 6 (not intense)	250 cm^{-1}	Leban & Kosec (2017), Genchev & Erbe (2016)	Kartsonakis & Charitidis (2020) reported a value of 273 cm^{-1} for goethite. Genchev & Erbe (2016) reported 253 cm^{-1} for mackinawite.
Magnetite (Fe_3O_4)	Day 6 and day 13 (very broad)	688 cm^{-1}, 660 cm^{-1}	Antunes *et al*. (2014), Genchev & Erbe (2016), Colomban *et al*. (2008), Bellot-Gurlet *et al.* (2009).	Kartsonakis & Charitidis (2020) reported a value of 683 cm^{-1}.

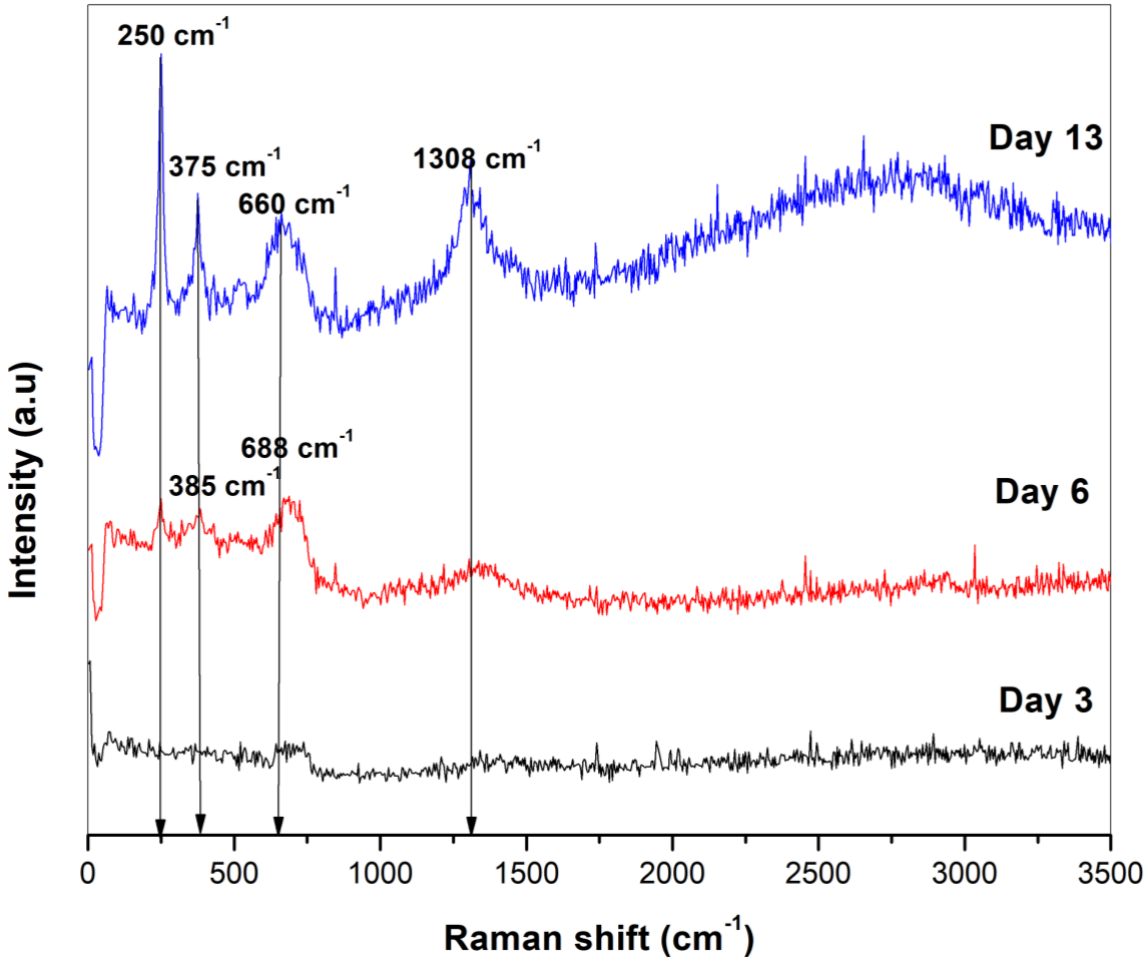

Figure 6.1: Raman spectra of alloy A after exposure on days 3, 6, and 13

In light of the results, FeS peaks (sharp and intense) were reported between 200 and 375 cm^{-1} (Dwivedi *et al.,* 2017, Genchev & Erbe 2016). In this study, peaks were observed in from day 6 to day 13 at 250 and 375 cm^{-1} respectively and were identified as the corrosion product mackinawite; however, in the study by Genchev and Erbe (2016), lepidocrocite and goethite were not identified, resulting in an overlap of these values, especially between 200 and 1308 cm^{-1}. On day 6, blackening of the batch reactor media (inoculated with bacteria) was observed. It was reported that *Clostridium sp.* can produce sulphide during growth, increasing iron-reduction (Shah, 2013). This was further supported by the Raman spectra where mackinawite was observed at 250 cm^{-1}. Elemental mapping results indicated a rapid decrease in iron content to 46.91%, indicating the presence of sulphur (Table 6.2). The control media without bacteria blackened only on day 13; this could be owing to lactate being an electron donor.

When sulphate is reduced to sulphide, it reacts with iron (either in the solution or solid) to produce black ferrous sulphide (Equations 6 and 7). (Little *et al*., 2006).

The electron donor is from lactate (lactic acid $C_3H_6O_3$) and metal, as in Equations 4 and 5.

4Fe + $SO_4^{2-} + 8H^+ \rightarrow 4FeS + 4H_2O$ (4)

$2C_3CHOHCOO^- + SO_4^{2-} + H^+ \rightarrow 2CH_3COO^- + 2CO_2 + HS^- + 2H_2O$ (5)

The corrosion products have these reactions:

$Fe^{2+} + S^{2-} \rightarrow FeS$ (6)

$Fe^{2+} + CO_2 + OH^- \rightarrow FeCO_3 + H^+$ (7)

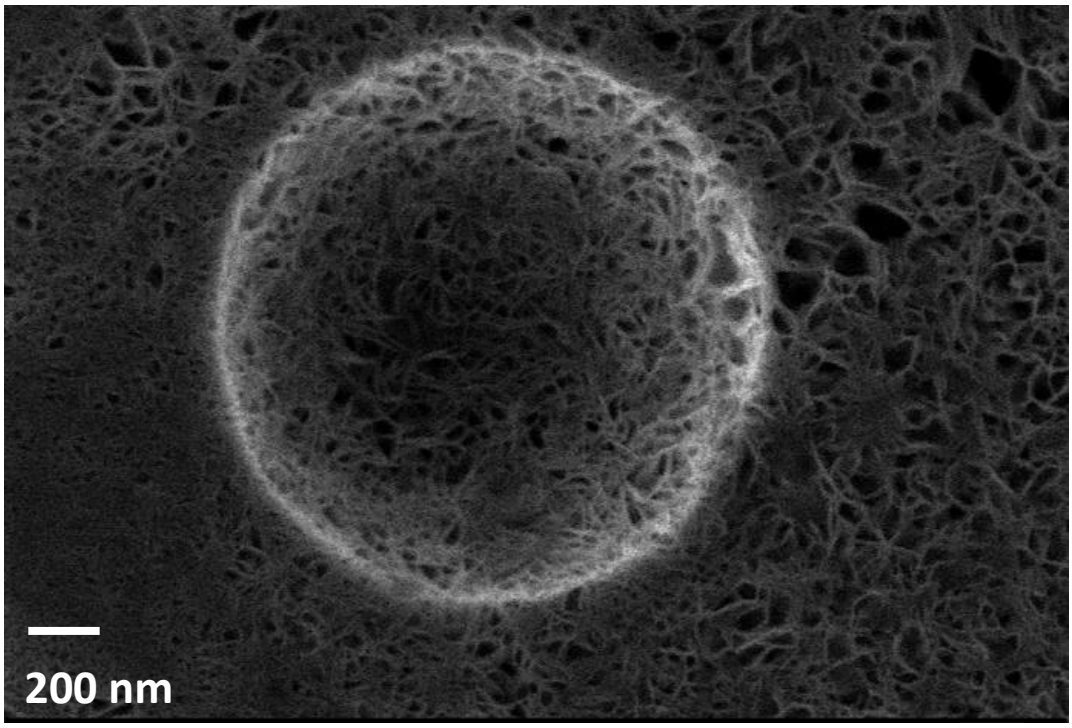

Figure 6.2: Sharp flower-like structures of lepidocrocite were observed in the pits, also seen in another study with carbon steel (Antunes *et al.*, 2014)

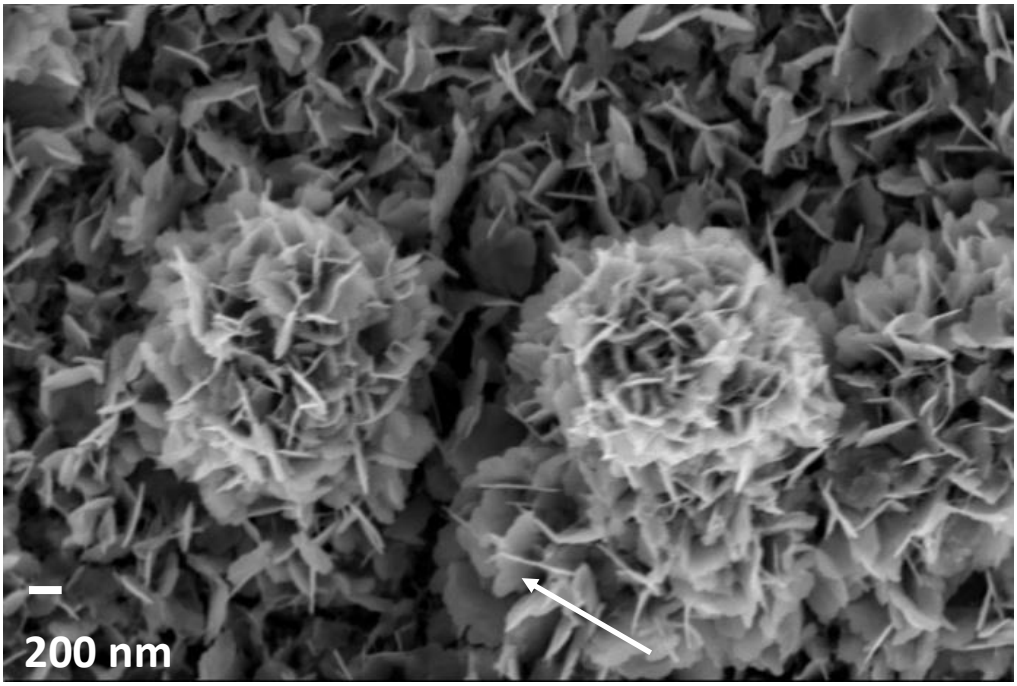

Figure 6.3: Lepidocrocite can be observed (white arrow) on day 3 as thin flower-like protruding structures

Similarly, seen in a study on carbon steel by Thalib et al. (2018).

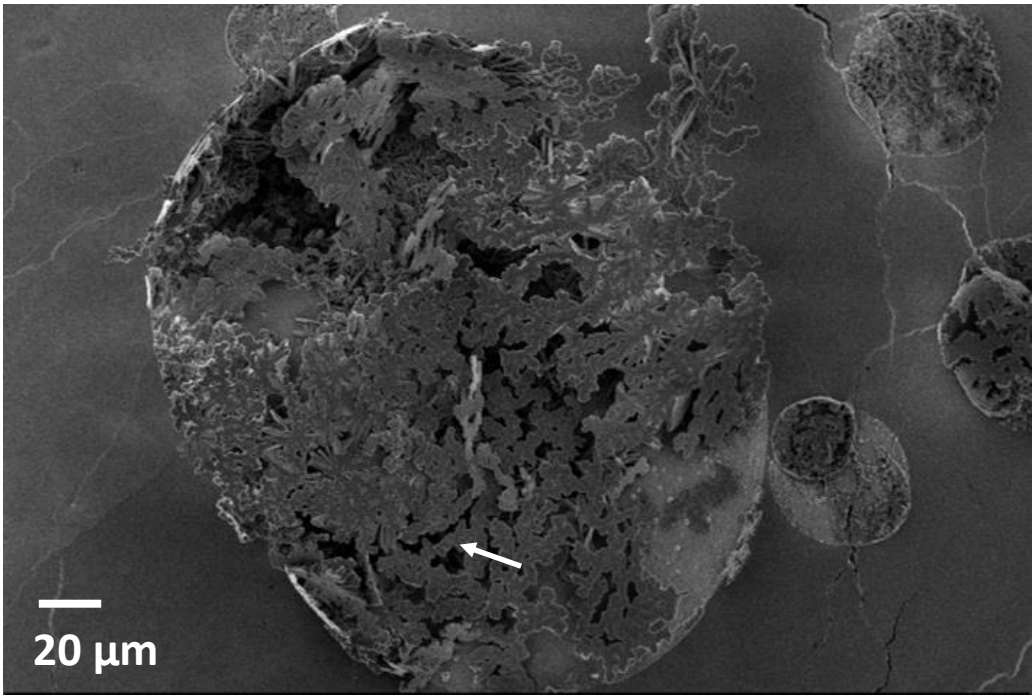

Figure 6.4: Flattened and dark discs (white arrow) of magnetite formed on top of the bulb-like structure

Also seen in another study with carbon steel (Antunes et al., 2014).

The attachment of dominant bacteria *Clostridium sp.* and *Pseudomonas sp.* with their metabolites (acetate) play an important role in the kinetics of steel. Functional groups further prove that these metabolites were observed from day 1 and are responsible for the accelerated corrosion rates observed on days 3 and 6.

6.5 KEY FUNCTIONAL GROUPS

Results in Figure 6.5 and Table 6.5 indicted that there were only slight differences in peak intensity over days 3, 6, and 13. Where day 13 indicated more intense peaks of carbonyls. There was an intense peak of acetylenic compounds observed on day 3.

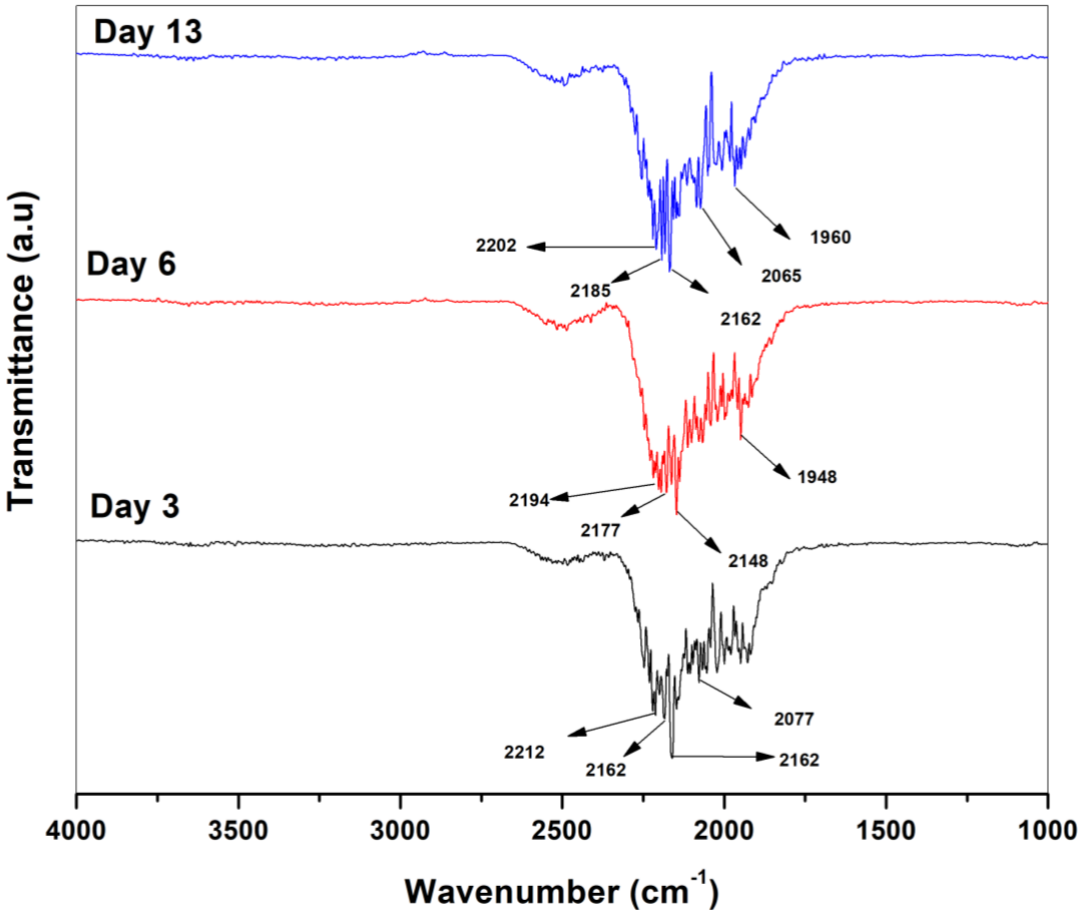

Figure 6.5: FTIR spectra of smooth alloy

It is hypothesised that acetate may be produced from the preliminary stages of bacterial growth as a sharp acetylenic peak (2162 cm^{-1}) was observed on day 3. Future work should be conducted to ascertain the presence of this metabolite.

Day 3 shows acetylenic compounds stretching at 2162 cm^{-1}. Day 6 showed the acetylenic compound peak was less intensified (2148 cm^{-1}), and the carbonyl peak was still present at 1948 cm^{-1}. Day 13 showed acetylenic compounds at a stretch of 2162 cm^{-1}, indicating decreased amounts of acetic acid by the bacteria.

Table 6.5: Functional groups

Origin	**Group frequency wavenumber cm^{-1}**	**Group frequency wavenumber cm^{-1} from literature**	**Assignment**	**Reference**
C ≡ C	2212, 2162, 2183, 2194, 2177, 2148, 2202, 2185, 2162	2260 cm^{-1} – 2100 cm^{-1}	Acetylenic compounds	Coates (2000)
Transition metal carbonyls	2077, 1948, 2085, 1960	2100 cm^{-1} – 1800 cm^{-1}	Transitional metal carbonyls	Coates (2000)

It was observed that the acetylenic compounds in the form of acetic acid were detected most intensely on the surface of the alloy from early stages of exposure (day 3 and day 6), in the region of 2500-2000 cm^{-1}. Corrosion results (Table 6.3) indicated high corrosion rates on day 6. A decrease in corrosion rates was observed on day 13; and was evidenced by the less intensified acetylenic peak on day 13 (Figure 6.5). The carbonyl peak was formed from day 3 and intensified on day 6 only. The intensified metal carbonyl peak on day 6 gives indication of C-Fe bonds. This further proved that the carbon-metal bonding is a possible phenomenon as discussed in Section 6.3. The bacteria had produced acetic acid—a mechanism of corrosion, a recent study reported that acetate was a requirement for bacterial growth of *Clostridium sp*. (Detman *et al.,* 2019).

CHAPTER 7 CONCLUSION

This industrial study proved that no residual phase was observed with the growth of this bacterial consortium; however, a long-term stationary phase was observed. The statistical data suggested that there were no significant time-related differences on the species abundance ($p(perm)>0.05$) and bacterial levels ($p>0.05$) the on surfaces. However, on day 3 the abundant *Clostridium sp*. bacteria was more prevalent on the rough finished surface. Time-related differences were observed on the RMS roughness ($p<0.05$) values with no significant differences in microbial corrosion rates within rough and smooth groups ($p>0.05$). It is worth mentioning that there were only significant differences on day 6 ($p<0.05$). At the peak of the exponential phase of bacterial growth, a decline in corrosion rate was observed. Furthermore, *Pseudomonas sp*. were seen to preferentially attach to the rough surfaces indicating higher corrosion rates than the smooth surface. Visually the dominant strains facilitated a more severe combination of corrosion attack. Presence of acetylenic compounds and sulphur induced high corrosion rates by formation of a magnetite film which involved the bacterial metabolism. Smooth steel A106 GB proved to be the best candidate steel to prevent biofilm facilitated corrosion.

CHAPTER 8 FUTURE WORK

Studies can be conducted on Gram-positive species and their long-term survival in nutrient-depleted conditions. Future work can be done in cultivating and identifying the unknown species to understand their ecology and impact in the petrochemical industry. Further research on carbon-metal bonding and enzymatic channelling of hydrogen by acetogenic bacteria on this alloy will be worthwhile. Metabolites, such as butyrate and acetate, with their corrosion-related properties, can be investigated further. New metabolic pathways can then be developed. Further investigation of spatial patterns can present more insight into the bacterial ecology in this system. More investigation is needed to prevent early colonisation of dominating and abundant species to the smooth-finished surface of alloy grade A 106 GB.

In this study it was impractical to conduct in-situ studies, implementation of a modified coupon rack may be designed to hold multiple coupons for analysis on different days. Early and middle colonisation should be taken into account, this includes implementation of sterile conditions for assessment of coupons. Bacterial growth and attachment should be evaluated in conditions where the media contains hydrocarbons. Manufacturing of a special plasmid with qPCR may be conducted on the abundant species *Clostridium sp.* that attached to the surface during early stages. This work may be used in the industry to control biofilm facilitated corrosion during new installations with focus on targeting attachment of the abundant and dominating bacteria.

REFERENCES

Achinas, S., Charalampogiannis, N., & Euverink, G. J. W. 2019. A Brief Recap of Microbial Adhesion and Biofilms. *Applied Sciences*. Molecular Diversity Preservation International and Multidisciplinary Digital Publishing Institute, 1-15.

An, Y. H. & Friedman, R. J. 1997. Laboratory methods for studies of bacterial adhesion. *Journal of Microbiological Methods, 30*(2): 141-152.

Anselme, K., Davidson, P., Popa, A. M., Giazzon, M., Liley, M., & Ploux, L. 2010. The interaction of cells and bacteria with surfaces structured at the nanometre scale. *Acta Biomaterialia*, 10(6): 3824-3846.

Antunes, R. A., Ichikawa, R. U., Martinez, L. G., & Costa, I. 2014. Characterization of corrosion products on carbon steel exposed to natural weathering and to accelerated corrosion tests. *International Journal of Corrosion,* 2014.

Arnold, J. W. & Bailey, G. W. 2000. Surface finishes on stainless steel reduce bacterial attachment and early biofilm formation: scanning electron and atomic force microscopy study. *Poultry Science*, 79(12): 1839-1845.

Babu, S. S., Möhwald, H., & Nakanishi, T. 2010. Recent progress in morphology control of supramolecular fullerene assemblies and its applications.

Balamurugan, P., Chandramohan, P., & Rao, T. S. 2016. Corrosion management of carbon steel material: Operational modes influence corrosion rate–An in vitro study. *RSC Advances*, 6(47): 41122-41129.

Balzer, M., Witt, N., Flemming, H. C., & Wingender, J. 2010. Faecal indicator bacteria in river biofilms. *Water Science and Technology*, 61(5): 1105-1111.

Bauer, S., Arpa-Sancet, M. P., Finlay, J. A., Callow, M. E., Callow, J. A., & Rosenhahn, A. 2013. Adhesion of Marine Fouling Organisms on Hydrophilic and Amphiphilic Polysaccharides. *Langmuir*. 29: 4039-4074.

Bazaka, K., Crawford, R. J., & Ivanova, E. P. 2011. Do bacteria differentiate between degrees of nanoscale surface roughness? *Biotechnology Journal, 6*:1103-1114.

Bazaka, K., Jacob, M. V., Crawford, R. J., & Ivanova, E.P. 2012. Efficient surface modification of biomaterial to prevent biofilm formation and the attachment of microorganisms. *Applied Microbiology and Biotechnology*, 95: 299–311.

Bazaka, K., Jacob, M. V., Truong, V. K., Crawford, R. J., & Ivanova, E. P. 2011. The Effect of Polyterpenol Thin Film Surfaces on Bacterial Viability and Adhesion. *Polymers*, 3: 388-404.

Beech, I. B., Smith, J. R., Steele, A. A., Penegar, I., & Campbell, S. A. 2002. The use of atomic force microscopy for studying interactions of bacterial biofilms with surfaces. *Colloids and Surfaces B: Biointerfaces*, 23(2-3): 231-247.

Bellot-Gurlet, L., Neff, D., Reguer, S., Monnier, J., Saheb, M., & Dillmann, P. 2009. Raman studies of corrosion layers formed on archaeological irons in various media. *Journal of Nano Research, 8*: 147-156.

Bergmans, L., Moisiadis, P., Van Meerbeek, B., Quirynen, M., & Lambrechts, P. 2005. Microscopic observation of bacteria: review highlighting the use of environmental SEM. *International Endodontic Journal, 38*(11): 775-788.

Bispo, P. J., Haas, W., & Gilmore, M. S. 2015. Biofilms in infections of the eye. *Pathogens*, 4(1): 111- 136.

Bliznakov, S., Liu, Y., Dimitrov, N., Garnica, J., & Sedev, R. 2009. Double-scale roughness and superhydrophobicity on metalized Toray carbon fibre paper. *Langmuir*, 25(8): 4760- 4766.

Boucherit, N., Delichere, P., Joiret, S., & Hugot le Goff, A. 1989. Passivity of iron and iron alloys studied by voltammetry and Raman spectroscopy. *In Materials Science Forum*, 44: 51-62.

Bouchet, P., Decock, W., Lonneville, B., Vanhoorne, B., & Vandepitte, L. 2023. Marine biodiversity discovery: the metrics of new species descriptions. *Frontiers in Marine Science*, 10:929989.

Boulangé-Petermann, L., Rault, J., & Bellon-Fontaine, M. N. 1997. Adhesion of Streptococcus thermophilus to stainless steel with different surface topography and roughness. *Biofouling*, 11(3): 201-216.

Callow, J. A. & Callow, M. E. 2011. Trends in the development of environmentally friendly fouling- resistant marine coatings. *Nature Communications*, 2: 244.

Carpentier, B. & Cerf, O. 1993. Biofilms and their consequences, with particular reference to hygiene in the food industry. *Journal of Applied Bacteriology, 75*(6): 499-511.

Castellanos, T., Ascencio, F., & Bashan, Y. 1997. Cell-surface hydrophobicity and cell-surface charge of Azospirillum. spp. *FEMS Microbiology Ecology*, 24(2): 159-172.

Cheng, B., Xia, R., Zhang, Y., Yang, Z., Hu, S., Guo, F., & Ma, S. 2019. Characterization and causes analysis for algae blooms in large river system. *Sustainable Cities and Society*, 51: 101707.

Chew, B. H. & Lange, D. 2009. Ureteral stent symptoms and associated infections: a biomaterials perspective. *Nature Reviews Urology*, 6: 440-448.

Chua, P. H., Neoh, K. G., Kang, E. T., & Wang, W. 2008. Surface functionalization of titanium with hyaluronic acid/chitosan polyelectrolyte multilayers and RGD for promoting osteoblast functions and inhibiting bacterial adhesion. *Biomaterials*, 29(10): 1412-1421.

Coates, J. 2000. Interpretation of infrared spectra, a practical approach. *Wiley*, Chichester, 10815- 10837.

Colomban, P., Cherifi, S., & Despert, G. 2008. Raman identification of corrosion products on automotive galvanized steel sheets. *Journal of Raman Spectroscopy: An International Journal for Original Work in all Aspects of Raman Spectroscopy, Including Higher Order Processes, and also Brillouin and Rayleigh Scattering, 39*(7): 881-886.

Corning, P. A. 2002. The re-emergence of “emergence”: A venerable concept in search of a theory. *Complexity*, 7(6): 18-30.

Costerton, J. W., Marrie, T. J., & Cheng, K. J. 1985. Phenomena of Bacterial Adhesion. In: Savage D.C., Fletcher M. (eds). *Bacterial Adhesion*. Springer, Boston, M: 3-43.

Costerton, J. W. & Lappin-Scott, H. M. 1995. Introduction to microbial biofilms. *Microbial Biofilms*. First Edition. New York: Cambridge University Press.

Costerton, J. W., Cheng, K. J., Geesey, G. G., Ladd, T. I., Nickel, J. C., Dasgupta, M., & Marrie, T. J. 1987. Bacterial biofilms in nature and disease. *Annual Reviews in Microbiology*, 41(1): 435-464.

Costerton, J. W., Lewandowski, Z., Caldwell, D. E., Korber, D. R., & Lappin-Scott, H. M. 1995. Microbial biofilms. *Annual Review of Microbiology*, 49(1): 711-745.

Costerton, J. W., Lewandowski, Z., DeBeer, D., Caldwell, D., Korber, D., & James, G. 1994. Biofilms, the customized microniche. *Journal of Bacteriology, 176*(8): 2137-2142.

Costerton, J. W., Montanaro, L., & Arciola, C. R. 2007. Bacterial Communications in Implant Infections: A Target for an Intelligence War. *The International Journal of Artificial Organs*. 30(9): 757-763.

Costerton, J. W., Stewart, P. S., & Greenberg, E. P. 1999. Bacterial biofilms: a common cause of persistent infections. Science, 284(5418): 1318-1322.

Crick, C. R., Ismail, S., Pratten, J., & Parkin, I. P. 2011. An investigation into bacterial attachment to an elastomeric superhydrophobic surface prepared via aerosol assisted deposition. *Thin Solid Films*, 519(11): 3722-3727.

Critchley, M. & Javaherdashti, R. 2004. Metals, microbes and MIC—a review of microbiologically influenced corrosion. *In Proceeding of Corrosion and Prevention*. 1-8.

Dan, N. 2003. The effect of charge regulation on cell adhesion to substrates: salt- induced repulsion. *Colloids and Surfaces B: Biointerfaces*, 27(1): 41-47.

Davey, M. E. & O'Toole, G. A. 2000. Microbiology and Molecular Biology Reviews. *Microbial Biofilms: from Ecology to Molecular Genetics*, 64: 847-867.

Davies, D. G. & Geesey, G. G. 1995. Regulation of the alginate biosynthesis gene algC in *Pseudomonas aeruginosa* during biofilm development in continuous culture. *Applied and Environmental Microbiology*, 61(3): 860-867.

De Nys, R. & Steinberg, P. D. 2000. Linking marine biology and biotechnology. *Current Opinion in Biotechnology*, 13(3): 244-248.

Detman, A., Mielecki, D., Chojnacka, A., Salamon, A., Błaszczyk, M. K., & Sikora, A. 2019. Cell factories converting lactate and acetate to butyrate: Clostridium butyricum and microbial communities from dark fermentation bioreactors. *Microbial cell factories*, 18(1): 1-12.

Dezelic, T. & Schmidlin, P. R. 2009. Multi-species biofilm formation on dental materials and an adhesive patch. *Oral Health & Preventive Dentistry*, 7(1): 47-53.

Di Ciccio, P., Vergara, A., Festino, A. R., Paludi, D., Zanardi, E., Ghidini, S., & Ianieri, A. 2015. Biofilm formation by Staphylococcus aureus on food contact surfaces: Relationship with temperature and cell surface hydrophobicity. *Food Control*, 50: 930-936.

Douglas. C. Elliott. Biomass, Chemicals from, Encyclopaedia of Energy 2004.

Drinan, D. F., Robin, S., & Cogan, T. M. 1976. Citric acid metabolism in hetero-and homofermentative lactic acid bacteria. *Applied and Environmental Microbiology*, 31(4): 481-486.

Duarte, P. M., Reis, A. F., Freitas, P. M., & Ota-Tsuzuki, C. 2009. Bacterial Adhesion on Smooth and Rough Titanium Surfaces After Treatment With Different Instruments. *Journal of Periodontology,* 8: 1-9.

Dufrêne, Y. F. 2008. Towards nanomicrobiology using atomic force microscopy. *Nature Reviews Microbiology*, 6(9), 674-680.

Dunne Jr, W. M. 2002. Bacterial adhesion: seen any good biofilms lately? *Clinical Microbiology Reviews*, 15(2): 155-166.

Dwivedi, D., Lepková, K., & Becker, T. 2017. Carbon steel corrosion: a review of key surface properties and characterisation methods. *RSC Advances*, 7(8): 4580-4610.

Elder, M. J., Stapleton, F., Evans, E., & Dart, J. K. 1995. Biofilm-related infections in ophthalmology. *Eye*, 9(1): 102-109.

Elliott, D.C., 2004. *Biomass, chemicals from* (No. PNNL-SA-36685). Pacific Northwest National Lab. (PNNL), Richland, WA (United States).

Fadeeva, E., Truong, V. K., Stiesch, M., Chichkov, B. N., Crawford, R. J., Wang, J., & Ivanova, E. P. 2011. Bacterial retention on superhydrophobic titanium surfaces fabricated by femtosecond laser ablation. *Langmuir*, 27(6): 3012-3019.

Fang, H. H., Chan, K. Y., & Xu, L. C. 2000. Quantification of bacterial adhesion forces using atomic force microscopy (AFM). *Journal of Microbiological Methods, 40*(1): 89-97.

Flemming, H.C. & Wingender, J., 2010. The biofilm matrix. *Nature Reviews Microbiology*, *8*(9): 623-633.

Flemming, H. C., Wingender, J., Szewzyk, U., Steinberg, P., Rice, S. A., & Kjelleberg, S. 2016. Biofilms: an emergent form of bacterial life. *Nature Reviews Microbiology*, 14(90): 563.

Genchev, G. & Erbe, A. 2016. Raman spectroscopy of mackinawite FeS in anodic iron sulfide corrosion products. *Journal of the Electrochemical Society, 163*(6): 333.

Gilbert, P., Das, J., & Foley, I. 1997. Biofilm susceptibility to antimicrobials. *Advances in Dental Research*, 11(1): 160-167.

Gilbert, P., Evans, D. J., Evans, E., Duguid, I. G., & Brown, M. R. W. 1991. Surface characteristics and adhesion of Escherichia coli and Staphylococcus epidermidis. *Journal of Applied Bacteriology, 71*(1): 72-77.

Guo, J., Zheng, Y., Teng, J., Wang, X., & Song, J. 2021. Characteristics of spatial distribution for microbial ecology inside and outside source water reservoir. *Journal of Cleaner Production*, 311: 127697.

Hall-Stoodley, L., Costerton, J. W., & Stoodley, P. 2004. Natural Environment to Infectious Diseases. *Nature Reviews Microbiology*, 2: 95-108.

Hannig, C., Follo, M., Hellwig, E., & Al-Ahmad, A. 2010. Visualization of adherent micro-organisms using different techniques. *Journal of Medical Microbiology, 59*(1): 1-7.

Hannig, C., Huber, K., Lambrichts, I., Gräser, J., D'Haen, J., & Hannig, M. 2007. Detection of salivary α-amylase and lysozyme exposed on the pellicle formed in situ on different materials. *Journal of Biomedical Materials Research Part A: An Official Journal of The Society for Biomaterials, The Japanese Society for Biomaterials, and The Australian Society for Biomaterials and the Korean Society for Biomaterials, 83*(1): 98-103.

Harris, L. G. & Richards, R. G. 2004. Staphylococcus aureus adhesion to different treated titanium surfaces. *Journal of Materials Science: Materials in Medicine, 15*(4): 311-314.

Hermansson, M. 1999. The DLVO theory in microbial adhesion. *Colloids and Surfaces B: Biointerfaces*, 14(1-4): 105-119.

Hoffman, M. D., Zucker, L. I., Brown, P. J., Kysela, D. T., Brun, Y. V., & Jacobson, S. C. 2015. Timescales and frequencies of reversible and irreversible adhesion events of single bacterial cells. *Analytical Chemistry*, 87(24): 12032-12039.

Ivanova, E. P., Hasan, J., Truong, V. K., Wang, J. Y., Raveggi, M., Fluke, C., & Crawford, R. J. 2011. The influence of nanoscopically thin silver films on bacterial viability and attachment. *Applied Microbiology and Biotechnology*, 91(4): 1149-1157.

Ivanova, E. P., Truong, V. K., Wang, J. Y., Berndt, C. C., Jones, R. T., Yusuf, I. I., Peake, I., Schmidt, H. W., Fluke, C., Barnes, D., & Crawford, R. J. 2010. Impact of nanoscale roughness of titanium thin film surfaces on bacterial retention. *Langmuir*, 26(3): 1973-1982.

Ivanova, E. P., Truong, V. K., Webb, H. K., Baulin, V. A., Wang, J. Y., Mohammodi, N., Wang, F., Fluke, C., & Crawford, R. J. 2011. Differential attraction and repulsion of Staphylococcus aureus and Pseudomonas aeruginosa on molecularly smooth titanium films. *Scientific Reports*, 1: 165.

Jamal, M., Ahmad, W., Andleeb, S., Jalil, F., Imran, M., Nawaz, M. A., Hussain, T., Ali, M., Rafiq, M., & Kamil, M. A. 2018. Bacterial biofilm and associated infections. *Journal of the Chinese Medical Association, 81*(1): 7-11.

Jeong, G., Kim, H.J., Kim, K.E., Kim, Y.J., Lee, T.K., Shim, W.J., & Jung, S.W. 2023. Selective attachment of prokaryotes and emergence of potentially pathogenic prokaryotes on four plastic surfaces: Adhesion study in a natural marine environment. *Marine Pollution Bulletin*, 193: 115149.

Jung, M.J., Kim, J., Lee, S.H., Whon, T.W., Sung, H., Bae, J.W., Choi, Y.E., & Roh, S.W., 2022. Role of combinated lactic acid bacteria in bacterial, viral, and metabolite dynamics during fermentation of vegetable food, kimchi. *Food Research International*, 157: 111261.

Jones, D. S., Adair, C. G., Mawhinney, W. M., & Gorman, S. P. 1996. Standardisation and comparison of methods employed for microbial cell surface hydrophobicity and charge determination. *International Journal of Pharmaceutics, 131*(1): 83-89.

Kadaifciler, D.G., Unsal, T., & Ilhan-Sungur, E. 2023. Long-term Evaluation of Culturable Fungi in a Natural Aging Biofilm on Galvanized Steel Surface. *Johnson Matthey Technology Review.*

Kartsonakis, I. A. & Charitidis, C. A. 2020. Corrosion Protection Evaluation of Mild Steel: The Role of Hybrid Materials Loaded with Inhibitors. *Applied Sciences*, 10(18): 6594.

Katsikogianni, M. & Missirlis, Y. F. 2004. Concise review of mechanisms of bacterial adhesion to biomaterials and of techniques used in estimating bacteria-material interactions. *European Cells and Materials*, 8: 37-57.

Kim, S. K., Park, I. J., Lee, D. Y., & Kim, J. G. 2013. Influence of surface roughness on the electrochemical behavior of carbon steel. *Journal of Applied Electrochemistry, 43*(5): 507-514.

Knutton, S. 1995. Electron microscopical methods in adhesion. *In Methods in Enzymology* 253: 145-158. Academic Press.

Kolter, R. & Greenberg, E. P. 2006. The superficial life of microbes. *Nature*, 441(7091): 300-302.

Konopka, A. 2009. What is microbial community ecology?. *The ISME journal, 3*(11): 1223-1230.

Kuang, F., Wang, J. Y. A. N. L., & Zhang, D. 2007. Effects of sulphate-reducing bacteria on the corrosion behaviour of carbon steel. *Electrochimica Acta*, 52(20): 6084-6088.

Kumar, C. G. & Anand, S. K. 1998. Significance of microbial biofilms in food industry: a review. *International Journal of Food Microbiology, 42*(1-2): 9-27.

Kumar, H., Sharma, S., & Kumari, R. 2022. Corrosion inhibition and adsorption mechanism of Morus nigra on mild steel in acidic medium: A sustainable and green approach. *Vietnam Journal of Chemistry*, 60(4): 417-434.

Leban, M. B. & Kosec, T. 2017. Characterization of corrosion products formed on mild steel in deoxygenated water by Raman spectroscopy and energy dispersive X-ray spectrometry. *Engineering Failure Analysis*, 79: 940-950.

Leung, J. W., Liu, Y. L., Desta, T., Libby, E., Inciardi, J. F., & Lam, K. 1998. Is there a synergistic effect between mixed bacterial infection in biofilm formation on biliary stents? *Gastrointestinal Endoscopy*, 48: 250–257.

Li, H., Zhou, E., Zhang, D., Xu, D., Xia, J., Yang, C., Feng, H., Jiang, Z., Li, X., Gu, T., & Yang, K. 2016. Microbiologically influenced corrosion of 2707 hyper-duplex stainless steel by marine *Pseudomonas aeruginosa* biofilm. *Scientific Reports*, 6(1): 1-12.

Liang, C. H., Wang, H., & Huang, N. B. 2014. Effects of sulphate-reducing bacteria on corrosion behaviour of 2205 duplex stainless steel. *Journal of Iron and Steel Research International, 21*(4): 444-450.

Little, B. J., Lee, J. S., & Ray, R. I. 2006. Diagnosing microbiologically influenced corrosion: a state-of- the-art review. *Corrosion*, 62(11): 1006-1017.

Little, B. J., Lee, J. S., & Ray, R. I. 2008. The influence of marine biofilms on corrosion: a concise review. *Electrochimica Acta*, 54(1): 2-7.

Ma, J., Sun, Y., Gleichauf, K., Lou, J., & Li, Q. 2011. Nanostructure on taro leaves resists fouling by colloids and bacteria under submerged conditions. *Langmuir*, 27(16): 10035-10040.

Madigan, M. T., Martinko, J. M., & Parker, J. 2000. *Brock Biology of Microorganisms*, 11:135–162. Prentice-Hall, Upper Saddle River, New Jersey.

Mahanta, D. J., Borah, M., & Saikia, P. 2014. Study on Kinetic Models for Analysing the Bacterial Growth Rate. *American International Journal of Research in Science, Technology, Engineering and Mathematics, 8*(1): 2328-3491.

Maier, R. M. & Pepper, I. L. 2015. Bacterial growth. *In Environmental Microbiology*, 37-56. Academic Press.

Marshall, K. C. 1992. Biofilms: an overview of bacterial adhesion, activity, and control at surfaces. *American Society for Microbiology*. News, 58: 202-207.

Martin, W.F. 2019. Carbon–metal bonds: rare and primordial in metabolism. 2019. *Trends in Biochemical Sciences, 44*(9): 807-818.

Mathew, N. T., Kronholm, J., Bertilsson, K., Despeisse, M., & Johansson, B. 2021. Environmental and Economic Impacts of Biofouling on Marine and Coastal Heat Exchangers. *In EcoDesign and Sustainability II*, 385-398. Springer, Singapore.

Medilanski, E., Kaufmann, K., Wick, L. Y., Wanner, O., & Harms, H. 2002. Influence of the surface topography of stainless steel on bacterial adhesion. *Biofouling*, 18(3), 193-203.

Mignard, S. & Flandrois, J. P. 2006. 16S rRNA sequencing in routine bacterial identification: a 30-month experiment. *Journal of Microbiological Methods, 67*(3): 574-581.

Mitik-Dineva, N., Wang, J., Truong, V. K., Stoddart, P., Malherbe, F., Crawford, R. J., & Ivanova, E. P. 2009. Escherichia coli, Pseudomonas aeruginosa, and Staphylococcus aureus attachment patterns on glass surfaces with nanoscale roughness. *Current Microbiology*, 58(3): 268-273.

Mitik-Dineva, N., Wang, J., Truong, V. K., Stoddart, P. R., Malherbe, F., Crawford, R. J., & Ivanova, E. P. 2009. Differences in colonisation of five marine bacteria on two types of glass surfaces. *Biofouling*, 25(7): 621-631.

Mueller, R. F., Characklis, W. G., Jones, W. L., & Sears, J. T. 1992. Characterization of initial events in bacterial surface colonization by two Pseudomonas species using image analysis. *Biotechnology and Bioengineering*, 39(11): 1161-1170.

Navarro Llorens, J.M., Tormo, A. and Martínez-García, E. 2010. Stationary phase in gram-negative bacteria. *FEMS Microbiology Reviews*, 34(4): 476-495.

Ninham, B. W., Pashley, R. M., & Nostro, P. L. 2017. Surface forces: Changing concepts and complexity with dissolved gas, bubbles, salt, and heat. *Current Opinion in Colloid and Interface Science*, 27: 25-32.

Nouri, A., Shirvan, A.R., Li, Y., & Wen, C. 2023. Surface modification of additively manufactured metallic biomaterials with active antipathogenic properties. *Smart Materials in Manufacturing*, 1: 100001.

Panjeshahi, M. H., Ataei, A., Gharaie, M., & Parand, R. 2009. Optimum design of cooling water systems for energy and water conservation. *Chemical Engineering Research and Design*, 87(2): 200-209.

Parham, J. P., Cobb, C. M., French, A. A., Love, J. W., Drisko, C. L., & Killoy, W. J. 1989. Effects of an air-powder abrasive system on plasma-sprayed titanium implant surfaces: an in vitro evaluation. *The Journal of Oral Implantology, 15*(2): 78-86. PMID: 2640245.

Park, J. W., An, J. S., Lim, W. H., Lim, B. S., & Ahn, S. J. 2019. Microbial changes in biofilms on composite resins with different surface roughness: An in vitro study with a multispecies biofilm model. *The Journal of Prosthetic Dentistry, 122*(5): 493-e1.

Pembrey, R. S., Marshall, K. C., & Schneider, R. P. 1999. Cell surface analysis techniques: what do cell preparation protocols do to cell surface properties?. *Applied and Environmental Microbiology*, 65(7): 2877-2894.

Persat, A., Nadell, C. D., Kim, M. K., Ingremeau, F., Siryaporn, A., Drescher, K., Wingreen, N. S., Bassler, B. L., Gitai, Z., & Stone, H. A. 2015. The mechanical world of bacteria. *Cell*, 161(5): 988-997.

Pohl, S., Madzgalla, M., Manz, W., & Bart, H. J. 2017. Interaction of E. coli and Autochthonous river water microorganisms with polymers in heat transfer applications. *In Proceeding of International Conference on Heat Exchanger Fouling and Cleaning*, Aranjuez (Madrid), Spain, 92-99.

Poortinga, A. T., Bos, R., Norde, W., & Busscher, H. J. 2002. Electric double layer interactions in bacterial adhesion to surfaces. *Surface Science Reports*, 47(1): 1-32.

Prithiraj, A., Otunniyi, I. O., Osifo, P., & van Der Merwe, J. 2019. Corrosion behaviour of stainless and carbon steels exposed to sulphate–reducing bacteria from industrial heat exchangers. *Engineering Failure Analysis*, 104: 977-986.

Queiroz, G.A.D., Andrade, J.S., Malta, T.B.S., Vinhas, G., & Lima, M.A.G.D.A. 2018. Biofilm formation and corrosion on carbon steel API 5LX60 in clayey soil. *Materials Research*, 21: 1-7.

Rajasekar, A., Maruthamuthu, S., Muthukumar, N., Mohanan, S., Subramanian, P., & Palaniswamy, N. 2005. Bacterial degradation of naphtha and its influence on corrosion. *Corrosion Science*, 47(1): 257-271.

Refait, P., Grolleau, A.M., Jeannin, M., Rémazeilles, C. & Sabot, R. 2020. Corrosion of carbon steel in marine environments: role of the corrosion product layer. *Corrosion and Materials Degradation*, 1(1): 10.

Rijnaarts, H. H., Norde, W., Bouwer, E. J., Lyklema, J., & Zehnder, A. J. 1995. Reversibility and mechanism of bacterial adhesion. *Colloids and Surfaces B: Biointerfaces*, 4(1): 5-22.

Rijnaarts, H. H., Norde, W., Lyklema, J., & Zehnder, A. J. 1999. DLVO and steric contributions to bacterial deposition in media of different ionic strengths. *Colloids and Surfaces B: Biointerfaces*, 14(1-4): 179-195.

Rolfe, M.D., Rice, C.J., Lucchini, S., Pin, C., Thompson, A., Cameron, A.D., Alston, M., Stringer, M.F., Betts, R.P., Baranyi, J., & Peck, M.W. 2012. Lag phase is a distinct growth phase that prepares bacteria for exponential growth and involves transient metal accumulation. *Journal of Bacteriology*, 194(3): 686-701.

Rozen, R., Bachrach, G., Zachs, B. & Steinberg, D. 2001. Growth rate and biofilm thickness of *Streptococcus sobrinus* and *Streptococcus mutans* on hydroxapatite. *Journal of Pathology, Microbiology and Immunology*, 109(2): 155-160.

Rudney, J. D., Chen, R., Lenton, P., Li, J., Li, Y., Jones, R. S., Reilly, C., Fok, A. S., & Aparicio, C. 2012. A reproducible oral microcosm biofilm model for testing dental materials. *Journal of Applied Microbiology, 113*(6): 1540-1553.

Russell, J. C., Hayden, K. W., Vi, K. T., Jafar, H., & Elena, P. I. 2012. Surface topographical factors influencing bacterial attachment. *Advances in Colloid and Interface Science*, 182 (179): 142-149.

Salta, M., Wharton, J. A., Stoodley, P., Dennington, S. P., Goodes, L. R., Werwinski, S., Mart, U., Wood, R.J., & Stokes, K.R. 2010. Designing Biomimetic antifouling surfaces. *Philosophical Transactions of the Royal Society*, 368: 4729-4754.

Santos, A. L. S. D., Galdino, A. C. M., Mello, T. P. D., Ramos, L. D. S., Branquinha, M. H., Bolognese, A. M., Columbano Neto, J., & Roudbary, M. 2018. What are the advantages of living in a community? A microbial biofilm perspective! *Memórias do Instituto Oswaldo Cruz*, 113(9): 1- 7.

Scardino, A. J. & de Nys, R. 2011. Mini review: Biomimetic models and bioinspired surfaces for fouling control. *Biofouling*. 27(1): 73-86.

Scardino, A. J., Zhang, H., Cookson, D. J., Lamb, R. N., & Nys, R. D. 2009. The role of nano-roughness in antifouling. *Biofouling*, 25(8): 757-767.

Shah, M. 2013. Iron oxide reduction by clostridial consortium: insights from physiological and genome analysis. *Doctorate thesis*. The State University of New Jersey. 1-114.

Sheng, W. H., Ko, W. J., Wang, J. T., Chang, S. C., Hsueh, P. R., & Luh, K. T. 2000. Evaluation of antiseptic-impregnated central venous catheters for prevention of catheter-related infection in intensive care unit patients. *Diagnostic Microbiology and Infectious Disease*, 38(1): 1-5.

Shi, Z., Neoh, K. G., Kang, E. T., Poh, C. K., & Wang, W. 2009. Surface functionalization of titanium with carboxymethyl chitosan and immobilized bone morphogenetic protein-2 for enhanced osseointegration. *Biomacromolecules*,10(6): 1603-1611.

Shokrollahzadeh, S., Azizmohseni, F., Golmohammad, F., Shokouhi, H., & Khademhaghighat, F. 2008. Biodegradation potential and bacterial diversity of a petrochemical wastewater treatment plant in Iran. *Bioresource Technology*, 99(14): 6127-6133.

Sikora, A., Błaszczyk, M., Jurkowski, M., & Zielenkiewicz, U. 2013. Lactic acid bacteria in hydrogen-producing consortia: on purpose or by coincidence?. *INTECH open Science Minds*, 488-514.

Sun, H., Shi, B., Lytle, D.A., Bai, Y., & Wang, D. 2014. Formation and release behavior of iron corrosion products under the influence of bacterial communities in a simulated water distribution system. *Environmental Science: Processes & Impacts*, 16(3): 576-585.

Tang, M., Chen, C., Zhu, J., Allcock, H. R., Siedlecki, C. A., & Xu, L. C. 2021. Inhibition of bacterial adhesion and biofilm formation by a textured fluorinated alkoxyphosphazene surface. *Bioactive Materials*, 6(2): 447-459.

Taylor, R. L., Verran, J., Lees, G. C., & Ward, A. J. P. 1998. The influence of substratum topography on bacterial adhesion to polymethyl methacrylate. *Journal of Materials Science: Materials in Medicine, 9*: 17–22.

Thalib, S., Ikhsan, M., Fonna, S., Huzni, S., & Ridha, S. 2018. Identification of corrosion product on medium carbon steel under the exposure of Banda Aceh's atmosphere. *In IOP Conference Series: Materials Science and Engineering*, 352(1): 12004.

Tjalsma, H., Bolhuis, A., Jongbloed, J. D., Bron, S., & van Dijl, J. M. 2000. Signal peptide-dependent protein transport in Bacillus subtilis: a genome-based survey of the secretome. *Microbiology and Molecular Biology Reviews*, 64(3): 515-547.

Tran, T.T.T., Kannoorpatti, K., Padovan, A., & Thennadil, S. 2021. A study of bacteria adhesion and microbial corrosion on different stainless steels in environment containing Desulfovibrio vulgaris. *Royal Society Open Science*, 8(1): 201577.

Truong, V. K., Lapovok, R., Estrin, Y. S., Rundell, S., Wang, J. Y., Fluke, C. J., Crawford, R. J., & Ivanova, E. P. 2010. The influence of nano-scale surface roughness on bacterial adhesion to ultrafine-grained titanium. *Biomaterials*, 31(13): 3674-3683.

Truong, V. K., Rundell, S., Lapovok, R., Estrin, Y., Wang, J. Y., Berndt, C. C., Barnes, D. G., Fluke, C. J., Crawford, R. J., & Ivanova, E. P. 2009. Effect of ultrafine-grained titanium surfaces on adhesion of bacteria. *Applied Microbiology and Biotechnology*, 83(5): 925-937.

Truong, V. K., Wang, J., Lapovok, R., Estrin, Y., Malherbe, F., Berndt, C., Crawford, R., & Ivanova, E. 2010. Bacterial Attachment Response on Titanium Surfaces with Nanometric Topographic Features. In: Trends in Colloid and Interface Science XXIII. *Progress in Colloid and Polymer Science*. Springer, Berlin, Heidelberg, 137: 41-45.

Tuck, B., Watkin, E., Forsyth, M., Somers, A., Ghorbani, M., & Machuca, L. L. 2021. Evaluation of a novel, multi-functional inhibitor compound for prevention of biofilm formation on carbon steel in marine environments. *Scientific Reports*, 11(1): 1-12.

Van der Wal, A., Norde, W., Zehnder, A. J., & Lyklema, J. 1997. Determination of the total charge in the cell walls of Gram-positive bacteria. *Colloids and surfaces B: Biointerfaces*, 9(1-2): 81-100.

Vert, M., Doi, Y., Hellwich, K. H., Hess, M., Hodge, P., Kubisa, P., Rinaudo, M., & Schué, F. 2012. Terminology for biorelated polymers and applications (IUPAC Recommendations 2012). *Pure and Applied Chemistry*, 84(2): 377-410.

Wang, Y. S., Liu, L., Fu, Q., Sun, J., An, Z. Y., Ding, R., Li, Y., & Zhao, X. D. 2020. Effect of *Bacillus subtilis* on corrosion behaviour of 10MnNiCrCu steel in marine environment. *Scientific Reports*, 10(1): 1-9.

Wang, J. & Yin, Y. 2021. *Clostridium* species for fermentative hydrogen production: An overview. *International Journal of Hydrogen Energy*, 46(70): 34599-34625.

Waters, C. M. & Bassler, B. L. 2005. Quorum sensing: cell-to-cell communication in bacteria. *Annual Reviews of Cell Developmental Biology*, 21: 319-346.

Whitehead, K. A., Rogers, D., Colligon, J., Wright, C., & Verran, J. 2006. Use of the atomic force microscope to determine the effect of substratum surface topography on the ease of bacterial removal. *Colloids and Surfaces B: Biointerfaces*, 51(1): 44-53.

Wimpenny, J. 2000. January. An overview of biofilms as functional communities. In Symposia Society for General Microbiology, 1-24. Cambridge; Cambridge University Press; 1999.

Wingender, J. & Flemming, H. C. 2010. The biofilm matrix. *Nature Reviews Microbiology*, 8: 623-633.

Xavier, J. B., Martinez-Garcia, E., & Foster, K. R. 2009. Social evolution of spatial patterns in bacterial biofilms: when conflict drives disorder. *The American Naturalist*, 174(1): 1-12.

Xavier, J. D. B., Picioreanu, C., & van Loosdrecht, M. C. 2005. A general description of detachment for multidimensional modelling of biofilms. *Biotechnology and Bioengineering*, 91(6): 651-669.

Xi, G., Zhao, X., Wang, S., Yang, J., Sun, J., An, Z., Li, Y., & Qu, X. 2020. Synergistic Effect Between Sulphate-reducing Bacteria and Pseudomonas Aeruginosa on Corrosion Behaviour of Q235 Steel. *International Journal of Electrochemical Science,* 15: 361-370.

Xu, Z., Sun, M., Liu, Z., Wang, B., & Di, H. 2020. Properties of the Iron Bacteria on Ni-P-rGO Coating. *Applied Sciences*, 10: 1567.

Yang, S. R., Xu, Z. M., & Sun, L. F. 2004. *Fouling and Counter Measures for Heat Transfer Equipment*, 2nd ed. Beijing, China.

Yuan, L., Hansen, M. F., Røder, H. L., Wang, N., Burmølle, M., & He, G. 2019. Mixed-Species biofilms in the food industry: Current knowledge and novel control strategies. Critical Reviews *In Food Science and Nutrition*, 60(13): 2277-2293.

Zhao, M., Tyson, C., Chen, H.C., Paudel, S., Gitaitis, R., Kvitko, B., & Dutta, B. 2022. *Pseudomonas alliivorans sp.* nov., a plant-pathogenic bacterium isolated from onion foliage in Georgia, USA. *Systematic and Applied Microbiology*, 45(1): 126278.

Zhao, Q., Lui, C., Liu, Y., & Wang, S. 2007. Bacterial and Protein Adhesion on NI-P-PTFE Coated Surfaces. *In Proceeding of 7th International Conference on Heat Exchanger Fouling and Cleaning.* Engineering Conferences International, Tomar, Portugal, 237-242.

Zhu, X. Y., Lubeck, J., & Kilbane, J. J. 2003. Characterisation of microbial communities in gas industry pipelines. *Applied and Environmental Microbiology*, 69(9): 5354-5363.

CHAPTER 9 APPENDICES

9.1 APPENDIX A: DATA

9.1.1 16S RDNA GENE SEQUENCING METAGENOMIC REPORT, INDICATING BACTERIAL SPECIES PRESENT ON THE EXPOSED ALLOYS.

It was observed that on both surface finishes on separate days, a large number of unknown species were detected.

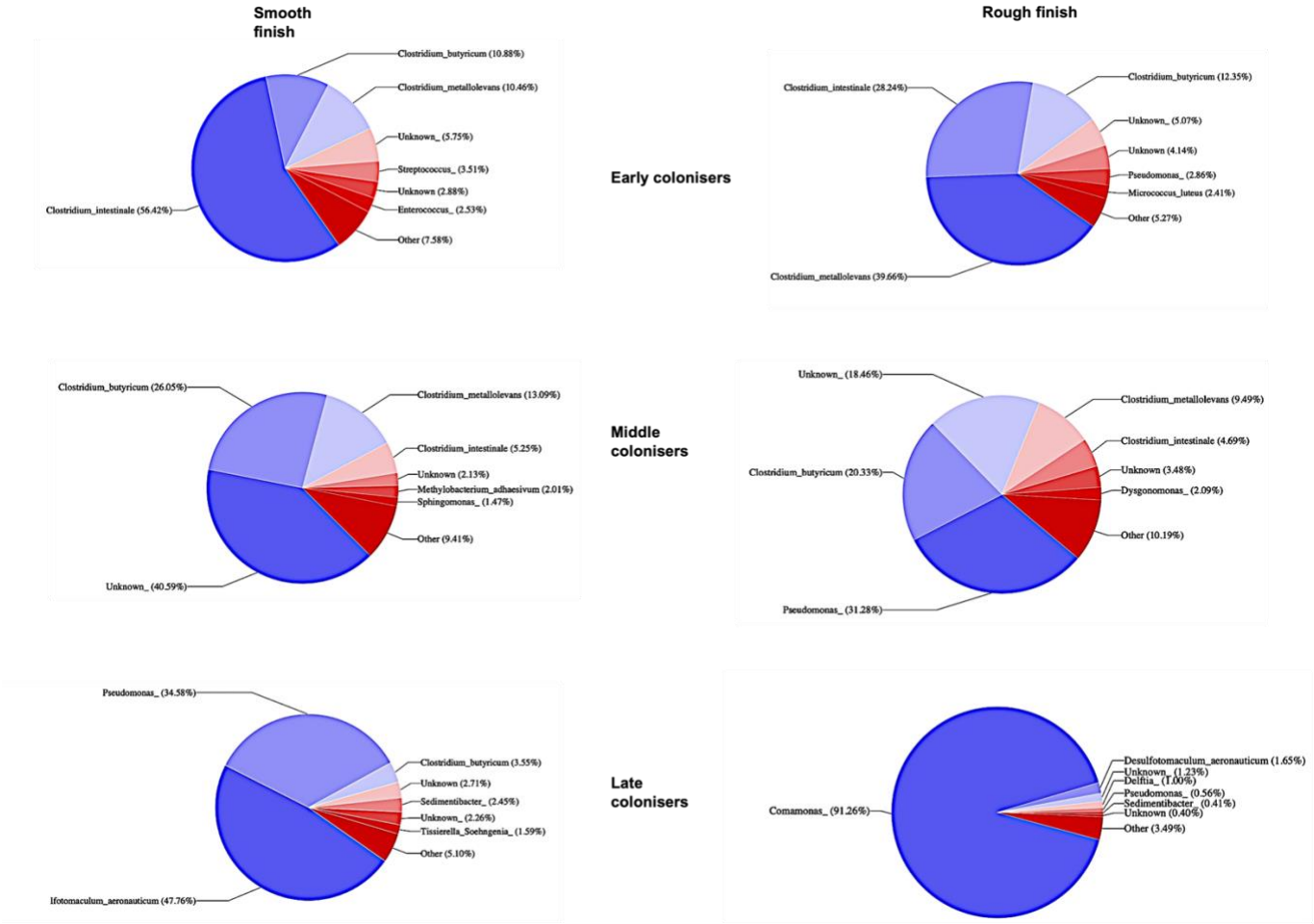

Figure 9.1: PI charts of the bacterial species attached to the steel surface on days 3, 6, and 13

Day 3 (Early colonisers), day 6 (Middle colonisers) and day 13 (Late colonisers).

9.1.2 Carbon mapping

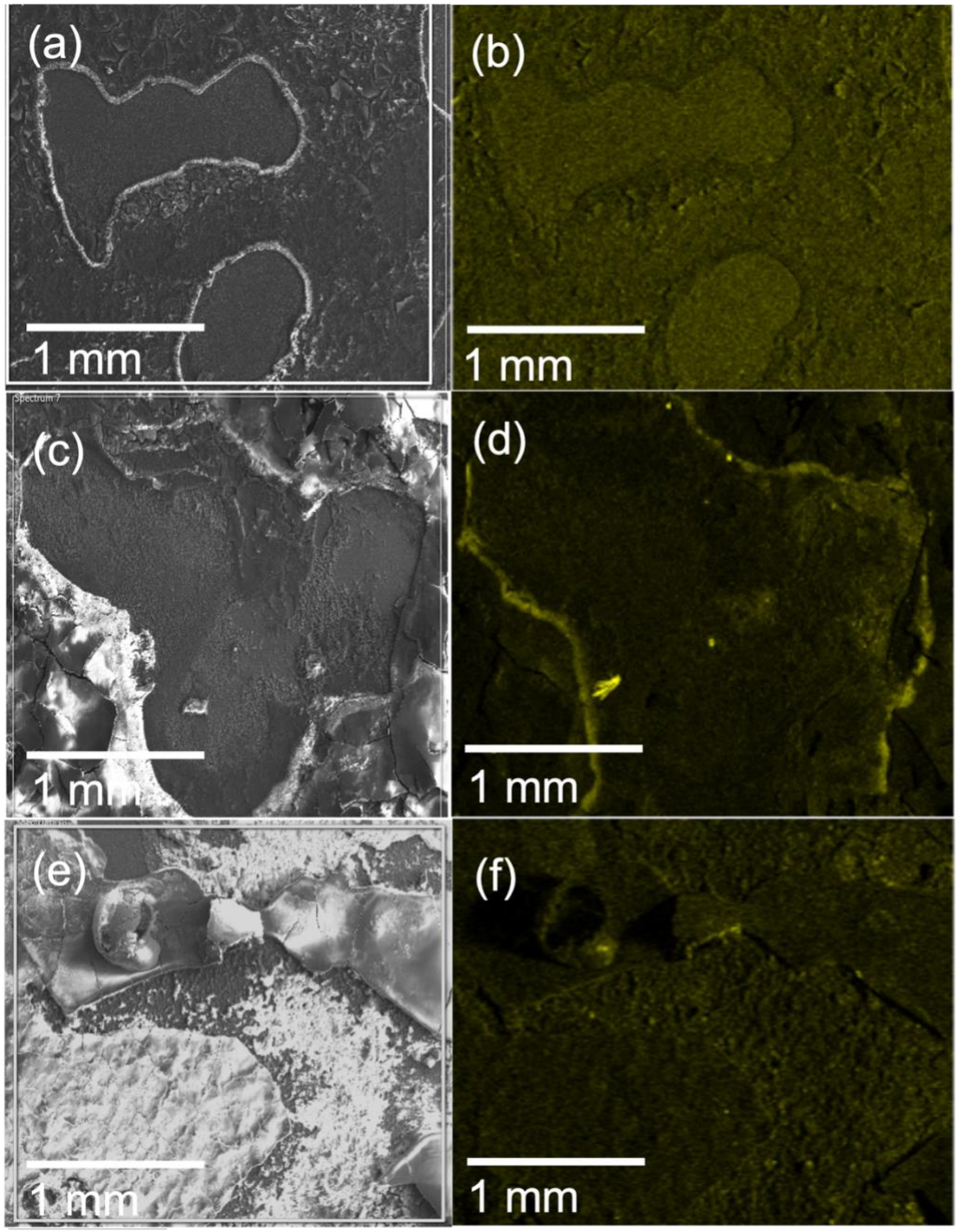

Figure 9.2: SEM/EDX images of carbon deposition on smooth alloy A after bacterial exposure on day 3 (a-b), day 6 (c-d), and day 13 (e-f)

9.1.3 Corrosion products

Table 9.1: Corrosion products according to literature

Corrosion products in the literature on carbon steel	**Wavenumber (cm^{-1}) reported in the literature**	**Literature references**
Lepidocrocite	245 cm^{-1} and 375 cm^{-1}	Antunes *et al*. (2014)
Goethite (FeOOH)	249 cm^{-1}, 303 cm^{-1}, 390 cm^{-1}, 476 cm^{-1}, 660 cm^{-1}	Leban & Kosec (2017)
Magnetite (Fe_3O_4)	671 cm^{-1}	Genchev & Erbe (2016), Colomban *et al*. (2008), Bellot-Gurlet *et al*. (2009)
Magnetite ($Fe_{(2,3)}O_4$)	670 cm^{-1}	Leban & Kosec (2017)
Magnetite (Fe_3O_4)	662 cm^{-1} and 535 cm^{-1}	Antunes *et al*. (2014)
Mackinawite (FeS)	200 cm^{-1}, 253 cm^{-1}, 287 cm^{-1}	Genchev & Erbe (2016)
Mixture of Lepidocrocite and Goethite	245 cm^{-1}, 299 cm^{-1}, 385 cm^{-1},479 cm^{-1} and 550	Antunes *et al*. (2014)
Mixture of magnetite and Goethite	245 cm^{-1},280 cm^{-1},375 cm^{-1} and 664 cm^{-1}	Leban & Kosec (2017)
Magnetite (Fe_3O_4)	683 cm^{-1}	Kartsonakis & Charitidis (2020)
Lepidocrocite	393	Kartsonakis & Charitidis (2020)
Goethite (FeOOH)	273	Kartsonakis & Charitidis (2020)
Ferrihydrite	1362 and 1613	Kartsonakis & Charitidis (2020)
Lepidocrocite	1307	Boucherit *et al*. (1989)

9.1.3.1 Different colour spectra observed on the surface of the alloy

The colours observed on the surface had similar spectra intensities on day 3; however, various areas observed on day 6 and day 13 alloys indicated that the spectra differed with intensity.

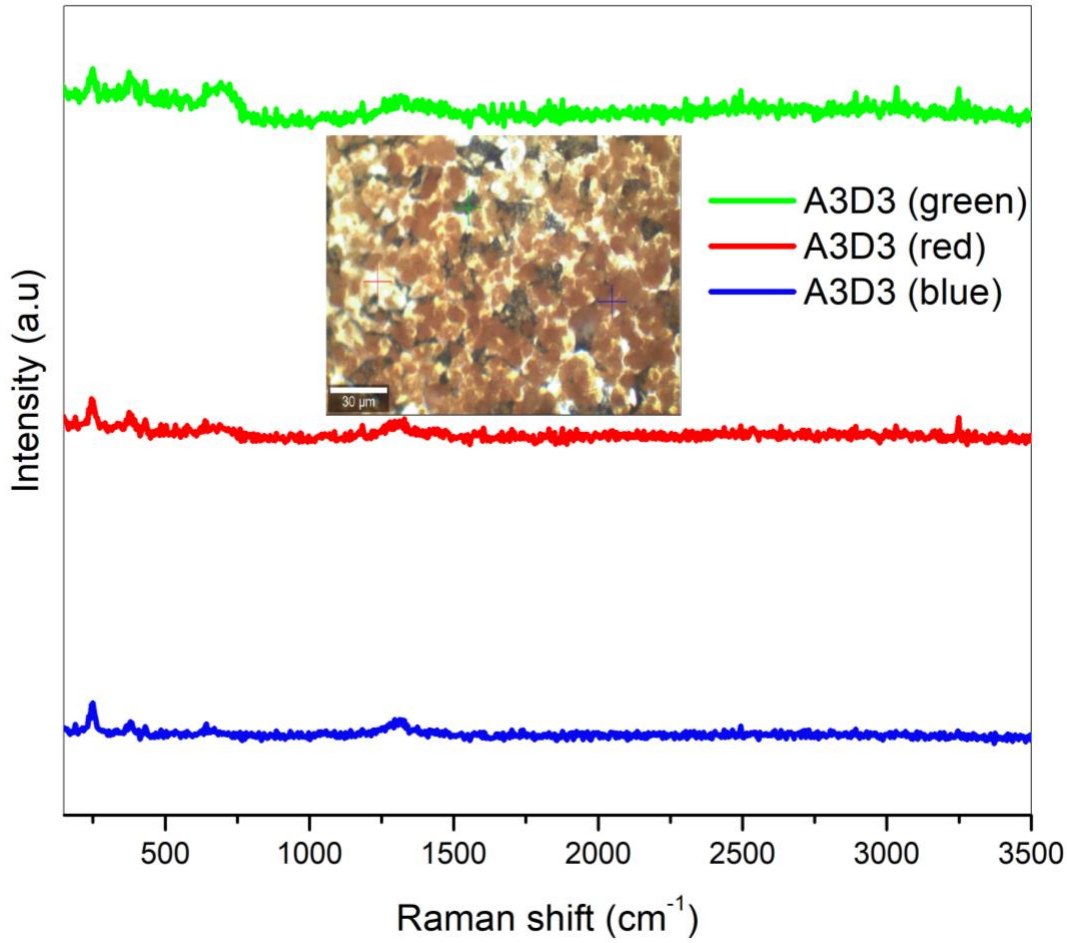

Figure 9.3: Raman spectra on day 3 of Area 1

Image (a) indicates the area where the spectra was taken.

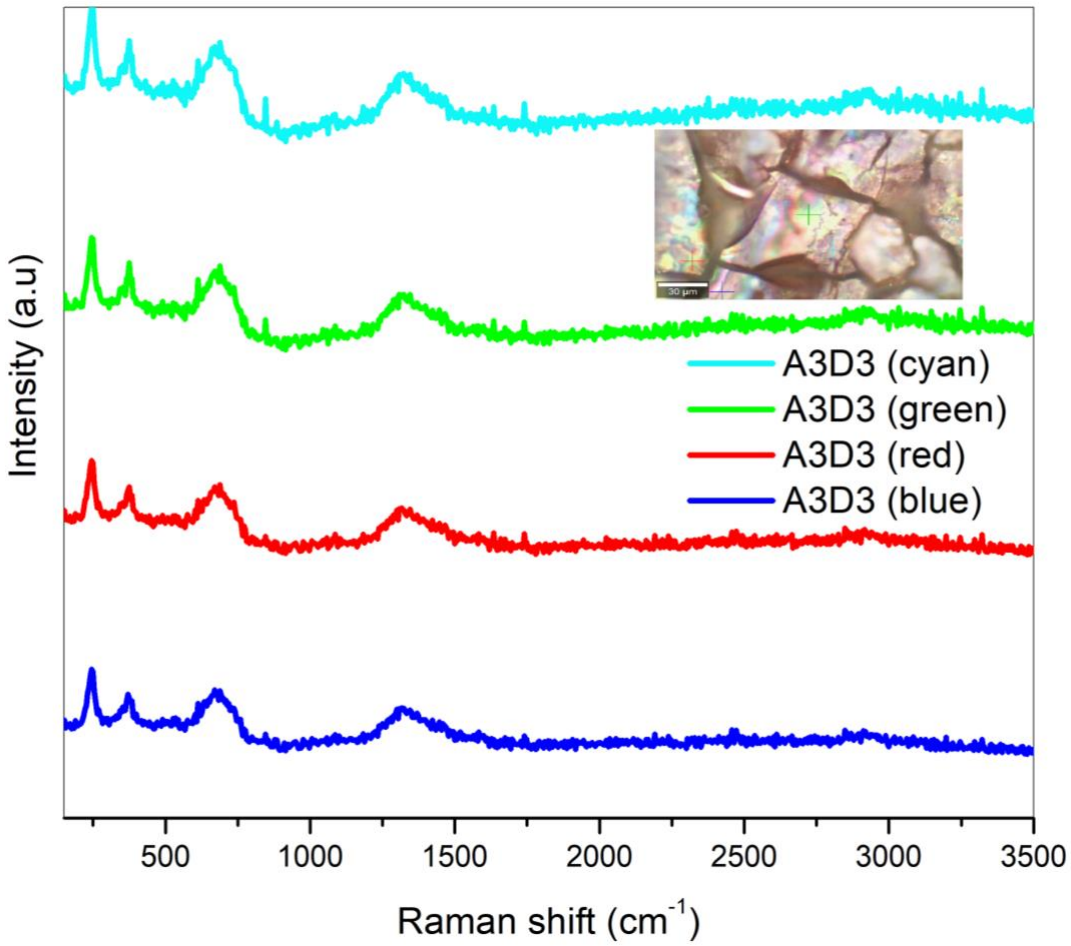

Figure 9.4: Raman spectra on day 3 of Area 2

Image (a) indicates the area where the spectra was taken.

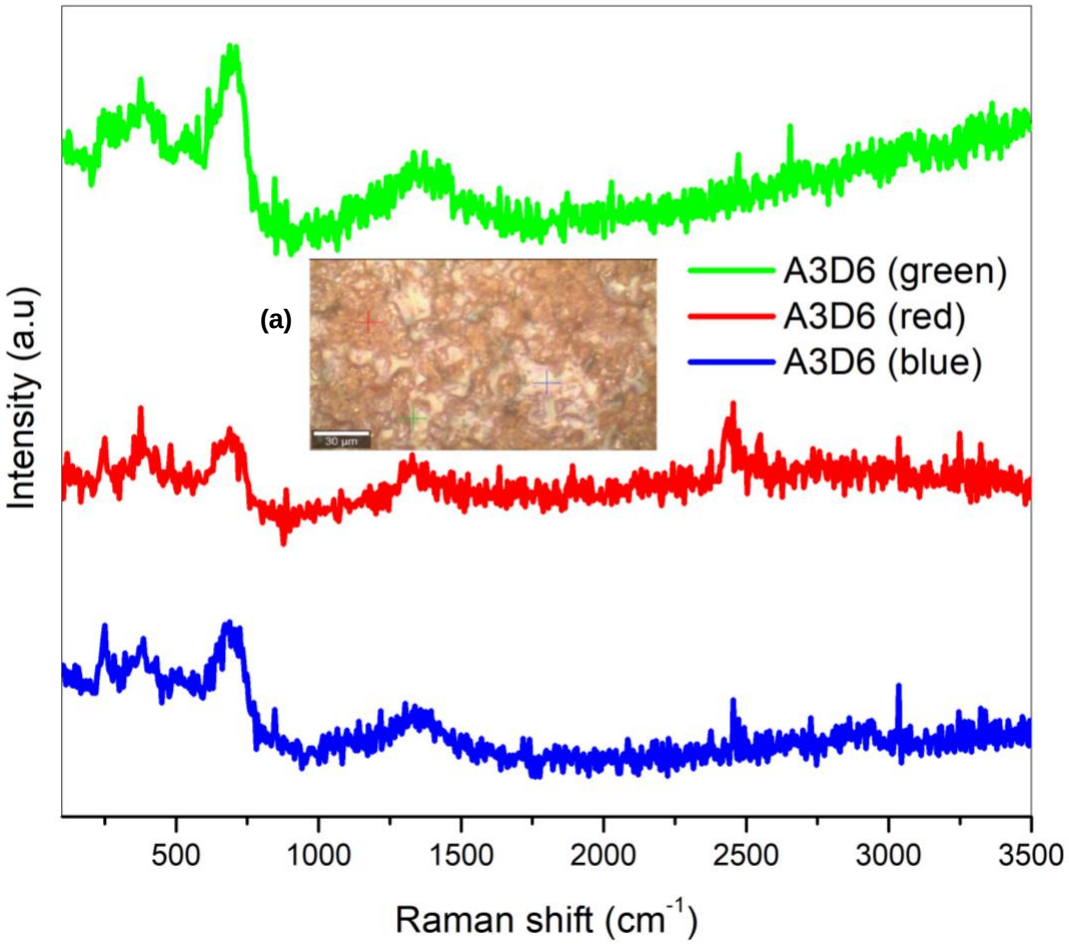

Figure 9.5: Raman spectra on day 6 of Area 1

Image (a) indicates the area where the spectra was taken.

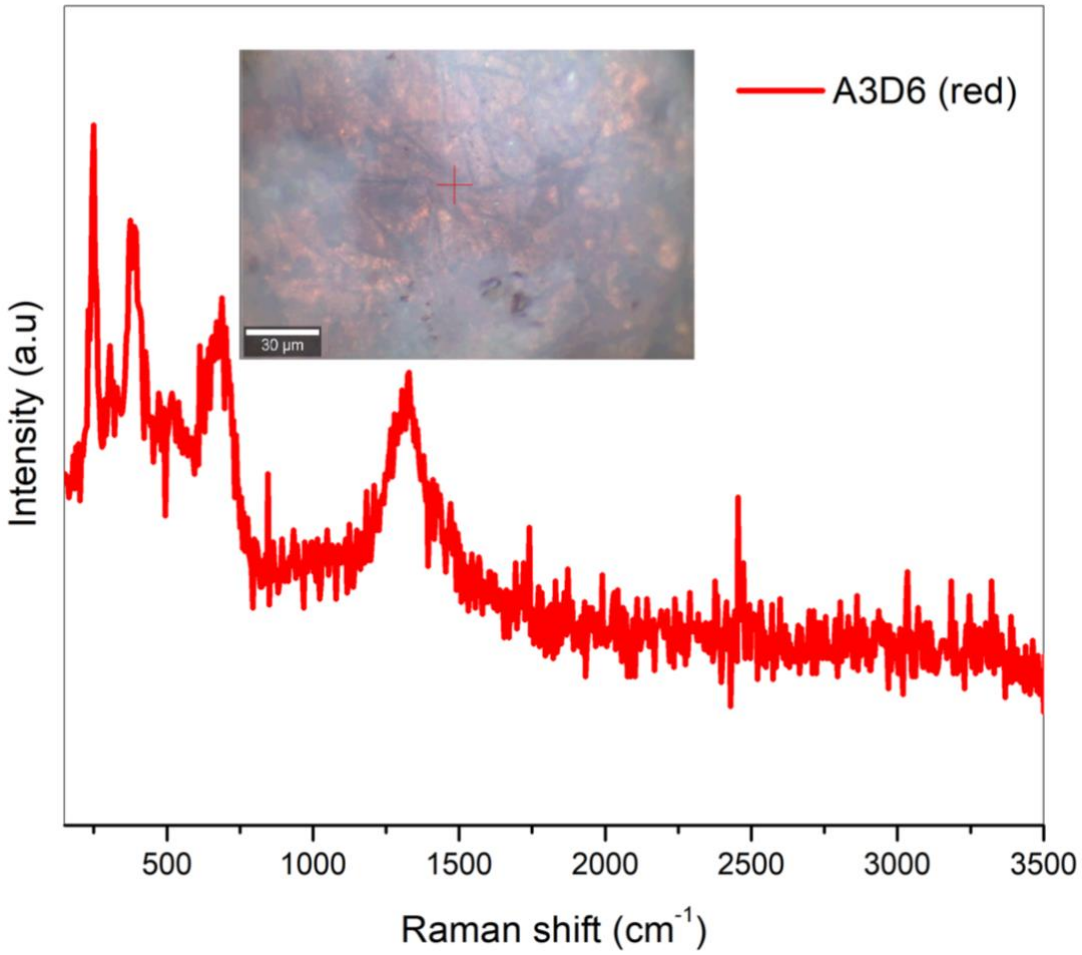

Figure 9.6: Raman spectra on day 6 of Area 2

Image (a) indicates the area where the spectra was taken.

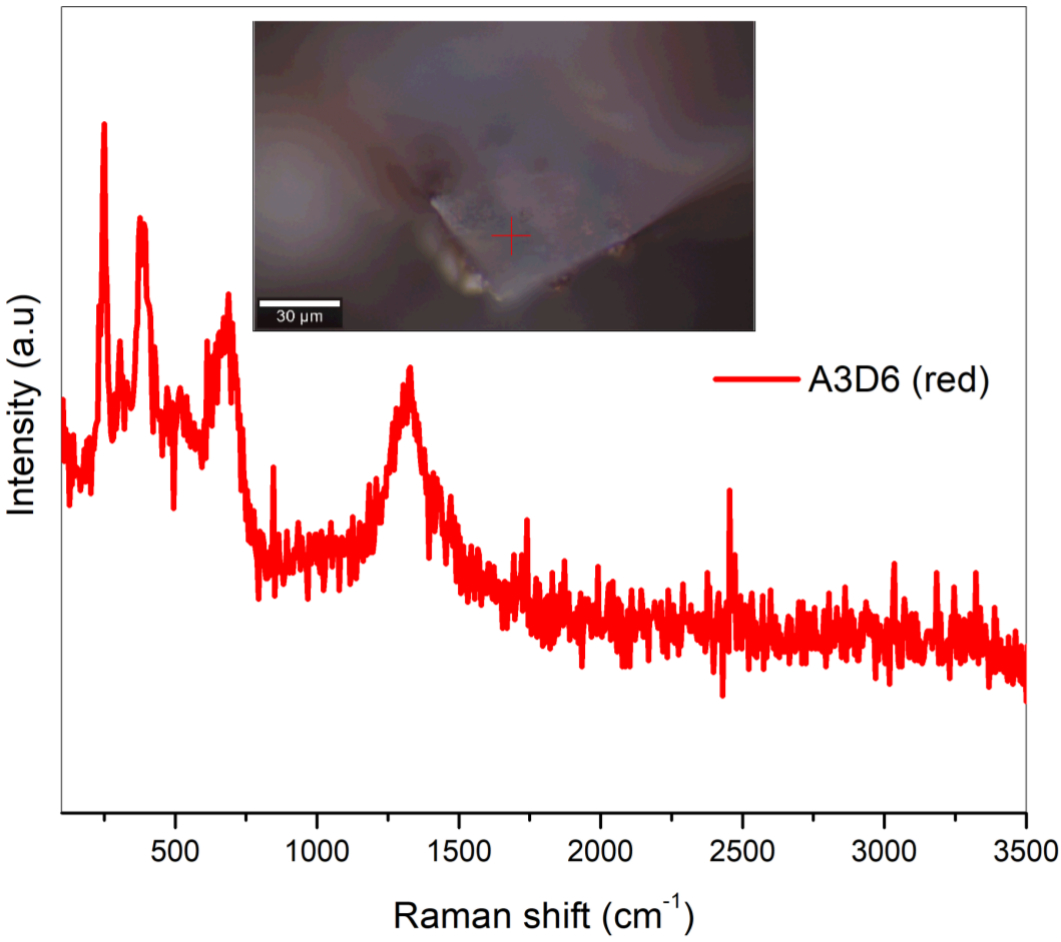

Figure 9.7: Raman spectra on day 6 of Area 3

Image (a) indicates the area where the spectra was taken.

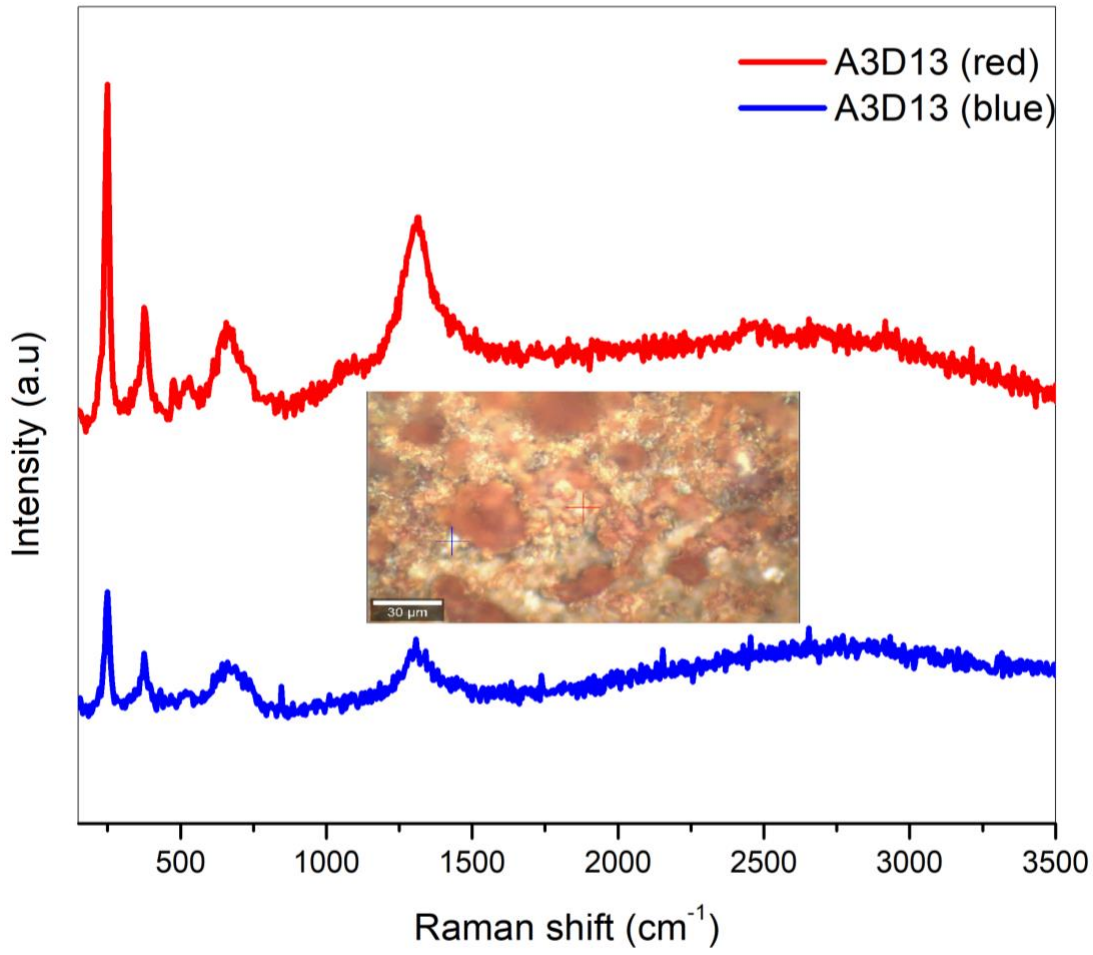

Figure 9.8: Raman spectra on day 13 of Area 1

Image (a) indicates the area where the spectra was taken.

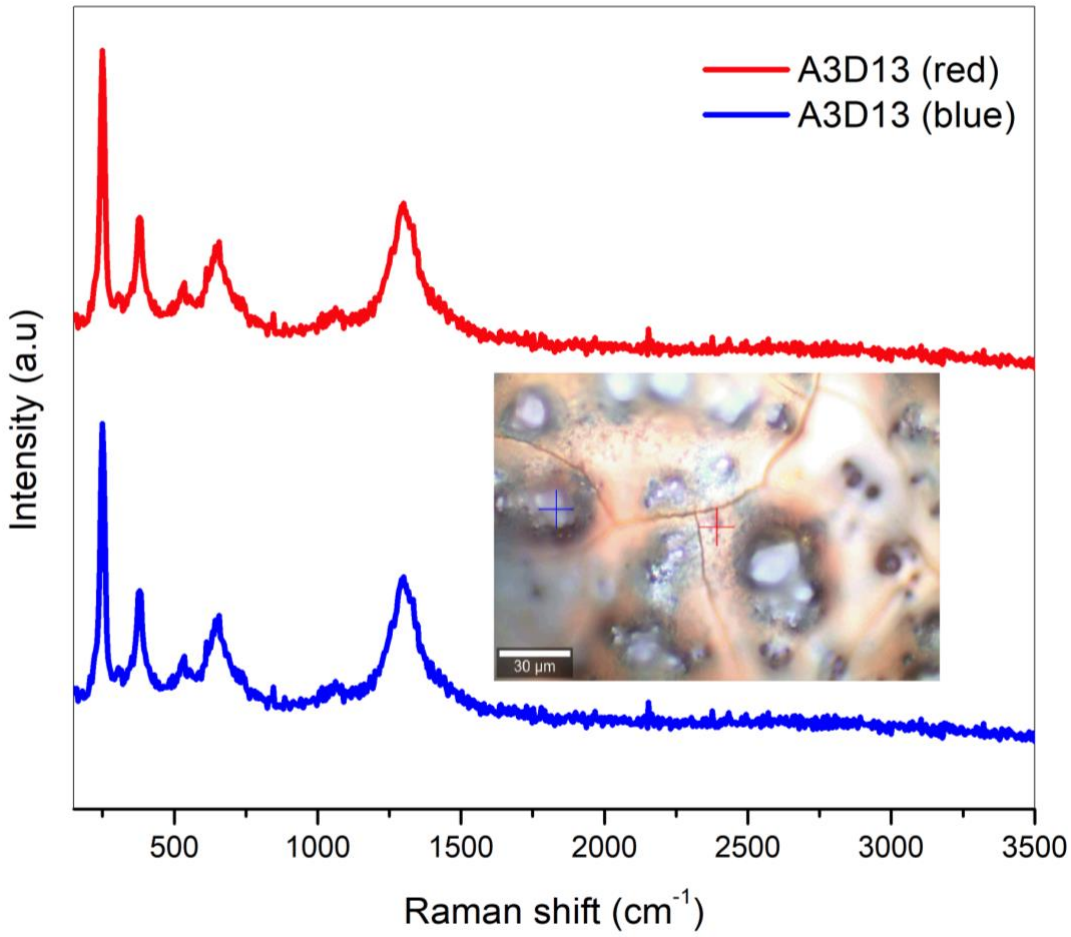

Figure 9.9: Raman spectra on day 13 of Area 2

Image (a) indicates the area where the spectra was taken.

9.1.4 SEM images of bacteria

Figure 9.10 depicts the SEM image of the bacteria attached to the surface on day 3(a) and day 6(b). Figure 9.11(a and b) depict the mature biofilm structures seen only on day 13, the structures take on a flower-like appearance and bulb-like structure as seen in Figure 9.11(a). Figure 9.11(b) is a higher magnification image of the multispecies biofilm structure.

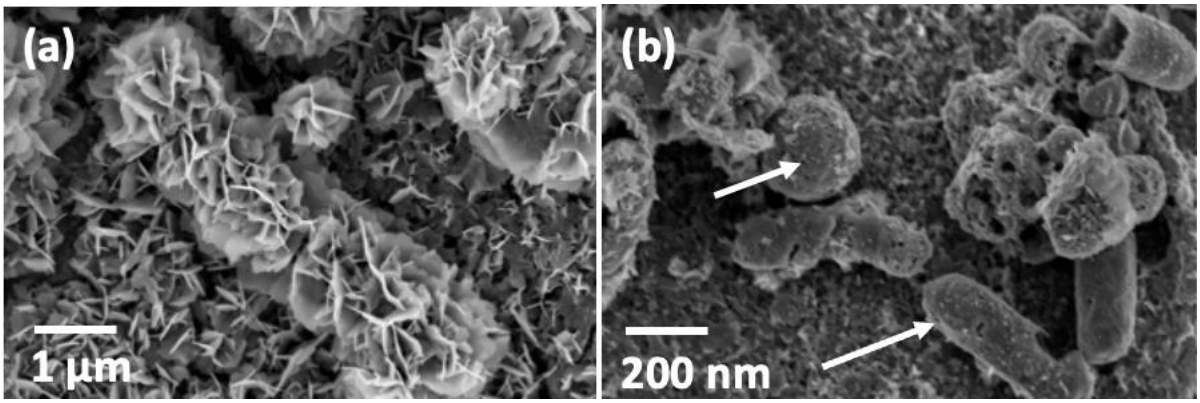

Figure 9.10: Day 3 SEM image of (a) smooth finish initial attachment of the rod-shaped bacteria (b) Day 6 smooth finish, where rod-shaped and spherical shaped bacteria can be observed (indicated by the white arrow)

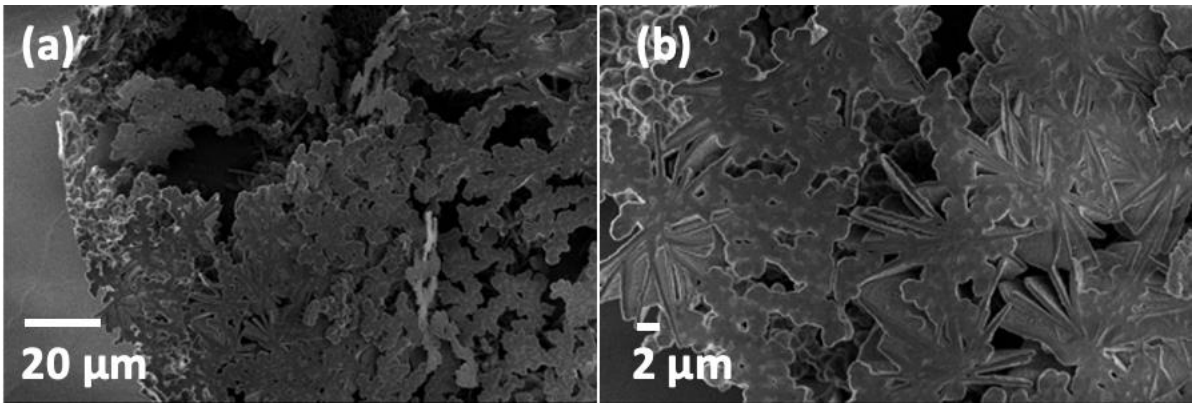

Figure 9.11: Day 13 SEM image of rough finish depicting the mature biofilm (a) with a mushroom-like structure and (b) the higher magnification of part of the structure

9.1.5 Compositional analysis

Table 9.2 indicates the cooling water composition taken on different days in May 2019, at the period the mesh coupon was installed in the coupon rack. The results indicate that there are minimal chlorides and phosphorus levels in the water when compared to Table 6.2 (elements presence on the surface after bacterial exposure). Table 9.3 presents composition of the stainless-steel mesh coupon that was inserted into the cooling tower coupon rack to collect bacteria.

Table 9.2: Composition of the cooling tower

Conductivity (µS/cm)	pH	Zn	Mg	Ca	Na	Fe	NH_3	P	M-Alk*	Silica	TOC**	
		mg/L										
543	8.59	0.53	24.12	34.28	32.34	0.17	0.10	0.00	156	4.38	10.26	
569	8.68	0.53	29.46	49.68	43.10	0.23	1.33	0.22	173	6.37	10.28	
479	6.72	0.43	21.59	29.09	35.61	0.08	0.56	0.00	133	5.15	10.84	
467	8.09	0.92	30.68	45.02	46.92	0.29	0.05	0.00	144	8.38	7.72	
522	7.70	0.70	30.52	39.04	37.40	0.19	0.35	0.12	156	4.09	8.38	

**M-Alkalinity (M-Alk) is the amount of carbonate in the water down to a pH of 4.6. **Hydrocarbon content (TOC).*

Table 9.3: Biofilm mesh coupon composition

Element	C	Cr	Fe	Mn	Mo	Ni	P	S	Si
Weight %	0.08	16.00	72.00	2.00	3.00	14.00	0.05	1.00	0.03

The quantification of bacteria on the rough and smooth surfaces was obtained using qPCR. Table 9.4 presents the data of the samples performed in triplicate, were averaged were determined and absolute copies were then calculated. Figure 9.12 is the standard curve; Figure 9.13 is the amplification of curve standards and Figure 9.14 represents the melt peak of standards.

9.1.6 Quantification of bacterial levels using qPCR

Table 9.4: Quantification of bacterial levels

Sample	Cq	Average Cq	Absolute Copies
Day 3 smooth	18.25	18.34	88524.41
Day 3 smooth	18.43		
Day 3 smooth	18.34		
Day 3 rough	25.77	25.62	1062.1
Day 3 rough	25.54		

Day 3 rough	25.55		
Day 6 smooth	25.18	25.20	1368.40
Day 6 smooth	25.23		
Day 6 smooth	25.20		
Day 6 rough	24.26	24.27	2412.29
Day 6 rough	24.28		
Day 6 rough	24.27		
Day 13 smooth	25.09	24.91	1633.69
Day 13 smooth	25.10		
Day 13 smooth	24.54		
Day 13 rough	22.25	22.27	8127.98
Day 13 rough	22.22		
Day 13 rough	22.35		

(a) *Three replicates were run for each DNA sample to obtain the average Cq.*

The equation below was used to calculate the absolute copy number:

$$Genome\ copy\ \# = \frac{DNA}{g\ to\ bp\ constant\ \times\ genome\ size}$$

Where 0.1 ng of DNA was used, with a genome size of 3505 bp and g to bp constant of 1.096 x 10^{-21} g.

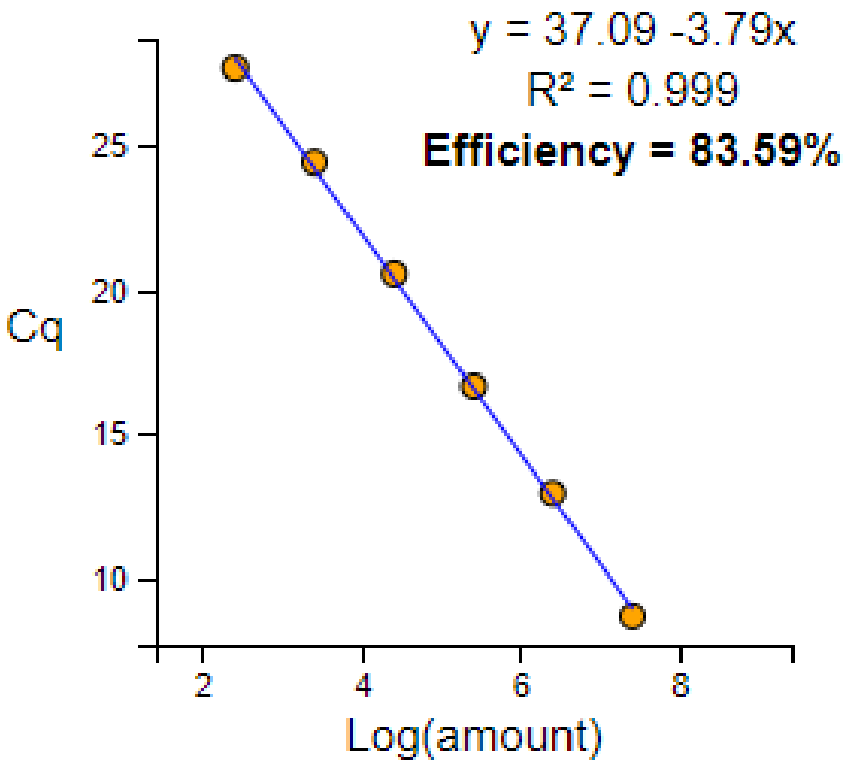

Figure 9.12: Standard curve with the 7 log dilutions (0.1 ng to 0.1 fg) and all the samples were calculated based on this curve

The PCR efficiency was calculated based on the below formula:

$$E = \frac{10 - 1}{slope - 1}$$

The percentage efficiency was calculated based on the below formula:

$$Percentage\ efficiency = (E - 1) \times 100$$

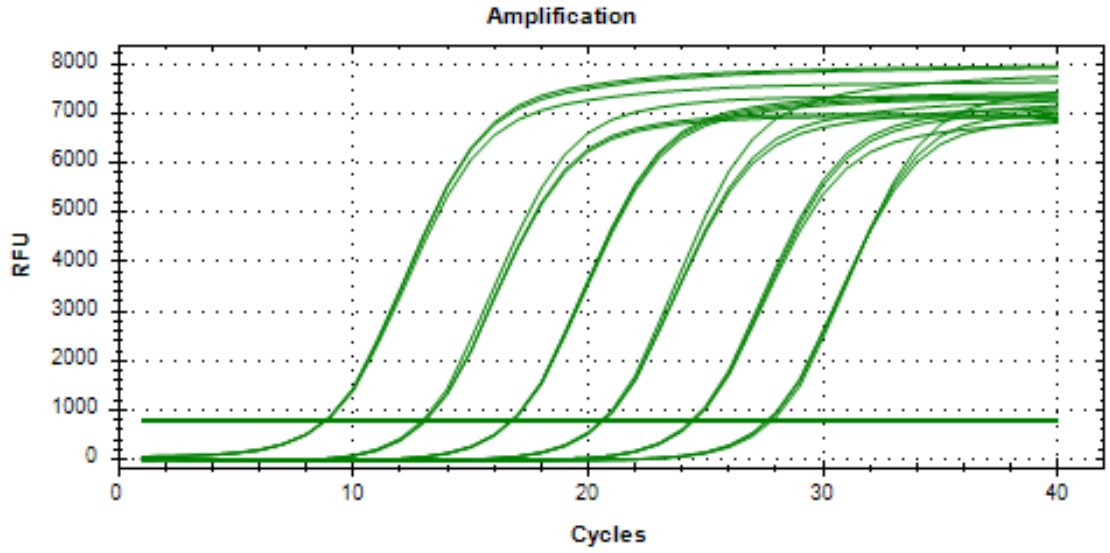

Figure 9.13: Amplification curves of standards

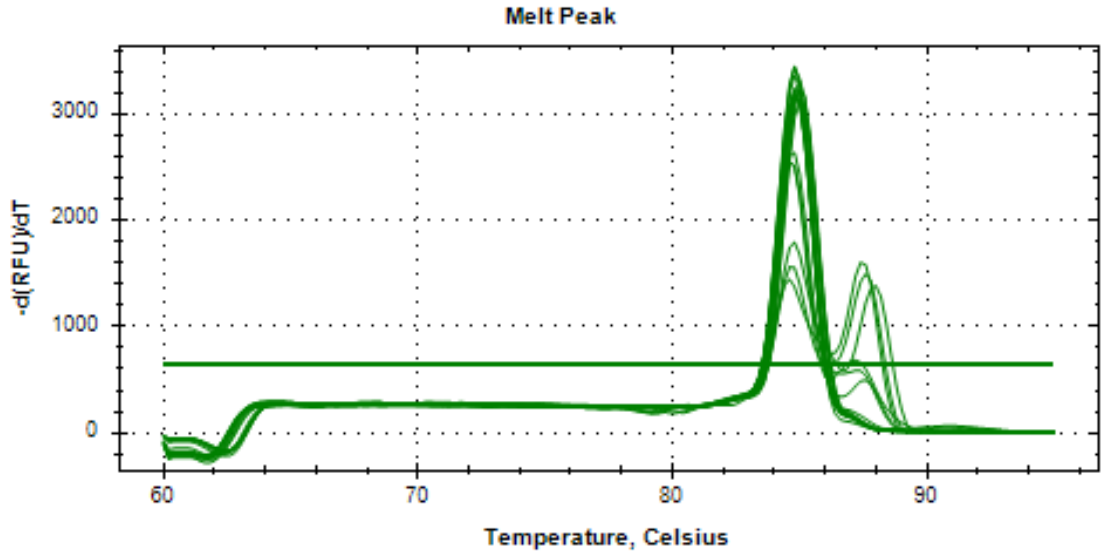

Figure 9.14: Melt peak of standards

9.1.7 AQUASIM lis.file.txt programme code

AQUASIM

Version 2.0 (win/mfc)

{AQUASYS}{{OPTIONS}{{3}{SECANT}{100}{FALSE}}{VARSYS}{{CONSTVAR
}{{1}{Ks}{Concentration for 1/2mumax}{g/l}{0.22}{1}{0}{10}{FAL
SE}{FALSE}}{CONSTVAR}{{1}{mumax}{Max specific growth rate }{1/
d}{0.455}{1}{0}{10}{FALSE}{FALSE}}{STATEVAR}{{1}{S}{Concentrat
ion of limiting nutrient}{g/l}{VOL}{1e-006}{1e-006}}{PROGVAR}{{
1}{t}{time (days)}{days}{T}}}{PROCSYS}{{DYNPROC}{{1}{Specific_
growth_rate_of_cells}{Specific growth rate of cells (mu)}{muma
x*S/(Ks+S)}{{S}{-1}}}}{COMPSYS}{{MIXCOMP}{{4}{Growth_rate}{Gro
wth}{0}{{Ks}{mumax}{S}{t}}{{Specific_growth_rate_of_cells}}{TR
UE}{0}{}{{0}{S}{1}}{TRUE}{1}{}{0.001}{0.001}{0.001}{0.001}}}{L
INKSYS}{}{CALCSYS}{{CALC}{{2}{calc1}{}{0}{0}{FALSE}{{0.1}{300}
}{TRUE}{FALSE}}}{FITSYS}{}{NUMPAR}{{2}{1}{1000}{0}{TRUE}{5}{10
00}{0.005}}{PLOTSYS}{{PLOTLISOPT}{{1}{4}{TAB}}{PLOTFILOPT}{{2}
{A4}{TRUE}{1}{1}{1}{1}{2.5}{2}{4}{10}{8}{8}{8}{TRUE}{TRUE}{FAL
SE}}{PLOTSCROPT}{{1}{600}{400}{25}{25}{25}{25}{50}{20}{14}{10}
{12}}{PLOT}{{2}{Specific_growth_rate}{Specific growth rate}{Sp
ecific growth rate}{Time (days)}{Specific growth rate (1/d)}{T
IME}{0}{TRUE}{5}{FALSE}{0}{TRUE}{1}{FALSE}{0}{TRUE}{5}{FALSE}{
0}{TRUE}{1}{FALSE}{{S}{0}{Growth_rate}{0}{0}{FALSE}{VAL}{}{Con
centration of citrate }{FALSE}{SOL}{2}{BLA}{TRUE}{CIRC}{2}{BLU
}{t}{0}{Growth_rate}{0}{0}{FALSE}{VAL}{}{Maximum specific grow

th rate}{TRUE}{DOT}{2}{GRE}{FALSE}{CIRC}{6}{GRE}}}}{STATESYS}{
{1}{2}{0}{{0}{{1}{0}{-0.3729508197}{0}}{0.1}{{0.9628332869}{0}
{-0.3703587935}{0}}{0.2}{{0.9259326967}{0}{-0.3676201634}{0}}{
0.3}{{0.8893128005}{0}{-0.364754072}{0}}{0.4}{{0.8529891669}{0
}{-0.3616997879}{0}}{0.5}{{0.8169792814}{0}{-0.3584654281}{0}}
{0.6}{{0.7813028995}{0}{-0.3550274186}{0}}{0.7}{{0.7459811012}
{0}{-0.3513716525}{0}}{0.8}{{0.7110364585}{0}{-0.3474817549}{0
}}{0.9}{{0.6764933134}{0}{-0.343338641}{0}}{1}{{0.6423778282}{
0}{-0.3389235722}{0}}{1.1}{{0.6087185479}{0}{-0.3342098983}{0}
}{1.2}{{0.575546598}{0}{-0.3291734405}{0}}{1.3}{{0.5428954589}
{0}{-0.3237893277}{0}}{1.4}{{0.510801481}{0}{-0.3180263496}{0}
}{1.5}{{0.4793038103}{0}{-0.3118564987}{0}}{1.6}{{0.4484447324
}{0}{-0.3052484369}{0}}{1.7}{{0.4182697657}{0}{-0.2981699348}{
0}}{1.8}{{0.3888276758}{0}{-0.2905856183}{0}}{1.9}{{0.36017053
39}{0}{-0.2824649713}{0}}{2}{{0.3323536504}{0}{-0.2737762568}{
0}}{2.1}{{0.3054351896}{0}{-0.2644911747}{0}}{2.2}{{0.27947584
89}{0}{-0.2545906516}{0}}{2.3}{{0.2545381166}{0}{-0.2440592605
}{0}}{2.4}{{0.230685242}{0}{-0.2328950496}{0}}{2.5}{{0.2079798
671}{0}{-0.2211103252}{0}}{2.6}{{0.18648254}{0}{-0.2087419207}
{0}}{2.7}{{0.166249326}{0}{-0.195841754}{0}}{2.8}{{0.147329379
1}{0}{-0.1824922867}{0}}{2.9}{{0.1297622493}{0}{-0.1688041062}

{0}}{3}{{0.113575248}{0}{-0.1549155977}{0}}{3.1}{{0.0987804542
}{0}{-0.1409873231}{0}}{3.2}{{0.08537290706}{0}{-0.1272048211}
{0}}{3.3}{{0.07332947872}{0}{-0.1137392044}{0}}{3.4}{{0.062608
08613}{0}{-0.1007868433}{0}}{3.5}{{0.05314880537}{0}{-0.088519
78775}{0}}{3.6}{{0.04487595941}{0}{-0.07708980335}{0}}{3.7}{{0
.03770177742}{0}{-0.06656512428}{0}}{3.8}{{0.03153010586}{0}{-
0.05703635681}{0}}{3.9}{{0.02626065071}{0}{-0.04852142002}{0}}
{4}{{0.02179235149}{0}{-0.04100956057}{0}}{4.1}{{0.018026664}{
0}{-0.03446046522}{0}}{4.2}{{0.01487036932}{0}{-0.02880994064}
{0}}{4.3}{{0.01223748666}{0}{-0.02397855415}{0}}{4.4}{{0.01005
034939}{0}{-0.01988024689}{0}}{4.5}{{0.008239991163}{0}{-0.016
42812953}{0}}{4.6}{{0.006746040448}{0}{-0.01353717734}{0}}{4.7
}{{0.005516342468}{0}{-0.01113008952}{0}}{4.8}{{0.004506306944
}{0}{-0.00913315463}{0}}{4.9}{{0.003678175054}{0}{-0.007482271
438}{0}}{5}{{0.003000196568}{0}{-0.006121474325}{0}}{5.1}{{0.0
0244582573}{0}{-0.00500261493}{0}}{5.2}{{0.001992989456}{0}{-0
.004084198137}{0}}{5.3}{{0.001623477972}{0}{-0.003331022382}{0
}}{5.4}{{0.001322231992}{0}{-0.002714426928}{0}}{5.5}{{0.00107
6778191}{0}{-0.002212212312}{0}}{5.6}{{0.0008766660924}{0}{-0.
001801668962}{0}}{5.7}{{0.0007137659676}{0}{-0.001468160149}{0
}}{5.8}{{0.0005809833777}{0}{-0.001195587429}{0}}{5.9}{{0.0004

728371412}{0}{-0.0009754053849}{0}}{6}{{0.0003846929833}{0}{-0
.000793620805}{0}}{6.1}{{0.0003129297975}{0}{-0.0006469200858}
{0}}{6.2}{{0.0002545652131}{0}{-0.000525454046}{0}}{6.3}{{0.00
02070839283}{0}{-0.0004270358129}{0}}{6.4}{{0.0001685034469}{0
}{-0.0003475647858}{0}}{6.5}{{0.0001371041829}{0}{-0.000282449
661}{0}}{6.6}{{0.0001115587598}{0}{-0.0002304830425}{0}}{6.7}{
{9.07590529e-005}{0}{-0.0001873166984}{0}}{6.8}{{7.381994259e-
005}{0}{-0.000152524207}{0}}{6.9}{{6.003686415e-005}{0}{-0.000
1241052562}{0}}{7}{{4.882683886e-005}{0}{-0.0001008488959}{0}}
{7.1}{{3.971682439e-005}{0}{-8.205329248e-005}{0}}{7.2}{{3.231
424446e-005}{0}{-6.658157651e-005}{0}}{7.3}{{2.629135046e-005}
{0}{-5.416766551e-005}{0}}{7.4}{{2.139576717e-005}{0}{-4.41137
9099e-005}{0}}{7.5}{{1.740454194e-005}{0}{-3.5934724e-005}{0}}
{7.6}{{1.415568397e-005}{0}{-2.926927935e-005}{0}}{7.7}{{1.151
078674e-005}{0}{-2.380948427e-005}{0}}{7.8}{{9.360146343e-006}
{0}{-1.935807381e-005}{0}}{7.9}{{7.618159262e-006}{0}{-1.56250
5866e-005}{0}}{8}{{6.212592837e-006}{0}{-1.25924222e-005}{0}}{
8.1}{{5.078872278e-006}{0}{-1.018608546e-005}{0}}{8.2}{{4.1679
99426e-006}{0}{-8.058944355e-006}{0}}{8.3}{{3.446098606e-006}{
0}{-6.454168044e-006}{0}}{8.4}{{2.861494688e-006}{0}{-5.321009
017e-006}{0}}{8.5}{{2.368865258e-006}{0}{-4.233424021e-006}{0}

}{8.6}{{1.986170223e-006}{0}{-3.461405996e-006}{0}}{8.7}{{1.66
8380958e-006}{0}{-2.936111608e-006}{0}}{8.8}{{1.390268893e-006
}{0}{-2.671818082e-006}{0}}{8.9}{{1.148140416e-006}{0}{-2.2091
48422e-006}{0}}{9}{{9.41891103e-007}{0}{-1.918006264e-006}{0}}
{9.1}{{7.649528243e-007}{0}{-1.614454275e-006}{0}}{9.2}{{6.154
129474e-007}{0}{-1.47697454e-006}{0}}{9.3}{{4.783662048e-007}{
0}{-1.257837288e-006}{0}}{9.4}{{3.65627193e-007}{0}{-9.8524893
97e-007}{0}}{9.5}{{2.842123165e-007}{0}{-6.257835998e-007}{0}}
{9.6}{{2.116017512e-007}{0}{-6.71918418e-007}{0}}{9.7}{{1.5293
77149e-007}{0}{-4.99668856e-007}{0}}{9.8}{{1.121521514e-007}{0
}{-3.128941512e-007}{0}}{9.9}{{8.521181094e-008}{0}{-2.5950542
66e-007}{0}}{10}{{6.363973626e-008}{0}{-1.753859814e-007}{0}}{
10.1}{{4.944463175e-008}{0}{-1.119660234e-007}{0}}{10.2}{{4.05
5654867e-008}{0}{-6.924555271e-008}{0}}{10.3}{{3.49055383e-008
}{0}{-4.722456925e-008}{0}}{10.4}{{3.042165192e-008}{0}{-4.590
307303e-008}{0}}{10.5}{{2.503494079e-008}{0}{-6.528106405e-008
}{0}}{10.6}{{2.545612657e-008}{0}{5.217209554e-008}{0}}{10.7}{
{3.119675405e-008}{0}{6.088787279e-008}{0}}{10.8}{{3.728318489
e-008}{0}{5.908816271e-008}{0}}{10.9}{{4.266387035e-008}{0}{4.
677296529e-008}{0}}{11}{{4.62872617e-008}{0}{2.394228053e-008}
{0}}{11.1}{{4.710181021e-008}{0}{-9.403891556e-009}{0}}{11.2}{

{4.405596715e-008}{0}{-5.326555098e-008}{0}}{11.3}{{4.29063208
5e-008}{0}{-4.244013415e-009}{0}}{11.4}{{4.20758297e-008}{0}{-
1.236580963e-008}{0}}{11.5}{{4.043315892e-008}{0}{-2.048760585
e-008}{0}}{11.6}{{3.797830853e-008}{0}{-2.860940207e-008}{0}}{
11.7}{{3.471127851e-008}{0}{-3.673119828e-008}{0}}{11.8}{{3.06
3206887e-008}{0}{-4.48529945e-008}{0}}{11.9}{{2.574067961e-008
}{0}{-5.297479072e-008}{0}}{12}{{2.397784657e-008}{0}{-1.73202
8267e-008}{0}}{12.1}{{2.22458183e-008}{0}{-1.732028267e-008}{0
}}{12.2}{{2.051379004e-008}{0}{-1.732028267e-008}{0}}{12.3}{{1
.878176177e-008}{0}{-1.732028267e-008}{0}}{12.4}{{1.70497335e-
008}{0}{-1.732028267e-008}{0}}{12.5}{{1.531770524e-008}{0}{-1.
732028267e-008}{0}}{12.6}{{1.358567697e-008}{0}{-1.732028267e-
008}{0}}{12.7}{{1.18536487e-008}{0}{-1.732028267e-008}{0}}{12.
8}{{1.012162043e-008}{0}{-1.732028267e-008}{0}}{12.9}{{8.38959
2166e-009}{0}{-1.732028267e-008}{0}}{13}{{7.815002042e-009}{0}
{-5.64512936e-009}{0}}{13.1}{{7.250489106e-009}{0}{-5.64512936
e-009}{0}}{13.2}{{6.68597617e-009}{0}{-5.64512936e-009}{0}}{13
.3}{{6.121463234e-009}{0}{-5.64512936e-009}{0}}{13.4}{{5.55695
0298e-009}{0}{-5.64512936e-009}{0}}{13.5}{{4.992437362e-009}{0
}{-5.64512936e-009}{0}}{13.6}{{4.427924426e-009}{0}{-5.6451293
6e-009}{0}}{13.7}{{3.86341149e-009}{0}{-5.64512936e-009}{0}}{1

3.8}{{3.298898554e-009}{0}{-5.64512936e-009}{0}}{13.9}{{2.7343
85618e-009}{0}{-5.64512936e-009}{0}}{14}{{2.547111801e-009}{0}
{-1.839894002e-009}{0}}{14.1}{{2.3631224e-009}{0}{-1.839894002
e-009}{0}}{14.2}{{2.179133e-009}{0}{-1.839894002e-009}{0}}{14.
3}{{1.9951436e-009}{0}{-1.839894002e-009}{0}}{14.4}{{1.8111542
e-009}{0}{-1.839894002e-009}{0}}{14.5}{{1.627164799e-009}{0}{-
1.839894002e-009}{0}}{14.6}{{1.443175399e-009}{0}{-1.839894002
e-009}{0}}{14.7}{{1.259185999e-009}{0}{-1.839894002e-009}{0}}{
14.8}{{1.075196599e-009}{0}{-1.839894002e-009}{0}}{14.9}{{8.91
2071986e-010}{0}{-1.839894002e-009}{0}}{15}{{8.301698035e-010}
{0}{-5.996691851e-010}{0}}{15.1}{{7.70202885e-010}{0}{-5.99669
1851e-010}{0}}{15.2}{{7.102359665e-010}{0}{-5.996691851e-010}{
0}}{15.3}{{6.50269048e-010}{0}{-5.996691851e-010}{0}}{15.4}{{5
.903021295e-010}{0}{-5.996691851e-010}{0}}{15.5}{{5.303352109e
-010}{0}{-5.996691851e-010}{0}}{15.6}{{4.703682924e-010}{0}{-5
.996691851e-010}{0}}{15.7}{{4.104013739e-010}{0}{-5.996691851e
-010}{0}}{15.8}{{3.504344554e-010}{0}{-5.996691851e-010}{0}}{1
5.9}{{2.904675369e-010}{0}{-5.996691851e-010}{0}}{16}{{2.70573
8669e-010}{0}{-1.954477387e-010}{0}}{16.1}{{2.510290931e-010}{
0}{-1.954477387e-010}{0}}{16.2}{{2.314843192e-010}{0}{-1.95447
7387e-010}{0}}{16.3}{{2.119395453e-010}{0}{-1.954477387e-010}{

0}}{16.4}{{1.923947714e-010}{0}{-1.954477387e-010}{0}}{16.5}{{
1.728499976e-010}{0}{-1.954477387e-010}{0}}{16.6}{{1.533052237
e-010}{0}{-1.954477387e-010}{0}}{16.7}{{1.337604498e-010}{0}{-
1.954477387e-010}{0}}{16.8}{{1.14215676e-010}{0}{-1.954477387e
-010}{0}}{16.9}{{9.46709021e-011}{0}{-1.954477387e-010}{0}}{17
}{{8.81870392e-011}{0}{-6.370148606e-011}{0}}{17.1}{{8.1816890
59e-011}{0}{-6.370148606e-011}{0}}{17.2}{{7.544674199e-011}{0}
{-6.370148606e-011}{0}}{17.3}{{6.907659338e-011}{0}{-6.3701486
06e-011}{0}}{17.4}{{6.270644477e-011}{0}{-6.370148606e-011}{0}
}{17.5}{{5.633629617e-011}{0}{-6.370148606e-011}{0}}{17.6}{{4.
996614756e-011}{0}{-6.370148606e-011}{0}}{17.7}{{4.359599896e-
011}{0}{-6.370148606e-011}{0}}{17.8}{{3.722585035e-011}{0}{-6.
370148606e-011}{0}}{17.9}{{3.085570174e-011}{0}{-6.370148606e-
011}{0}}{18}{{2.87424427e-011}{0}{-2.076196605e-011}{0}}{18.1}
{{2.66662461e-011}{0}{-2.076196605e-011}{0}}{18.2}{{2.45900494
9e-011}{0}{-2.076196605e-011}{0}}{18.3}{{2.251385289e-011}{0}{
-2.076196605e-011}{0}}{18.4}{{2.043765628e-011}{0}{-2.07619660
5e-011}{0}}{18.5}{{1.836145968e-011}{0}{-2.076196605e-011}{0}}
{18.6}{{1.628526307e-011}{0}{-2.076196605e-011}{0}}{18.7}{{1.4
20906647e-011}{0}{-2.076196605e-011}{0}}{18.8}{{1.213286986e-0
11}{0}{-2.076196605e-011}{0}}{18.9}{{1.005667326e-011}{0}{-2.0

76196605e-011}{0}}{19}{{9.367907341e-012}{0}{-6.766863075e-012
}{0}}{19.1}{{8.691221034e-012}{0}{-6.766863075e-012}{0}}{19.2}
{{8.014534727e-012}{0}{-6.766863075e-012}{0}}{19.3}{{7.3378484
19e-012}{0}{-6.766863075e-012}{0}}{19.4}{{6.661162112e-012}{0}
{-6.766863075e-012}{0}}{19.5}{{5.984475804e-012}{0}{-6.7668630
75e-012}{0}}{19.6}{{5.307789497e-012}{0}{-6.766863075e-012}{0}
}{19.7}{{4.631103189e-012}{0}{-6.766863075e-012}{0}}{19.8}{{3.
954416882e-012}{0}{-6.766863075e-012}{0}}{19.9}{{3.277730574e-
012}{0}{-6.766863075e-012}{0}}{20}{{3.053243903e-012}{0}{-2.20
5496134e-012}{0}}{20.1}{{2.83269429e-012}{0}{-2.205496134e-012
}{0}}{20.2}{{2.612144676e-012}{0}{-2.205496134e-012}{0}}{20.3}
{{2.391595063e-012}{0}{-2.205496134e-012}{0}}{20.4}{{2.1710454
49e-012}{0}{-2.205496134e-012}{0}}{20.5}{{1.950495836e-012}{0}
{-2.205496134e-012}{0}}{20.6}{{1.729946223e-012}{0}{-2.2054961
34e-012}{0}}{20.7}{{1.509396609e-012}{0}{-2.205496134e-012}{0}
}{20.8}{{1.288846996e-012}{0}{-2.205496134e-012}{0}}{20.9}{{1.
068297382e-012}{0}{-2.205496134e-012}{0}}{21}{{9.951313555e-01
3}{0}{-7.188283764e-013}{0}}{21.1}{{9.232485179e-013}{0}{-7.18
8283764e-013}{0}}{21.2}{{8.513656802e-013}{0}{-7.188283764e-01
3}{0}}{21.3}{{7.794828426e-013}{0}{-7.188283764e-013}{0}}{21.4
}{{7.076000049e-013}{0}{-7.188283764e-013}{0}}{21.5}{{6.357171

673e-013}{0}{-7.188283764e-013}{0}}{21.6}{{5.638343297e-013}{0
}{-7.188283764e-013}{0}}{21.7}{{4.91951492e-013}{0}{-7.1882837
64e-013}{0}}{21.8}{{4.200686544e-013}{0}{-7.188283764e-013}{0}
}{21.9}{{3.481858168e-013}{0}{-7.188283764e-013}{0}}{22}{{3.24
3391115e-013}{0}{-2.342848063e-013}{0}}{22.1}{{3.009106309e-01
3}{0}{-2.342848063e-013}{0}}{22.2}{{2.774821502e-013}{0}{-2.34
2848063e-013}{0}}{22.3}{{2.540536696e-013}{0}{-2.342848063e-01
3}{0}}{22.4}{{2.30625189e-013}{0}{-2.342848063e-013}{0}}{22.5}
{{2.071967083e-013}{0}{-2.342848063e-013}{0}}{22.6}{{1.8376822
77e-013}{0}{-2.342848063e-013}{0}}{22.7}{{1.60339747e-013}{0}{
-2.342848063e-013}{0}}{22.8}{{1.369112664e-013}{0}{-2.34284806
3e-013}{0}}{22.9}{{1.134827858e-013}{0}{-2.342848063e-013}{0}}
{23}{{1.057105262e-013}{0}{-7.635949315e-014}{0}}{23.1}{{9.807
45769e-014}{0}{-7.635949315e-014}{0}}{23.2}{{9.043862758e-014}
{0}{-7.635949315e-014}{0}}{23.3}{{8.280267827e-014}{0}{-7.6359
49315e-014}{0}}{23.4}{{7.516672895e-014}{0}{-7.635949315e-014}
{0}}{23.5}{{6.753077964e-014}{0}{-7.635949315e-014}{0}}{23.6}{
{5.989483032e-014}{0}{-7.635949315e-014}{0}}{23.7}{{5.22588810
1e-014}{0}{-7.635949315e-014}{0}}{23.8}{{4.462293169e-014}{0}{
-7.635949315e-014}{0}}{23.9}{{3.698698238e-014}{0}{-7.63594931
5e-014}{0}}{24}{{3.445380146e-014}{0}{-2.488753874e-014}{0}}{2

4.1}{{3.196504758e-014}{0}{-2.488753874e-014}{0}}{24.2}{{2.947
629371e-014}{0}{-2.488753874e-014}{0}}{24.3}{{2.698753983e-014
}{0}{-2.488753874e-014}{0}}{24.4}{{2.449878596e-014}{0}{-2.488
753874e-014}{0}}{24.5}{{2.201003209e-014}{0}{-2.488753874e-014
}{0}}{24.6}{{1.952127821e-014}{0}{-2.488753874e-014}{0}}{24.7}
{{1.703252434e-014}{0}{-2.488753874e-014}{0}}{24.8}{{1.4543770
46e-014}{0}{-2.488753874e-014}{0}}{24.9}{{1.205501659e-014}{0}
{-2.488753874e-014}{0}}{25}{{1.122938725e-014}{0}{-8.111494184
e-015}{0}}{25.1}{{1.041823783e-014}{0}{-8.111494184e-015}{0}}{
25.2}{{9.60708841e-015}{0}{-8.111494184e-015}{0}}{25.3}{{8.795
938991e-015}{0}{-8.111494184e-015}{0}}{25.4}{{7.984789573e-015
}{0}{-8.111494184e-015}{0}}{25.5}{{7.173640155e-015}{0}{-8.111
494184e-015}{0}}{25.6}{{6.362490736e-015}{0}{-8.111494184e-015
}{0}}{25.7}{{5.551341318e-015}{0}{-8.111494184e-015}{0}}{25.8}
{{4.740191899e-015}{0}{-8.111494184e-015}{0}}{25.9}{{3.9290424
81e-015}{0}{-8.111494184e-015}{0}}{26}{{3.65994847e-015}{0}{-2
.643746277e-015}{0}}{26.1}{{3.395573842e-015}{0}{-2.643746277e
-015}{0}}{26.2}{{3.131199215e-015}{0}{-2.643746277e-015}{0}}{2
6.3}{{2.866824587e-015}{0}{-2.643746277e-015}{0}}{26.4}{{2.602
449959e-015}{0}{-2.643746277e-015}{0}}{26.5}{{2.338075331e-015
}{0}{-2.643746277e-015}{0}}{26.6}{{2.073700704e-015}{0}{-2.643

746277e-015}{0}}{26.7}{{1.809326076e-015}{0}{-2.643746277e-015
}{0}}{26.8}{{1.544951448e-015}{0}{-2.643746277e-015}{0}}{26.9}
{{1.280576821e-015}{0}{-2.643746277e-015}{0}}{27}{{1.192872105
e-015}{0}{-8.616654613e-016}{0}}{27.1}{{1.106705559e-015}{0}{-
8.616654613e-016}{0}}{27.2}{{1.020539013e-015}{0}{-8.616654613
e-016}{0}}{27.3}{{9.343724666e-016}{0}{-8.616654613e-016}{0}}{
27.4}{{8.482059205e-016}{0}{-8.616654613e-016}{0}}{27.5}{{7.62
0393744e-016}{0}{-8.616654613e-016}{0}}{27.6}{{6.758728283e-01
6}{0}{-8.616654613e-016}{0}}{27.7}{{5.897062821e-016}{0}{-8.61
6654613e-016}{0}}{27.8}{{5.03539736e-016}{0}{-8.616654613e-016
}{0}}{27.9}{{4.173731899e-016}{0}{-8.616654613e-016}{0}}{28}{{
3.88787949e-016}{0}{-2.808391159e-016}{0}}{28.1}{{3.607040374e
-016}{0}{-2.808391159e-016}{0}}{28.2}{{3.326201258e-016}{0}{-2
.808391159e-016}{0}}{28.3}{{3.045362142e-016}{0}{-2.808391159e
-016}{0}}{28.4}{{2.764523026e-016}{0}{-2.808391159e-016}{0}}{2
8.5}{{2.48368391e-016}{0}{-2.808391159e-016}{0}}{28.6}{{2.2028
44794e-016}{0}{-2.808391159e-016}{0}}{28.7}{{1.922005678e-016}
{0}{-2.808391159e-016}{0}}{28.8}{{1.641166562e-016}{0}{-2.8083
91159e-016}{0}}{28.9}{{1.360327446e-016}{0}{-2.808391159e-016}
{0}}{29}{{1.267160734e-016}{0}{-9.153274975e-017}{0}}{29.1}{{1
.175627985e-016}{0}{-9.153274975e-017}{0}}{29.2}{{1.084095235e

-016}{0}{-9.153274975e-017}{0}}{29.3}{{9.925624851e-017}{0}{-9

.153274975e-017}{0}}{29.4}{{9.010297354e-017}{0}{-9.153274975e

-017}{0}}{29.5}{{8.094969856e-017}{0}{-9.153274975e-017}{0}}{2

9.6}{{7.179642359e-017}{0}{-9.153274975e-017}{0}}{29.7}{{6.264

314861e-017}{0}{-9.153274975e-017}{0}}{29.8}{{5.348987364e-017

}{0}{-9.153274975e-017}{0}}{29.9}{{4.433659866e-017}{0}{-9.153

274975e-017}{0}}{30}{{4.130005395e-017}{0}{-2.983289649e-017}{

0}}}}}

9.1.8 Metabolic activity (Growth rate)

The Metabolic activity was determined by using the spectrophotometer at 550 nm at 35° C.

Metabolic activity at time (t) = unfiltered absorbance - filtered absorbance

Table 9.5: Metabolic activity

Day	Filtered Sample 1	Filtered Sample 2	Unfiltered Sample 1	Unfiltered Sample 2	Metabolic activity 1	Metabolic activity 2
1	0.010	0.010	0.107	0.107	0.097	0.097
2	0.005	0.011	0.156	0.166	0.151	0.155
3	0.010	0.011	0.096	0.100	0.086	0.089
4	0.012	0.013	0.120	0.122	0.108	0.109
5	0.014	0.018	0.176	0.181	0.162	0.163
6	0.025	0.026	0.201	0.202	0.176	0.176
7	0.011	0.012	0.183	0.185	0.172	0.173
8	0.011	0.017	0.249	0.251	0.238	0.234
9	0.025	0.027	0.302	0.306	0.277	0.279
10	0.036	0.035	0.334	0.334	0.298	0.299
11	0.080	0.081	0.471	0.482	0.391	0.401
12	0.102	0.104	0.499	0.502	0.397	0.398
13	0.229	0.234	0.674	0.668	0.445	0.434
14	0.069	0.068	0.335	0.336	0.266	0.268
15	0.013	0.014	0.183	0.185	0.170	0.171

9.2 ANOVA CONDUCTED ON DAY 6 CORROSION RATE

Table 9.6: ANOVA for day 6 corrosion rate

SUMMARY	Count	Sum	Average	Variance		
Groups						
Smooth	6	102.38	17.06	720.22		
Rough	6	90.43	-15.07	560.87		
Source of Variation	**SS**	**df**	**MS**	**F**	**P-value**	**F crit**
Between Groups	3097.73	1	3097.73	4.84	0.05	4.96
Within Groups	6405.44	10	640.54			
Total	9503.17	11				

9.3 APPENDIX B: LANGUAGE EDITING CERTIFICATE

Nr: 202700

ACADEMIC AND PROFESSIONAL EDITING SERVICES

Tel nr: USA: +1 (773) 217-4568/ NZ: +64 22 359 2202 SA +27 81 534 3590/
www.apespro.com; Facebook: www.facebook.com/apespro

LANGUAGE EDITING CERTIFICATE

Report title:	Multispecies bacterial attachment to industry finished steels used in heat exchangers
Author/s:	Alicia Prithiraj
Institution:	University of Pretoria
Date Issued:	21 December 2022

This document certifies that the report listed above was edited for proper English language, grammar, punctuation, spelling, and overall style. Neither the research content nor the author's intentions were altered in any way during the editing process. Documents receiving this certification should be English-ready for publication; however, the author has the ability and choice to accept or reject our suggestions and changes.

We do not take responsibility for plagiarism.

If you have any questions or concerns about this document or certification, kindly contact: Info@apespro.com

APES is committed to providing high-quality services for professionals and researchers. To find out more about APES, visit www.apespro.com.

Warm regards

Elizabeth Marx

SAFREA member (2019 Western Cape Exco member)

Attended the EFA International Editors' Conference – Chicago: August 2019 https://www.the-efa.org/efas-2019-conference-announcement/